공학박사학위논문

Modification of Polyurethane Film by Ion Implantation and Its Application to Tissue Engineering

이온 주입법에 의한 폴리우레탄 필름의 개질 및 조직공학에의 응용

2012년 8월

서울대학교 대학원

재료공학부

양 찬 오

Modification of Polyurethane Film by Ion Implantation and Its Application to Tissue Engineering

이온 주입법에 의한 폴리우레탄 필름의 개질 및 조직공학에의 응용

지도교수 **강 태 진**

이 논문을 공학박사 학위논문으로 제출함
2012년 4월

서울대학교 대학원
재료공학부

양 찬 오

양 찬 오의 공학박사 학위논문을 인준함
2012년 6월

위 원 장 _____ (인)

부위원장 _____ (인)

위 원 _____ (인)

위 원 _____ (인)

위 원 _____ (인)

Modification of Polyurethane Film by Ion Implantation and Its Application to Tissue Engineering

ADVISOR: TAE JIN KANG, PROFESSOR

BY

CHAN OH YANG

SUBMITTED FOR THE DEGREE OF
DOCTOR OF PHILOSOPHY

IN THE
DEPARTMENT OF MATERIALS SCIENCE AND ENGINEERING
GRADUATE SCHOOL
AT
SEOUL NATIONAL UNIVERSITY

AUGUST 2012

ABSTRACT

Biomaterials are defined as artificial or natural substances or their composites, other than drugs, that can be used to treat, reinforce, replace or repair any tissue or organ of the human body for a short- or long-term period of time. Materials intended for use as biomaterials should have mechanical strength and functional characteristics similar to those of living tissues and provide the essential properties of biochemical compatibility. Currently, biomaterials are used mainly in areas such as dentistry, orthopedics, plastic surgery and otolaryngology. Even though research on biomaterials began in the early 1900s, biomaterials-related markets have witnessed a rapid growth worldwide over the last 30 years. Some prime reasons for such a growth include an increase in patients under rehabilitation due to wars and accidents, an increase in the aged population due to lengthened human lifespan and decreased natural mortality, the development of new biomaterials, surgery-related medical advances and people's pursuit of higher quality of life. Therefore, biomaterials for encouraging excellent performance are urgently needed in the fields of tissue engineering.

Polyurethane (PU) is a typical block copolymer which consists of soft polyol segments and hard urethane segments. Because of its excellent mechanical properties and relatively good biocompatibility, PU is commonly used in blood-containing devices or materials for artificial organs. Especially, in the case of biomedical application, PU has been relatively well-studied and is known to have better blood compatibility than any other polymer. Despite such advantages, however, PU itself does not have wide applications yet for biomedical use because it is still unsatisfactory

in blood compatibility and causes biodegradation and calcification by calcium deposit or bacterial infections as found in both *in vivo* and *in vitro* experiments. Thus, for biomedical use as a long-term implantable material, PU is required to meet such property requirements as bio-stability, anti-calcification and inhibition of infections as well as blood compatibility. Hence, surface modification is required for the enhancement of the biocompatibility of PU.

In this thesis, as a simple and very effective method that is currently used to improve the biocompatibility of polymeric materials, ion implantation was applied to PU. To investigate the surface modification of thermally treated PU films by ion implantation, argon ion (Ar^+) implantation was carried out using conventional ion implanter. In order to change the intrinsic properties of PU films such as phase separation, two different types of thermal treatment were applied to solvent-cast PU films before Ar^+ implantation. It was found that thermal treatment caused change to the degree of phase separation and the distribution of soft segment matrix and hard segment domains on the surfaces of PU films. Before ion implantation, in the case of a PU film cured at a higher temperature, its surface was enriched with hydrophobic soft segments to minimize interfacial free energy. On the other hand, in the case of a PU film cured at a lower temperature, hard segment domains were increased on the surface of it due to a higher degree of phase separation and the relatively slow molecular mobility of soft segments. After ion implantation, as for PU films cured at a higher temperature, an increase in surface wettability at lower ion doses was mainly caused by the formation of hydrophilic functional groups on the surfaces of ion-implanted PU films. However, a decrease in surface wettability at higher ion doses was induced by increased surface roughness and the carbonization of surface layer. As for PU films cured at a lower temperature, through the whole range of ion dose from 1×10^{13} to 1×10^{16} ions/cm^2, surface wettability was enhanced by an increase in hydrophilic

functional groups and a relatively small increase in surface roughness even at higher ion doses. The size of surface wrinkles induced by ion implantation was increased with increasing ion dose. Due to the hard segment domains on the surfaces of PU films cured at a lower temperature, wrinkle formation and its propagation were retarded.

Focused ion beam (FIB), a beam-line type gallium ion (Ga^+) implantation method, was also utilized to modify the surfaces of PU substrates. To investigate the effect of FIB-treated PU substrates on cell adhesion and cell growth, NIH3T3 fibroblasts derived from mouse embryo were cultured on them. With the sample washing after FIB treatment, the implanted gallium ions was not detected implying that the influence of Ga^+ on cell growth is negligible. Furthermore, most of RAW 264.7 monocytes/macrophages, which were derived from mouse, on the FIB-treated PU substrates did not produce multinucleated giant cells indicating that PU substrates showed no toxicity after FIB treatment. From the results of immunofluorescence staining, it was also found that NTH3T3 fibroblasts synthesized a trace amount of apoptosis-related caspase 3 during 3-days cell culture. Compared to conventional Ar^+ implantation, FIB treatment created more functional groups that increase the surface wettability of PU substrates producing more hydrophilic groups such as carbonyl and carboxyl groups. And surface wrinkles that had submicron-scale dimensions were also produced even at a low ion fluence of 1×10^{13} ions/cm^2. By these chemical and physical modifications, FIB-treated PU substrates showed enhanced biocompatibility leading to better proliferation than non-treated and Ar^+-implanted ones.

FIB and oxygen (O_2) plasma treatments are environment-friendly dry processes which can facilitate the morphological and chemical surface modifications of polymeric materials. To mimic the morphological and chemical properties of the extracellular matrix (ECM) of human body, both treatments were applied to PU substrates. And the effect of both surface modification methods on the adhesion and

proliferation of human dermal fibroblasts was also investigated. On the surfaces of ECM-like PU scaffolds fabricated by both treatments, it was observed that more filopodia protruded from the cell body of fibroblasts. Due to the various types of surface wrinkles, whose wavelength and amplitude were in the submicron range, and increased surface wettability, ECM-like PU scaffolds showed enhanced biocompatibility and cell proliferation during cell culture.

Keywords: polyurethane, ion implantation, focused ion beam, surface modification, surface wrinkles, surface wettability, biocompatibility, biomaterials, tissue-engineering

Student Number: 2001-30386

CONTENTS

LIST OF FIGURES

LIST OF TABLES

I. Introduction

The human body consists of very complex cell-based systems, and cells maintain their lives through interactions with three-dimensional nano- and micro-structures, called extracellular matrices (ECM), which contain proteins, glycosaminoglycans and their composites (i.e., proteoglycans and glycoproteins). Cells, through receptor-ligand

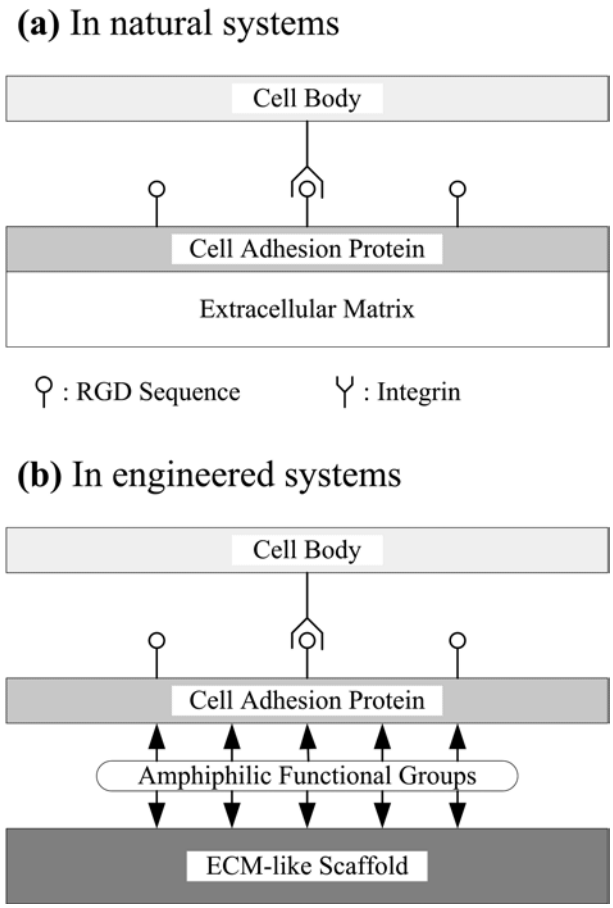

Figure 1.1. Schematics of cell adhesion in: (a) natural system and (b) engineered system.

binding to the ECM, settle in three-dimensional space, maintain their own unique forms and manifest their own unique phenotypes. For example, Figure 1.1 shows schematics of cell adhesion in natural and engineered systems. They communicate with their surrounding cells and help organs function properly through the processes of adhesion, growth and differentiation. Accordingly, tissue engineering refers to all the possible processes and methods of regulating cellular functions using engineering techniques which control the biologically-functioning cells and their surroundings and ultimately restoring such functions as desired by cell transplantation into patients with damaged tissues [1-2].

Biomaterials should have mechanical strengths and functional characteristics similar to those of living tissues and organs. Also, they should provide the property of biocompatibility (which is herein used in a narrow sense, meaning biochemical compatibility) [3]. Since biomaterials are used in direct contact with human tissues and organs, they must offer biochemical resistance to corrosion in the human body and ensure bio-stability and bio-affinity without causing severe side effects or adverse reactions. Therefore, biomaterials need to meet biocompatibility requirements for use in humans.

Biocompatibility has been defined in a number of different ways, but currently the most widely accepted definition of biocompatibility is that of D. F. Williams [4-5]. He defined it as *"the ability of a material to perform with an appropriate host response in a specific application."* More detailedly speaking, biocompatibility is defined as *"the ability of a biomaterial to perform its desired function with respect to a medical therapy, without eliciting any undesirable local or systemic effects in the recipient or beneficiary of that therapy, but generating the most appropriate beneficial cellular or tissue response in that specific situation, and optimizing the clinically relevant performance of that therapy."*

Accordingly, biocompatibility is defined as the ability of a material to perform its desired function in the human body without inhibiting normal cell division in tissues surrounding an implant and inducing any acute or chronic inflammatory reactions, and in a broad sense the term "biocompatibility" covers three dimensions: biological compatibility, chemical compatibility, and mechanical compatibility.

Biocompatibility, on the other hand, consists of hemocompatibility [6] and histocompatibility, though this definition has not received wide acceptance compared to that of Williams. Hemocompatibility, or blood compatibility, of a biomaterial depends on the chemical composition and uniformity of its surface and is determined by interactions in the interface between the material and blood. These interactions include thrombogenesis and complement activation. Histocompatibility, or tissue compatibility, means the ability of a material to induce cell proliferation effectively without causing necrosis of cells and their surrounding tissues.

Consequently, biomaterials must have infinitesimal or no toxicity, carcinogenicity and antigenicity to humans. Furthermore, bioactivity that allows biomaterials to achieve their desired purposes in response to tissues is also required. In addition, the biomaterials should have biologically similar strength and elastic modulus to peripheral tissues -so that they can replace the original tissues for quite a long time- and should not hinder or impede repair of peripheral tissues. In an economical sense, they should be easy to process and reasonable enough in price. As the case may be, biomaterials should be biodegradable. This means that they should remain attached onto surrounding tissues during the early post-transplant stages but be replaced by newly grown tissue by losing their shapes and structures after a certain period of time.

The structural biomimicry of the natural ECM is essential for the biocompatibility of materials to be properly achieved as described above. Human tissue does not consist

of cells alone, and macromolecules secreted by cells form a complicated interlocking mesh structure in extracellular space. This mesh structure, called extracellular matrix (ECM), is made up of many different polysaccharides and proteins. The ECM which provides a basic environment where cells can live and grow determines the shape of tissue and helps cells work properly. In a structural respect, the ECM consists of nano-sized wrinkles, pores, fibers and pits; therefore, the complicated structure should be created to the fullest possible extent through biomimicry. Figure 1.2 shows examples of the ECM in an embryonic chick limb bud (Figure 1.2(a)) and the cornea of a rat (Figure 1.2(b)) [7].

Biomaterials include metals, ceramics, polymers and their composites. Among them, polymer materials represent the largest proportion of biomaterials. Metals or ceramics are easy to use for the hard tissues of human body such as bones or teeth. However, for the replacement of soft tissues such as skin, organs and blood vessels, polymers should be used because they are most similar to such tissues in mechanical properties. That's why the demand for biomedical polymers has steadily increased every year. Biomedical polymers that are commonly used include natural polymers such as natural rubber, silk and cellulose and synthetic polymers such as polyvinylchloride (PVC), polyethylene (PE), polypropylene (PP), polycarbonate (PC), silicone rubber, polytetrafluoroethylene (PTFE) and polyurethane (PU) [8]. They are mainly used for artificial kidney filters, heart valves, artificial vessels, urethras, blood transfusion bags and nerve conduits, and synthetic polymers are used in artificial organs to replace most parts of the body, except for the brain.

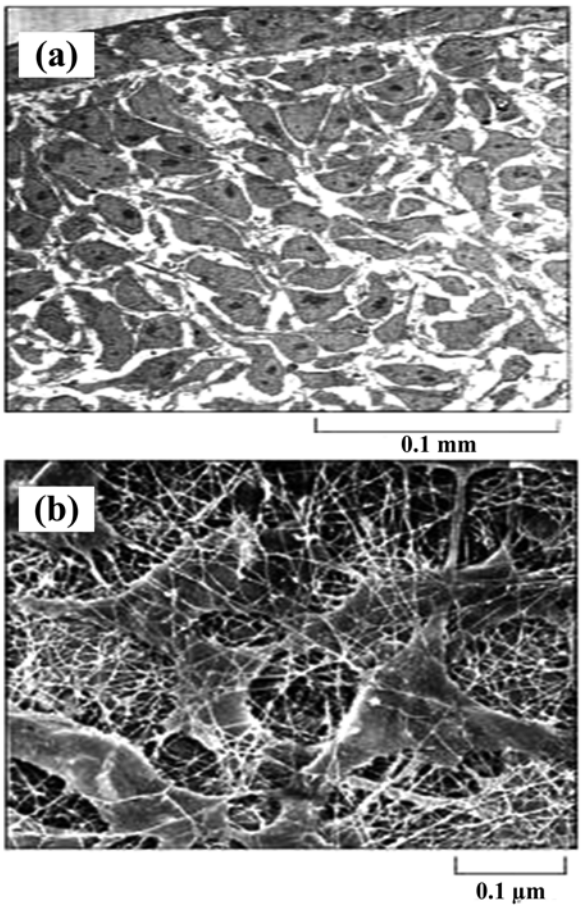

Figure 1.2. Images of ECM obtained from: (a) an embryonic chick limb bud and (b) the cornea of a rat [7].

In this thesis, to improve the biocompatibility of polymeric materials, ion implantation was applied to PU as a simple and effective method for the morphological and chemical changes of material surfaces. Up to the present, most of the fundamental studies of ion implantation have mainly focused on the effect of instrument parameters on the surface property changes of PU substrates [9-14]. However, the influence of the intrinsic properties of PU, such as the distribution of hard and soft segments, on the

surface property changes has received relatively little attention. Thus, different thermal treatments were applied to PU substrates and inactive argon ions (Ar^+) were implanted into them. After ion implantation, the correlation between the intrinsic properties of PU substrates and the surface property changes of ion-implanted PU surfaces was investigated.

Focused ion beam (FIB), one of beam-line type ion implantation methods, was also utilized to modify the surfaces of PU substrates. In most cases, the contribution of FIB to biomedical applications has been limited to the site-specific analysis of the interfaces between cells and substrates by milling process in combination with scanning electron microscopy (SEM) [15-18]. However, at low ion doses, surface wrinkles can be formed on FIB-treated polymer substrates. It is well-known that nano- or micro-scale pattern and structure can affect cell adhesion and cell growth. Therefore, both wrinkle formation and chemical changes induced by FIB treatment can be expected to enhance the biocompatibility of PU substrates. To confirm the influence of the FIB-treated PU surface on the adhesion and growth of cells, NIH3T3 fibroblasts, which derived from mouse embryo, were cultured on the FIB-treated PU substrates. Experimental results of the FIB-treated PU samples were compared with those of non-treated and Ar^+-implanted PU ones.

However, it is revealed that nanostructures make material surfaces more hydrophobic due to the existence of trapped air [19-22]. In the case of the FIB-treated PU substrates, due to the surface wrinkles whose size were in the submicron range, the hydrophobicity of them was increased in spite of increasing hydrophilic functional groups. Because, on the hydrophobic surface, the amount of adsorbed cell adhesion-related proteins such as fibronectin can be decreased, a decrease in the hydrophilicity of the FIB-treated PU substrates should be resolved. To overcome this problem and develop ECM-like scaffolds, oxygen (O_2) plasma treatment was applied to the FIB-

treated PU substrates. In comparison with the non-treated and FIB-treated substrates, PU scaffolds fabricated by both FIB and O_2 plasma treatments showed enhance surface wettability and better cell adhesion and proliferation of human dermal fibroblasts.

II. Literature Review

2.1. Biomedical applications of PU

2.1.1. Requirements of biomedical materials

The human desire for health and longevity has been the driving force behind the efforts to live free from disease and overcome physical disabilities. With the natural growth of the world population and the improvement of dietary life and housing environment, people's average life expectancy has been extended and the increasing aged population has led to a continued increase in the demand for medical care. As a result, the medical industry closely related to public health has been emerging as a future core industry.

Biomaterials refer to any materials that can be used as means for the diagnosis, treatment and prevention of diseases and basic materials that can be also used to replace damaged or dysfunctional human tissues or organs. The primary requirement for biomaterials is biocompatibility that prevents living tissue from necrotizing or clotting blood when in contact with them. Biocompatibility can be explained in terms of hemocompatibility and histocompatibility which are considered important according to application purposes.

2.1.2. Blood-material interactions

In general, biomaterials include polymers, metals, ceramics and their composites. They should ensure excellent biocompatibility to serve their purposes of use and are required to provide mechanical and physical properties including moldability and processability according to their purposes and applications. Polyurethanes currently available for medical use are applied in a wide variety of fields because they have excellent mechanical properties and relatively good biocompatibility. In particular, they are known to have excellent blood compatibility compared to most polymer materials and thus are widely applied in blood-contacting medical devices or implants; it is therefore important to consider blood-material interactions [23-24].

Blood mainly consists of cellular elements: plasma, erythrocyte, leucocytes and platelets. The first phenomenon that occurs when a material comes into contact with blood is the adsorption or desorption of plasma proteins such as fibrinogens, albumins and gamma-globulins. When the adsorbed proteins are denatured, they induce interactions with platelets and white blood cells and activate blood clotting mechanisms. As a consequence, blood clots are formed as fibrin cross-linking takes place on the surfaces of materials. Platelets are anuclear cells that are 2 - 4 μm in diameter, and normal blood contains 150,000 - 300,000 platelets/μl. They play an important role in the formation of blood clots. Adherent platelets release a variety of substances including granules via structural transformation which induces the initial formation of blood clots by attracting more platelets. The platelet adhesion on the surface of the implanted material occurs usually in tens of seconds when the thickness of absorbed protein layers reaches 100 - 200 Å. This platelet adhesion is influenced by

the properties of protein layers. Fibrinogens and gamma-globulins are known to induce the platelet adhesion, whereas albumins are reported to inhibit the platelet adhesion [25].

Polyurethane (PU) as a biomaterial has been most widely studied in terms of blood-material interactions. It is well known that hydrophilic PU is less likely to interact with blood than hydrophobic PU. An ESCA-based analysis of surface composition shows that soft segments present at the surface and their micro-phase separation have an important influence on blood-material interactions and that higher phase separation is associated with better blood compatibility [26]. Since differences in processing techniques cause the material to have different surface characteristics, they can also influence the blood compatibility of the material. As a result, large quantities of commercially produced PUs have been used for the fabrication of artificial blood vessels, catheters, pacemaker leads and so on. A brief summary of commercially produced PUs was presented well in Table 2 of the chapter 3 of ref. [8]. It is noted that not all of the polyurethanes presented in the table are currently available due to low biocompatibility, potential product liability lawsuits, etc. And Figure 2.1 shows the molecular structures of well-known three commercial biomedical polyurethanes, namely Pellethane®, Biomer® and Tecoflex®.

Pellethane®

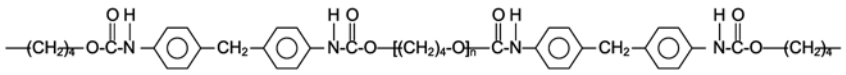

Extrudable grade Biomer®

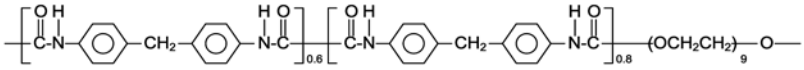

Solution grade Biomer®

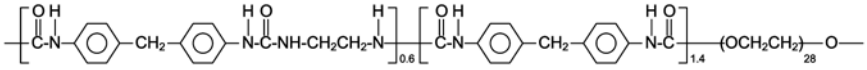

Tecoflex®

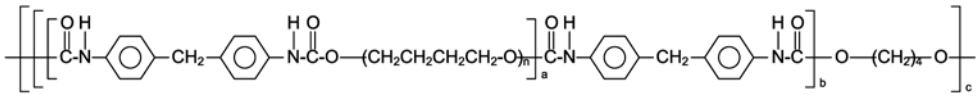

Figure 2.1. Molecular structures of well-known commercial biomedical polyurethanes.

2.1.3. Research trends in PU for biomedical use

One of the methods that are currently used to improve the biocompatibility and physical properties of medical PU is chemical modification by surface and bulk reactions. Chemical modification is a technique of physically and chemically reforming the surface characteristics of the existing PU and can be divided into two main types, physicochemical surface modification and biological surface modification, based on changes in surface composition. In general, physicochemical surface modification is conducted by increasing hydrophilicity or chemically introducing hydrophilic groups through plasma, UV radiation, gamma radiation, electron beams or ion beam treatments, or by simple coating or the fixation of bioactive substances. The procedures of biological surface modification include cell culture, protein absorption, and the fixation of bioactive substances. Heparin and cell-adhesive RGD peptide are

mainly used as bioactive substances. Recently, there have been attempts to study how to design and introduce bio-mimicking structures from the structural characteristics of bioactive substances [27-30]. For example, Figure 10 in ref. [28] shows SEM images of adhered platelets on the surfaces of heparinized segmented polyurethaneurea demonstrating the improvement of blood compatibility.

2.2. Methods for the morphological mimicry of ECM

One of the key issues in current tissue engineering is the physical mimicry of ECM so that the adhesion, spreading, migration, orientation and proliferation of cells are enhanced during *in vitro* or *in vivo* study. To mimic morphological characterization of the ECM, various methods such as photolithography, electrospinning, ion implantation, X-ray lithography [31-32], electron-beam lithography [33-34], electropolishing, sandblasting [35], etc. have been applied to polymeric materials, ceramics and metals. They have been fully reviewed elsewhere in detail by many researchers [36-41]. Here, three representative methods -photolithography, electrospinning and ion implantation- which have been studied well are dealt in priority.

2.2.1. Photolithography

Photolithography is a photo-printing technique for patterning integrated circuits, thin-film circuits and printed circuits mainly on semiconductor surfaces. A photo-resist solution is evenly coated onto the clean surface of a silicon substrate by way of spin-coating, spraying or immersion. After drying, UV lights, X-rays or electron beams are selectively irradiated through a mask. The depolymerized regions of the resist can be removed by an appropriate solvent. The polymerized regions act as a barrier to etching

or as a mask for deposition. Figure 2.2 shows a schematic diagram of the photolithography and pattern transfer processes. The application of this technique to the surface of polymeric material leads to the formation of patterns in the range of a few microns to tens of nanometers. There have been many studies of cell adhesion and growth resulting from such surface properties [42-53]. Photolithography involves the additional processes of mask making and photo-resist removal for sample fabrication and requires a solvent for photo-resist removal. Moreover, because the technique is mostly used to form simple patterns such as grooves and ridges, it has limitations in mimicking extracellular matrices (ECM).

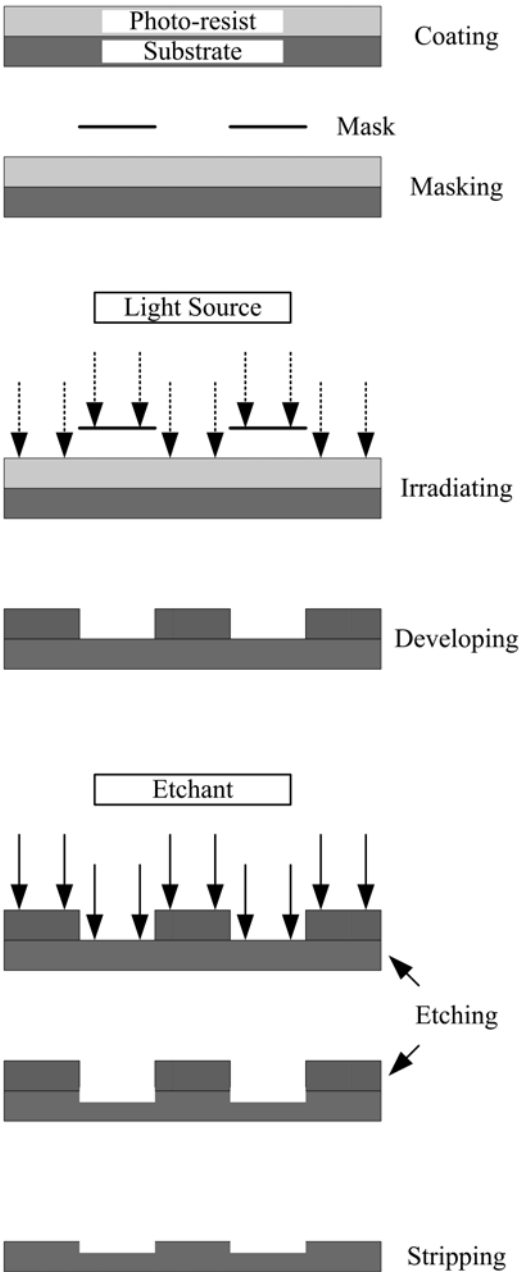

Figure 2.2. A schematic diagram of photolithography and pattern transfer processes.

2.2.2. Electrospinning

Electrospinning has been recognized as a highly practical technique that enables the efficient and inexpensive fabrication of one-dimensional nanostructures, that is to say, nanofibers [54]. Since electrospinning can be successfully used to fabricate composites such as polymer/metal oxide nanofibers and polymer nanofibers in which enzymes, drugs or nanoparticles are embedded, many studies of the technique have been conducted in application fields including chemical and biological sensors, tissue engineering scaffolds, drug delivery systems and energy storage. Electrospinning is the most powerful and straightforward method that enables the mass production of nanofibrous non-woven fabrics. When the electrical force on the surface of a suspended drop of polymer solution which is at the tip of a glass pipette or a syringe needle overcomes the surface tension of the polymer solution, a charged jet is ejected toward the collector plate. Subsequent splitting and/or stretching of the jet incorporated with solvent evaporation make finer mini-jets of which diameter range is from a few micrometers down to tens of nanometers. These mini-jets or nanofibers deposit in the form of nonwoven fabric on the surface of the collector plate. Figure 2.3 shows a schematic diagram of the electrospinning process.

In recent more than ten years, the electrospinning technique has been used to make nanofiber-based scaffolds in the fields of tissue engineering and is now attracting attention as a method of artificially mimicking the structural characteristics of the extracellular matrix where cells grow in human tissues [55-62]. However, such nanofiber-based scaffolds take non-woven fabric forms created by simple tanglement of electrospun nanofibers. Therefore, they can shrink in contact with water or blood if an appropriate post-treatment process with cross-linking agents such as glutaraldehyde and hexamethylenediamine is not applied to them. Moreover, it is difficult to orient

cells in a consistent direction because nanofibers are randomly oriented.

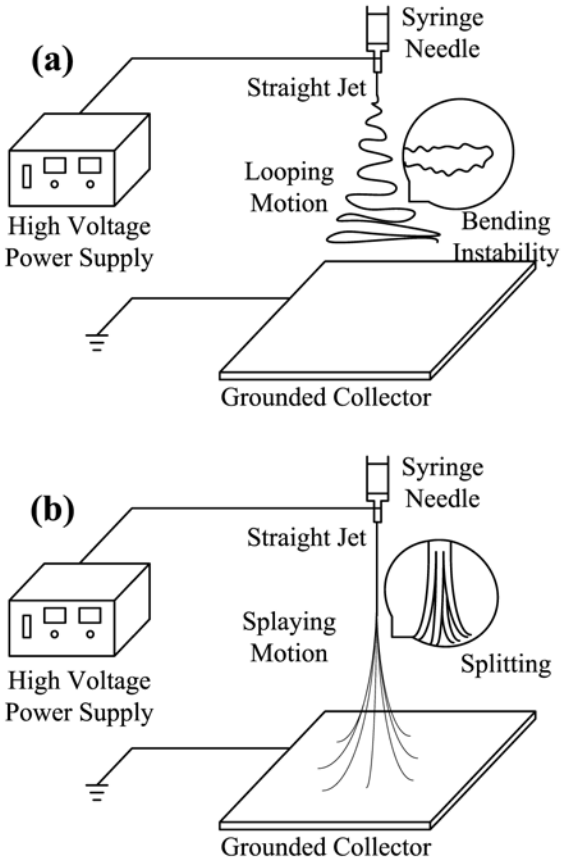

Figure 2.3. A schematic diagram of electrospinning process: (a) Looping-dominated type and (b) Splaying-dominated type.

2.2.3. Ion implantation

Ion implantation is a surface modification technology for adjusting the physical, chemical and mechanical properties of material surface by ionizing specific elements

to form an ion beam and then accelerate the beam at high energy and by injecting ions into materials to change the chemical composition and structure of the surface [63-64]. Although the ion implantation technology has been mainly employed to add impurities to semiconductors, it is being studied on how to use different types of elements to control the surface structure and composition of polymer materials or improve their properties.

The mechanism for the formation of surface wrinkles on a polymeric substrate using ion implantation is closely related to the crosslinking and the carbonization processes of polymer chains and to the diffusion of heat generated during ion implantation. The surface layer of a polymer substrate thermally expands during ion implantation. At the same time, the crosslinking and the carbonization of polymer chains occurs inside the surface layer to form a hard skin on the surface of the polymer substrate. Afterwards, the release of heat from the polymer substrate induces compressed stress and surface deformation, resulting in surface wrinkles. Figure 2.4 shows a schematic diagram of the surface wrinkle formation during ion implantation.

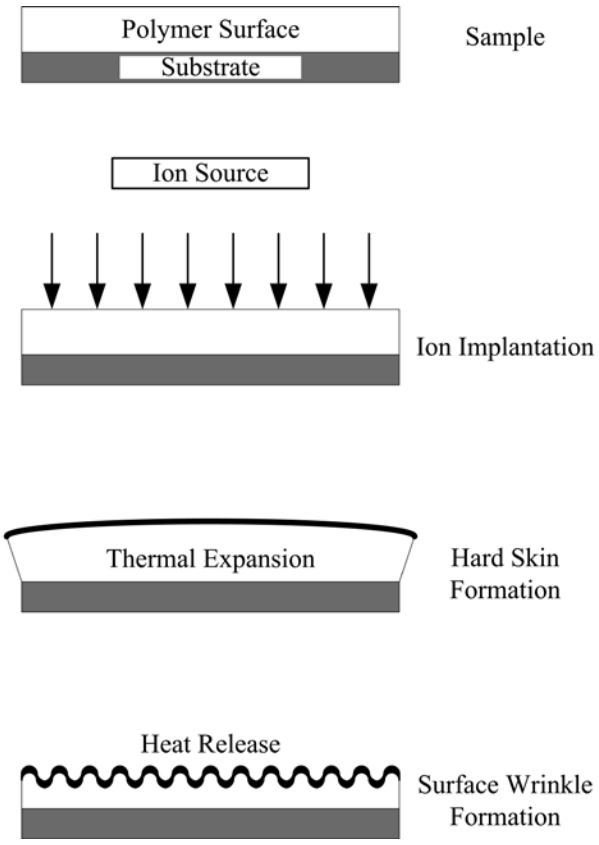

Figure 2.4. A schematic diagram of surface wrinkle formation by ion implantation.

2.2.3.1. Conventional ion implantation

Polymer materials are used in many different fields of industry and everyday life, because they are easy to mold and process and available at low production cost. On the other hand, however, polymers have a limited range of applications, because they are poor in mechanical properties such as hardness and abrasiveness and rather exhibit the typical properties of insulators with low electric conductivity, compared to metals. Since the 1980s, ion implantation has been actively studied as a way to transform

electric and mechanical properties of polymers without changing their bulk properties. The ion implantation of biopolymers has also been studied from the early 1990s, and currently it is applied in a variety of biomedical fields [65-66].

In early studies, the purposes of ion implantation of polymer materials were mostly to improve the hydrophilicity of their surfaces for biomedical applications. Because the morphological transformation of their surfaces was not taken into account or was thought to be relatively less important, the enhancement of the hydrophilicity of their surfaces could be evaluated by chemical surface modification alone which was associated with the reactions of radical ions and hydrophilic functional groups formed by ion implantation [67-70]. However, the morphological changes (wrinkle formation) of the material surface during ion implantation can play an important role in the growth of cells because, in many cases, cells grow along the pattern or direction of surface micro- or nanostructures. This can be also known as contact guidance of cells [71-75]. Thus, in the case of one-directional surface wrinkles or grooves, they can be applicable to artificial muscles and artificial blood vessels on which cells are oriented in one direction. Furthermore, non-directional irregularly-patterned wrinkles can be also used to mimic the ECM. Therefore, in-depth studies are needed on the morphological changes of the ion-implanted material surface.

2.2.3.2. Focused Ion Beam (FIB)

Focused ion beam (FIB) lithography or milling is a technique for drawing a desired pattern on a substrate by irradiating a finely focused ion beam without a mask [76]. Also, FIB is used especially in the semiconductor industry. FIB has weak scattering in

the resist membrane compared to electron beams and thus can be used to draw precise patterns of less than 100 nanometers. The FIB technique has been widely used to prepare specimens for Transmission electron microscopy (TEM) [77] especially in the semiconductor field, but recently it is used for the precise fabrication of three-dimensional nanostructures and technical development for its application is being continued. In recent years, the use of the FIB technique has rapidly grown in a wide variety of ultrahigh-precision nanofabrication applications [78], including electronics, communications, medicine and biology as well as semiconductor products requiring high-precision processes. The application of the FIB technique to polymers can etch the surface of a material at high ion doses [79-81] but form wrinkles on the surface at low ion doses [82-85]. Another advantage of the technique is that it enables a variety of different patterns to be quickly created. However, the FIB requires much time in large-area treatment, because it is designed for use with small-area samples. Currently, in the biological field, the FIB technique is used for site-specific analysis of the interfaces between cells and substrates [15-18].

2.2.4. Morphologies of PU substrates fabricated by photolithography, electrospinning and FIB treatment

Finally, Figure 2.5 shows examples of PU substrates fabricated by above-mentioned three methods and a corneal epithelial basement membrane of Macaque monkey [36]. For the fabrication of PU substrates, ether-based Pellethane® 2103-80AE was used in this thesis. Figure 2.6 shows a schematic diagram of the synthesis of ether-based Pellethane®.

An 11 wt% PU solution was prepared by dissolving Pellethane® 2103-80AE in a mixture of DMF and THF (70:30 w/w). Electrospinning of the prepared PU solution

was conducted at 25 °C and 30 % RH. With this PU solution, pristine PU substrates for photolithography and FIB treatment were also fabricated using solvent casting method under ambient conditions (25 °C and 50 % RH) and cured in a vacuum oven at 90 °C for 72 hours. Details of each process were specified in the caption of Figure 2.5.

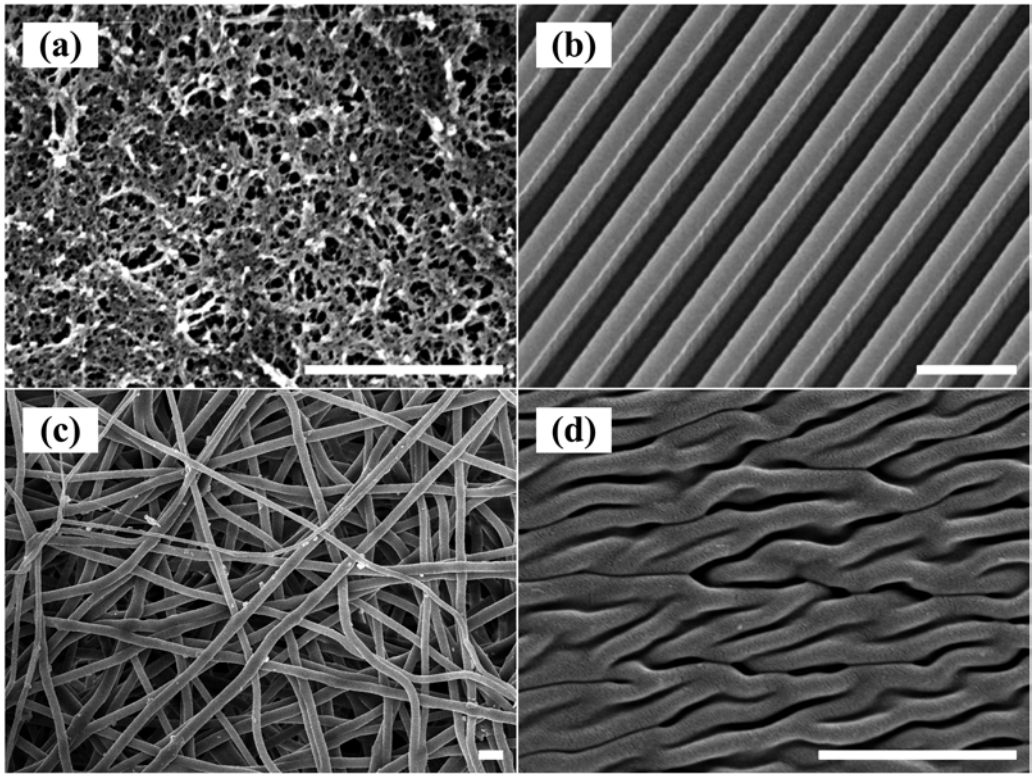

Figure 2.5. SEM images of various scaffolds (bar size = 1 μm): (a) The ECM of Macaque monkey [22], (b) PU substrate fabricated by photolithography (UV light source, anisotropic etching), (c) PU substrate fabricated by electrospinning (applied voltage = 11 kV, tip-to-target distance = 15 cm, flow rate = 1 ml/h, needle gauge = 21 G) and (d) PU substrate fabricated by FIB treatment (ion dose = 1×10^{14} ions/cm^2, acceleration voltage = 30 kV, ion current = 9.3 nA, dwell time = 10 μs).

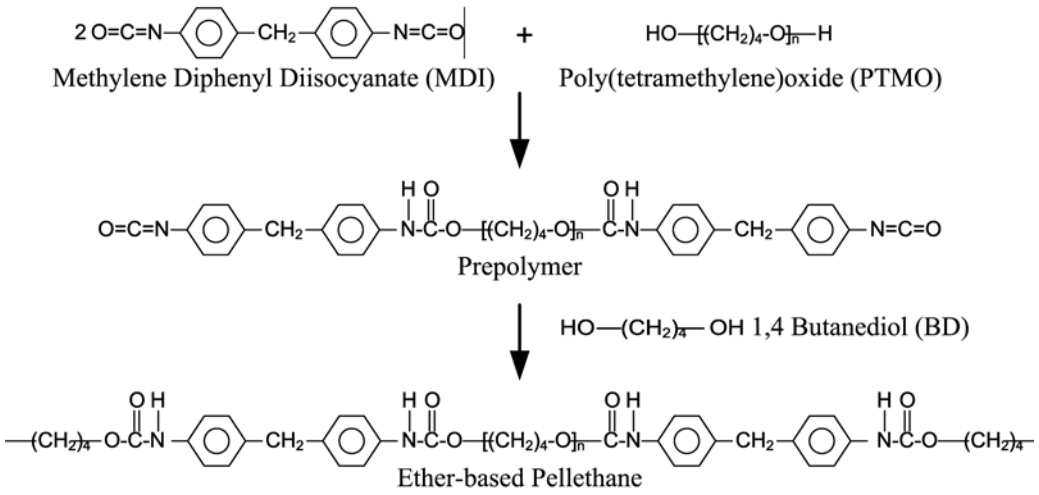

Figure 2.6. Synthesis of ether-based Pellethane®.

III. Surface Modification of Thermally Treated Polyurethane Films by Ion Implantation

3.1. Introduction

Ion implantation is an engineering process which has gained the attention of biomaterial researchers during the last two decades because it can easily and effectively transform the surface properties of biomaterials. It is well known that the surface modification induced by ion implantation can improve the wettability, adhesion and hardness of polymer-based biomaterials without changing their bulk properties [86]. Furthermore, the formation of surface wrinkles during ion implantation makes it possible to emulate human tissue such as extracellular matrix. Therefore, these surface property changes play an important role in biomedical applications of polymers such as heart valves, small diameter vascular grafts, etc. [65-66].

Polyurethane (PU) is a typical block copolymer which consists of soft polyol segments and hard urethane segments. Many combinations of these two segments are possible so that various urethane polymers have been synthesized and used in hundreds of applications across all the fields. Especially, in the case of biomedical application, PU has been relatively well-studied and is known to have better blood compatibility, an essential factor of biomaterials, than any other polymers [8, 87].

Most of the fundamental studies of ion implantation have mainly focused on the effect of instrument parameters such as ion source, amount of ion dose and acceleration voltage on the surface property changes of PU substrates [9-14]. However, the influence of the intrinsic properties of PU, such as the distribution of hard and soft

segments and the degree of phase separation, on the surface property changes induced by ion implantation has received relatively little attention although these properties might play an important role in the physico-chemical changes of the ion-implanted PU surface.

In this study, PU films were prepared by solvent casting method and different heat treatments were applied to them in order to change their intrinsic properties. Before argon ions (Ar^+) were implanted into these films, the thermal properties and degree of phase separation of PU films were investigated. After ion implantation, surface chemical composition and surface wettability were analyzed as a function of ion dose. Also, the surface morphologies of the ion-implanted PU films were observed. From the results, the correlation between the intrinsic properties of PU films and the surface property changes of ion-implanted PU films was drawn.

3.2. Experimental

3.2.1. Materials

Pellethane® 2103-80AE, commercial ether-based thermoplastic PU, was obtained from Dow Chemical Co. (USA) and used after thorough washing with distilled water. Tetrahydrofuran (THF) and dimethylformamide (DMF) were purchased from Samchun Chemical Co. Ltd. (Republic of Korea) and used without further purification.

3.2.2. Preparation and thermal treatment of PU films

An 11 wt% PU solution was prepared by dissolving 5.0 g of Pellethane® 2103-80AE in a mixture of DMF and THF (70:30 w/w) at room temperature for 6 hours with

stirring. After dissolving, the PU solution was kept in a thermostat oven at 25 °C overnight to be stabilized. PU films were fabricated under ambient conditions by solvent casting method and cured in a vacuum oven at 90 °C for 48 hours to eliminate residual solvent in the PU films. The thickness of the produced PU films was about 120 μm.

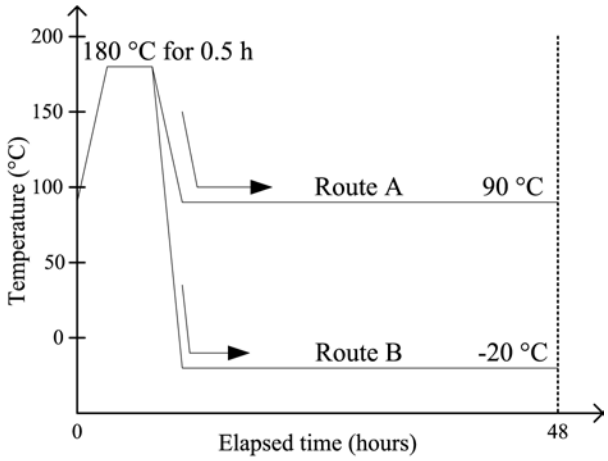

Figure 3.1. A schematic diagram of thermal treatment processes.

As shown in Fig. 3.1, two different thermal treatments were applied to the prepared PU films. After Samples were heated from 90 °C to 180 °C, the temperature was held at 180 °C for 30 minutes. And then, the heat-treated samples were cooled to 90 °C (Route A) or -20 °C (Route B). The heating rate was 10 °C/min for all samples. The cooling rates of Route A and Route B were 10 and 30 °C/min, respectively. Each of the films obtained from Route A and Route B was designated by C90 and C-20. Non-treated PU samples were just kept in a thermostat oven at 90 °C for additional 48 hours after solvent elimination process.

3.2.3. Ion implantation of PU films

Ar^+-implanted PU films were fabricated using a custom-made ion implanter installed at Korea Atomic Energy Research Institute (KAERI, Republic of Korea). Samples were moved into the vacuum chamber under a pressure of 1×10^{-5} Pa. Ion implantation was carried out at an energy of 30 keV with ion doses ranging from 1×10^{13} to 1×10^{16} ions/cm^2 at room temperature. To eliminate thermal effect, the beam current was kept constant at 2 μA/cm^2.

3.2.4. Characterization of ion-implanted PU films

For the thermal analysis of PU films, differential scanning calorimeter (DSC) results were obtained with DSC 200 F3 Maia® (Netzsch, Germany). Aluminum pans with a diameter of approximately 6.3 mm were used. Samples were heated from -80 °C to 200 ℃ at a rate of 5 °C/min.

To investigate the degree of phase separation of PU films, attenuated total reflectance Fourier Transform infrared spectroscopy (ATR FT-IR) was conducted with Nicolet 6700 FT-IR spectrometer (Thermo Scientific, USA) before ion implantation. The absorbance spectra of PU films in the range of 1800-1650 cm^{-1} were measured with 32 scans per sample at a spectral resolution of 4 cm^{-1}.

The surface chemical composition of PU films were confirmed by Sigma Probe X-ray photoelectron spectroscopy (XPS) system (Thermo VG scientific, UK). To minimize the charging effects of the nonconductive PU specimens, neutralization was carried out. The monochromatic Al-Kα (100 W) source was used. The survey scan was performed within the binding energy range of 0-1000 eV. The pass energy of 50 eV was applied to the samples during the survey scan. To calculate the elemental

composition of the PU samples, the XPS spectra were processed using the Avantage data system (Thermo VG scientific, UK). The binding energies of all the spectra were referenced to the 285 eV corresponding to the peaks of C-C and/or C-H groups (C1s).

To verify the surface modification by ion implantation, the water contact angles of PU films were calculated using PHOENIX 300 contact angle analyzer (SEO, Republic of Korea). The static sessile drop method was applied. A drop of distilled water with a volume of about 5 μl was used for each measurement.

For the observation of surface morphology, scanning electron microscope (SEM) images of PU films were obtained from JSM-6700F microscope (JEOL, Japan). Because PU films are highly nonconductive, a layer of gold (4 nm thickness) was coated onto their surface by a sputter coater to avoid surface charging.

To obtain quantitative 3-dimensional topography for large area (150 μm × 150 μm), Wyko NT2000 optical profiling system (Veeco, USA) was utilized. Tungsten halogen lamp with a wavelength of 630 nm was used. The root mean square roughness of PU films were determined from obtained 3-dimensional images captured at a magnification of 29×. For small area surface metrology, atomic force microscopy (AFM) images using XE-100 (Park Systems Corp., Republic of Korea) was carried out. Dynamic non-contact mode with a silicon tip was applied and the scan rate of 1 Hz was used for measurements.

The properties of crystalline phase of PU films were measured using D8 DISCOVER (Bruker, Germany) high resolution X-ray diffractometer (HRXRD) system. XRD patterns were recorded in the 2θ range from 10° to 35° at a scanning rate of 2° per minute and CuKα irradiation was used.

To estimate the thickness of surface hard skin which was formed during ion implantation, time-of-flight secondary ion mass spectrometry (TOF-SIMS) was conducted by TOF-SIMS 5 (ION-TOF, Germany). Cesium ions were used to ionize

molecules on the surfaces of PU films. Depth profiling up to 1000 nm from the surface was carried out.

3.3. Results

3.3.1. Thermal analysis of PU films

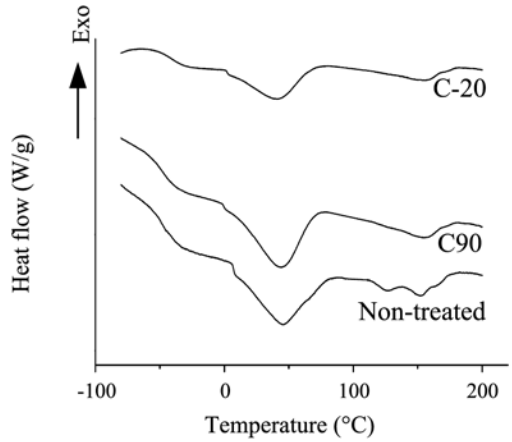

Figure 3.2. DSC thermograms of non-treated and thermally treated PU films.

Table 3.1. DSC results of PU films.

Sample	T_g (°C)			T_1 (°C)	T_2 (°C)	T_m (°C)
	onset	mid	inflection			
Non-treated	-53.3	-45.8	-49.2	45.8	119.6	152.0
C90	-55.0	-47.2	-45.0	44.1	-	154.8
C-20	-69.4	-61.3	-65.9	40.7	-	155.7

Figure 3.2 shows the results of the thermo-analysis of PU films before ion implantation. Typical glass transition temperature of soft segments (T_g), short-range

order disruption of hard segment domains (T_1), dissociation of domains containing long-range order (T_2) and melting temperature of hard segments (T_m) were observed [8, 88-89]. The DSC results of the PU films are summarized in Table 3.1. Both non-treated and C90 samples showed similar thermal behavior in the whole temperature range except the existence of the T_2 of the non-treated one. However, the T_g of a C-20 sample was quite lower than those of the non-treated and C90 samples. On the other hand, the T_m of the C-20 sample was slightly higher than those of the non-treated and C90 samples.

3.3.2. Phase separation of PU films

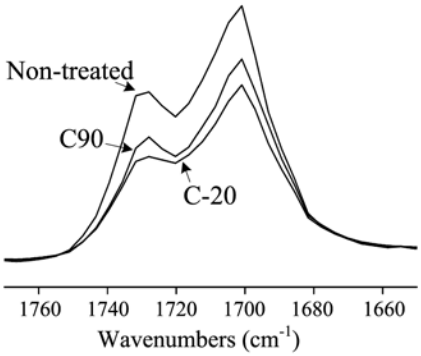

Figure 3.3. ATR FT-IR spectra of PU films before ion implantation.

Figure 3.3 shows the infrared absorption spectra of PU films before ion implantation. The peaks at 1700 and 1730 cm^{-1} are assigned to the urethane carbonyl groups hydrogen bonded to N-H group and the free urethane carbonyl group of ether-based PU, respectively [90]. If the number of hydrogen bonds between urethane groups

in a PU film increases, the degree of phase separation and the sizes of both crystalline hard segments and hard segment domains will also increase. Therefore, by carrying out the band deconvolution of the IR spectra and calculating the area under each peak, the percentage of hard segments getting involved in the formation of hard segment domains in the PU film can be obtained. In this study, their percentages of non-treated, C90 and C-20 PU films were 58.7 %, 59.4 % and 61.2 %, respectively.

3.3.3. Surface chemical properties of PU films

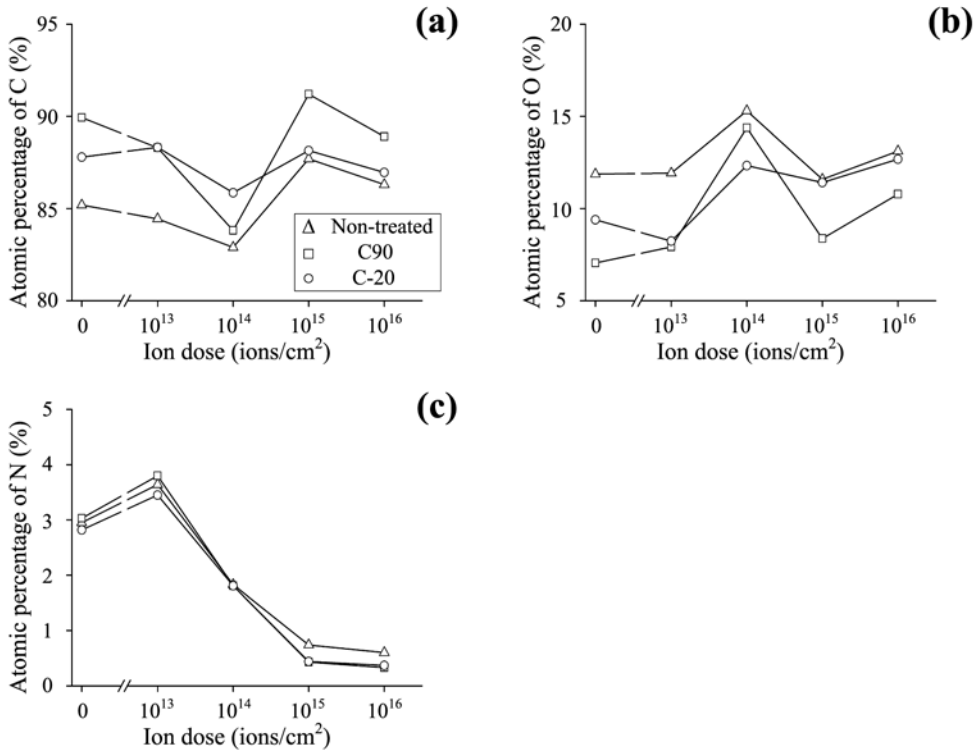

Figure 3.4. Surface elemental atomic percentages of PU films calculated from the XPS spectra of: (a) C1s, (b) O1s and (c) N1s.

Figure 3.4 presents the elemental composition of PU films as a function of ion dose. All PU films showed their minimum atomic percentage of carbon and maximum atomic percentage of nitrogen at ion doses of 1×10^{14} and 1×10^{13} ions/cm^2, respectively. However, non-treated and C90 PU samples had their maximum atomic percentage of oxygen at an ion dose of 1×10^{14} ions/cm^2. On the other hand, in the case of a C-20 sample, it appeared at an ion dose of 1×10^{16} ions/cm^2 (Figure 3.4(b)). Meanwhile, Figures 3.5, 3.6 and 3.7 show carbon, oxygen and nitrogen-containing functional groups on the surfaces of the PU films determined from XPS spectra, respectively. All PU samples did not show any consistent trend indicating the dependence of the amount of each functional group on ion dose.

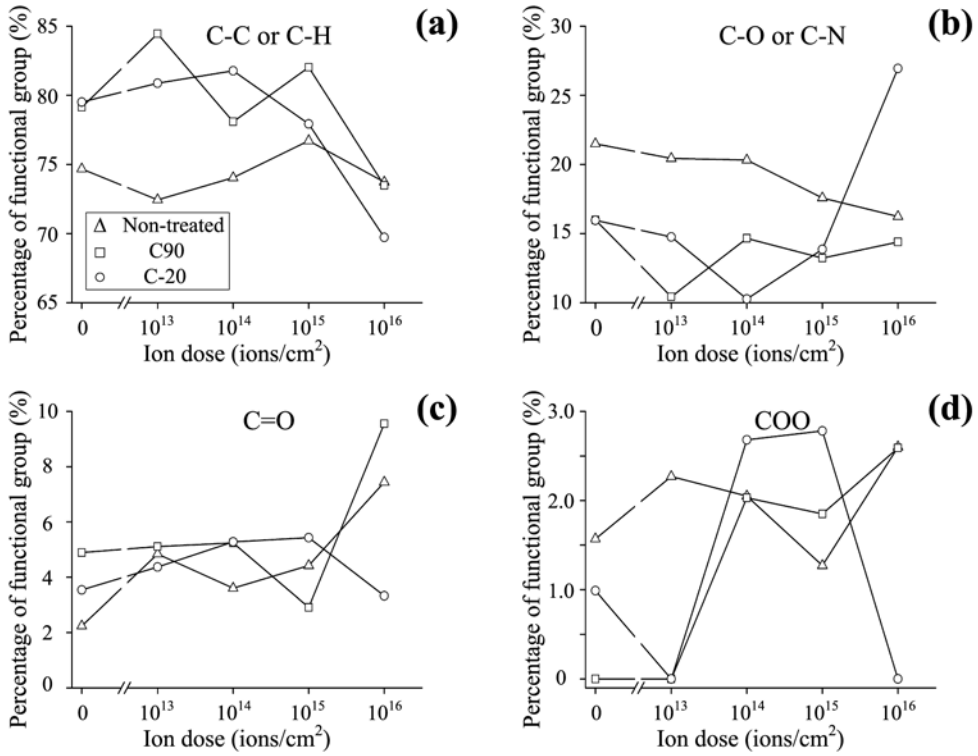

Figure 3.5. Carbon-containing functional groups of PU films.

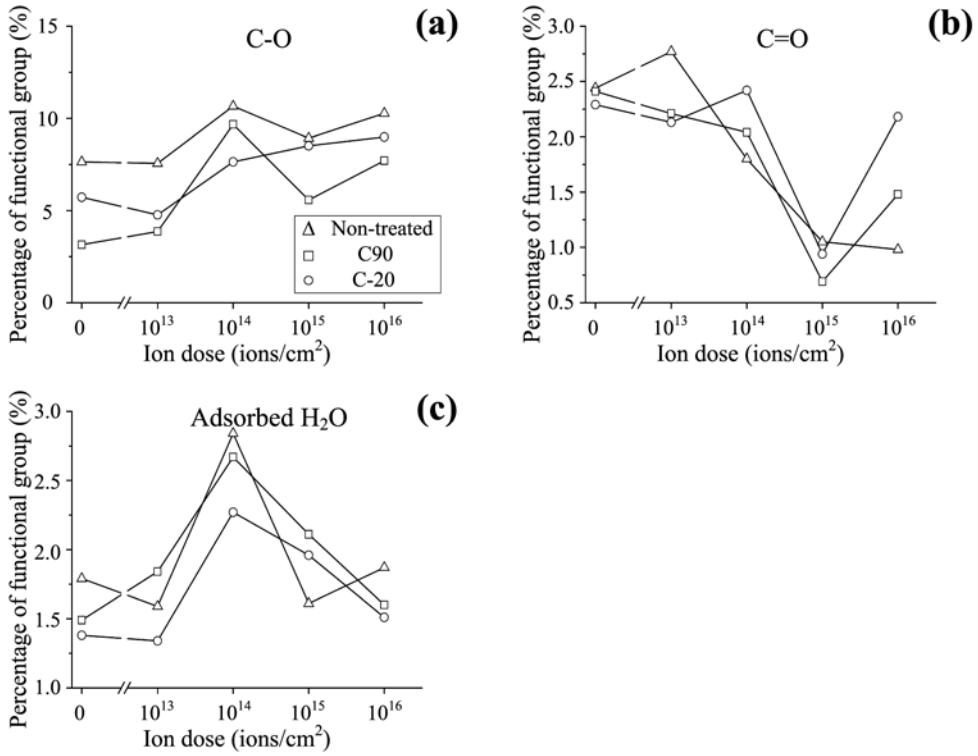

Figure 3.6. Oxygen-containing functional groups of PU films.

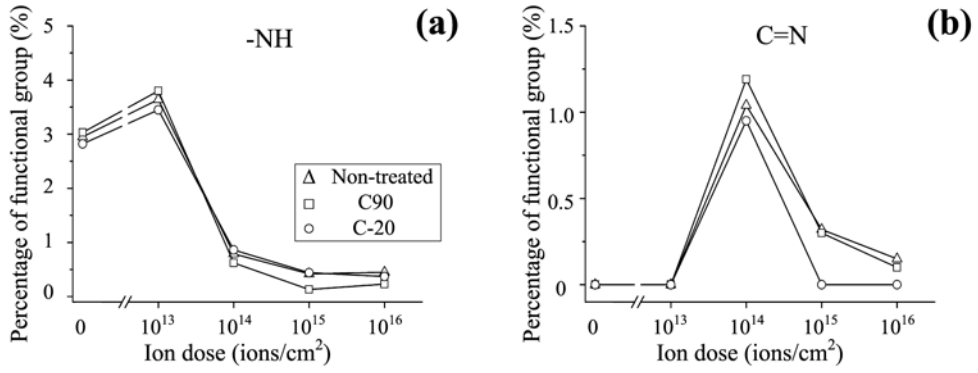

Figure 3.7. Nitrogen-containing functional groups of PU films.

3.3.4. Surface wettability of PU films

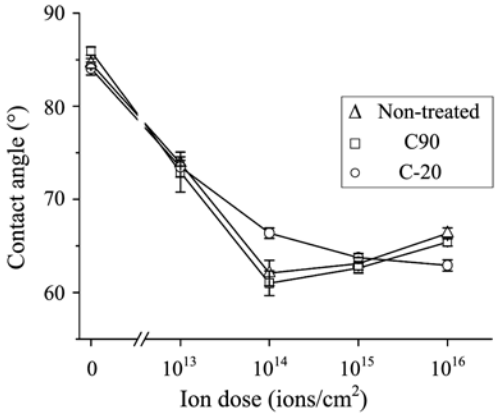

Figure 3.8. Water contact angles of PU films as a function of ion dose.

It is well known that surface wettability, which is an essential prerequisite for biomaterials [65, 69, 91], closely related to the surface chemical state of PU films. The more hydrophilic the surface of a PU film becomes, the better the surface wettability is. Figure 3.8 shows the contact angle changes of PU films as a function of ion dose. Like DSC results, non-treated and C90 films showed a quite similar tendency. The contact angles of these PU films decreased with increasing ion dose up to 1×10^{14} ions/cm^2. And then, the water contact angles slightly increased at higher ion doses. On the other hand, the contact angle of a C-20 PU film decreased with increasing ion dose through the whole range in this study.

3.3.5. Surface morphologies of PU films

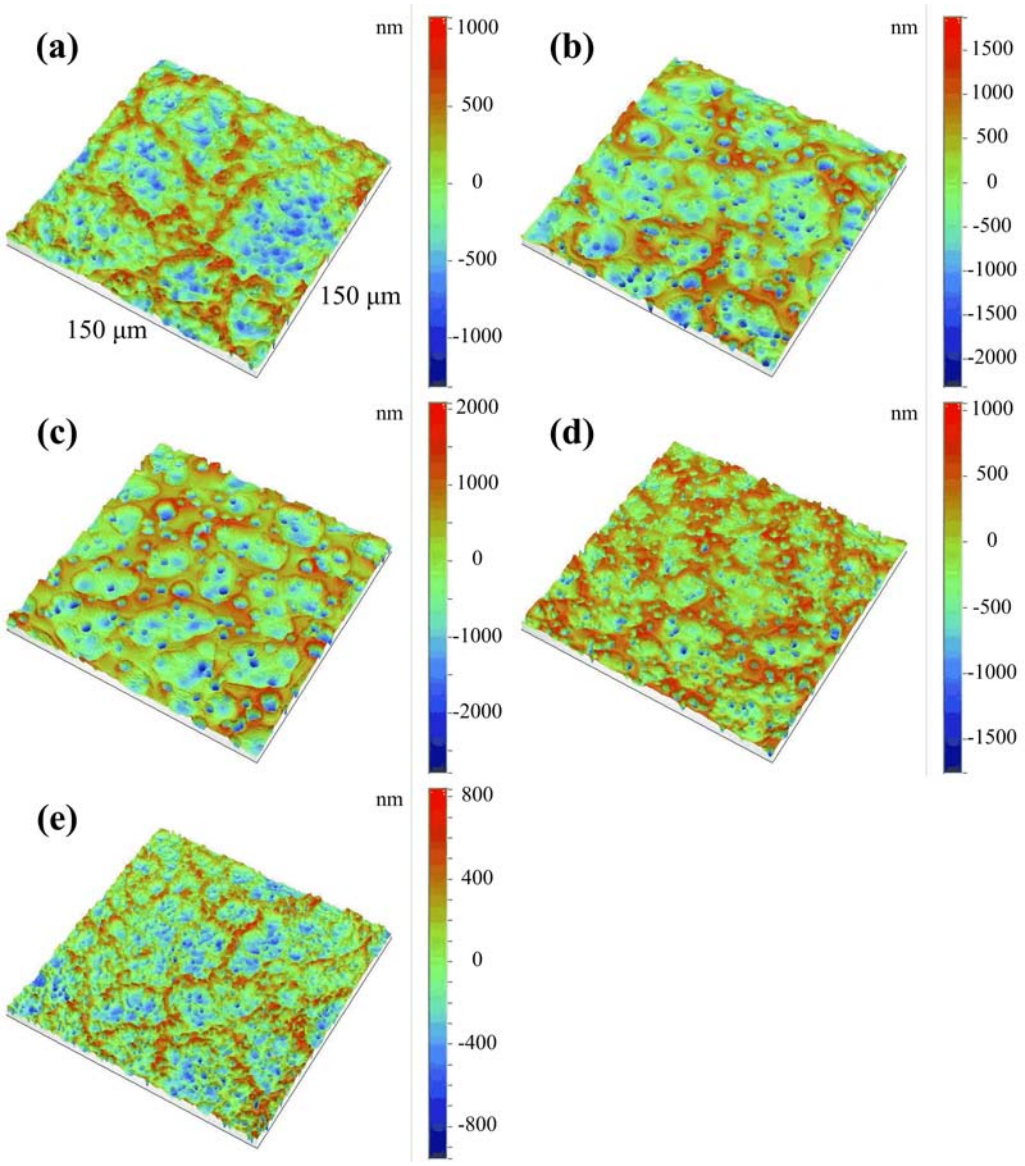

Figure 3.9. Three-dimensional topographic images of ion-implanted non-treated PU films: (a) Pristine, (b) 1×10^{13} ions/cm^2, (c) 1×10^{14} ions/cm^2, (d) 1×10^{15} ions/cm^2 and (e) 1×10^{16} ions/cm^2.

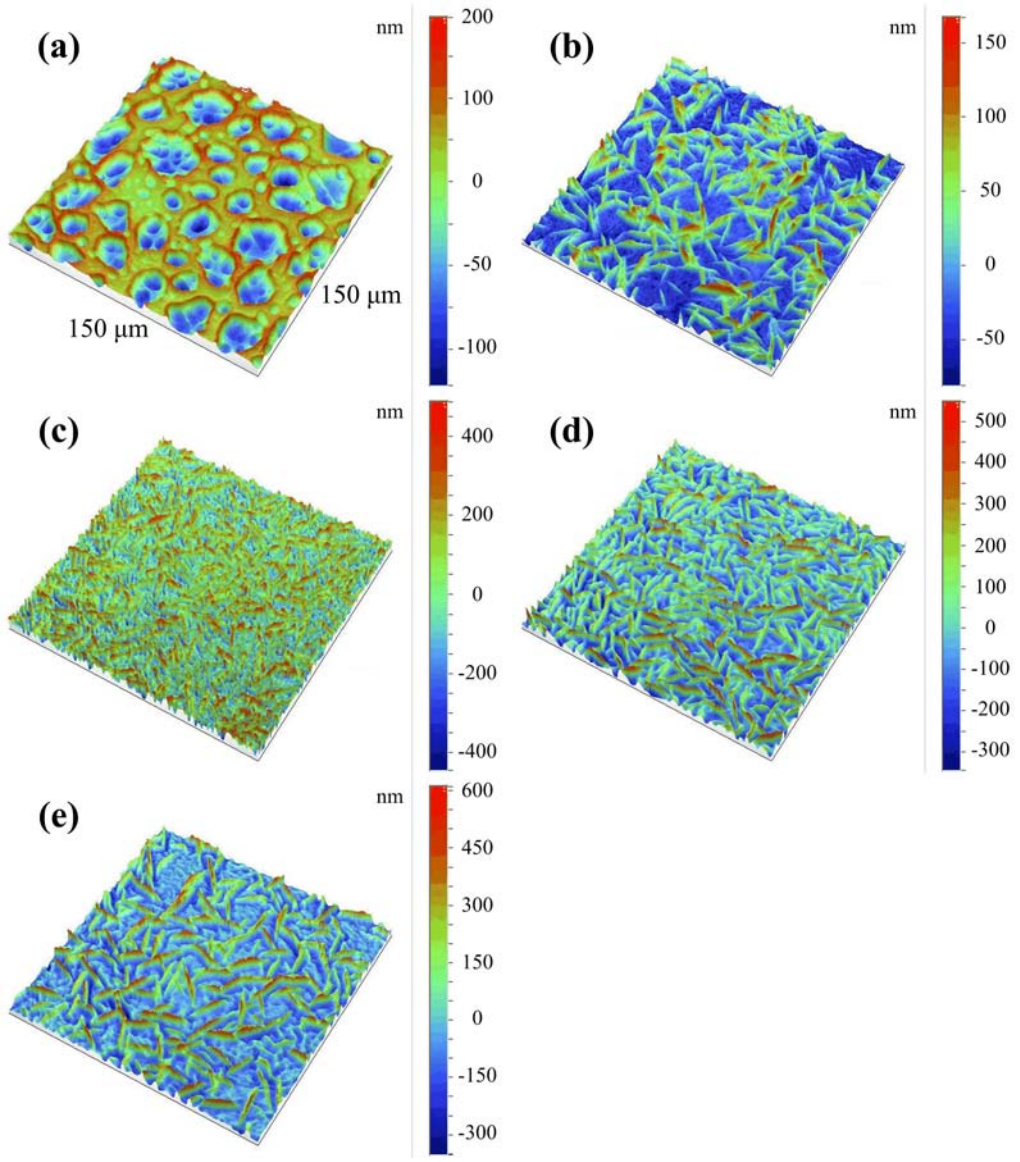

Figure 3.10. Three-dimensional topographic images of ion-implanted C90 PU films: (a) Pristine, (b) 1×10^{13} ions/cm^2, (c) 1×10^{14} ions/cm^2, (d) 1×10^{15} ions/cm^2 and (e) 1×10^{16} ions/cm^2.

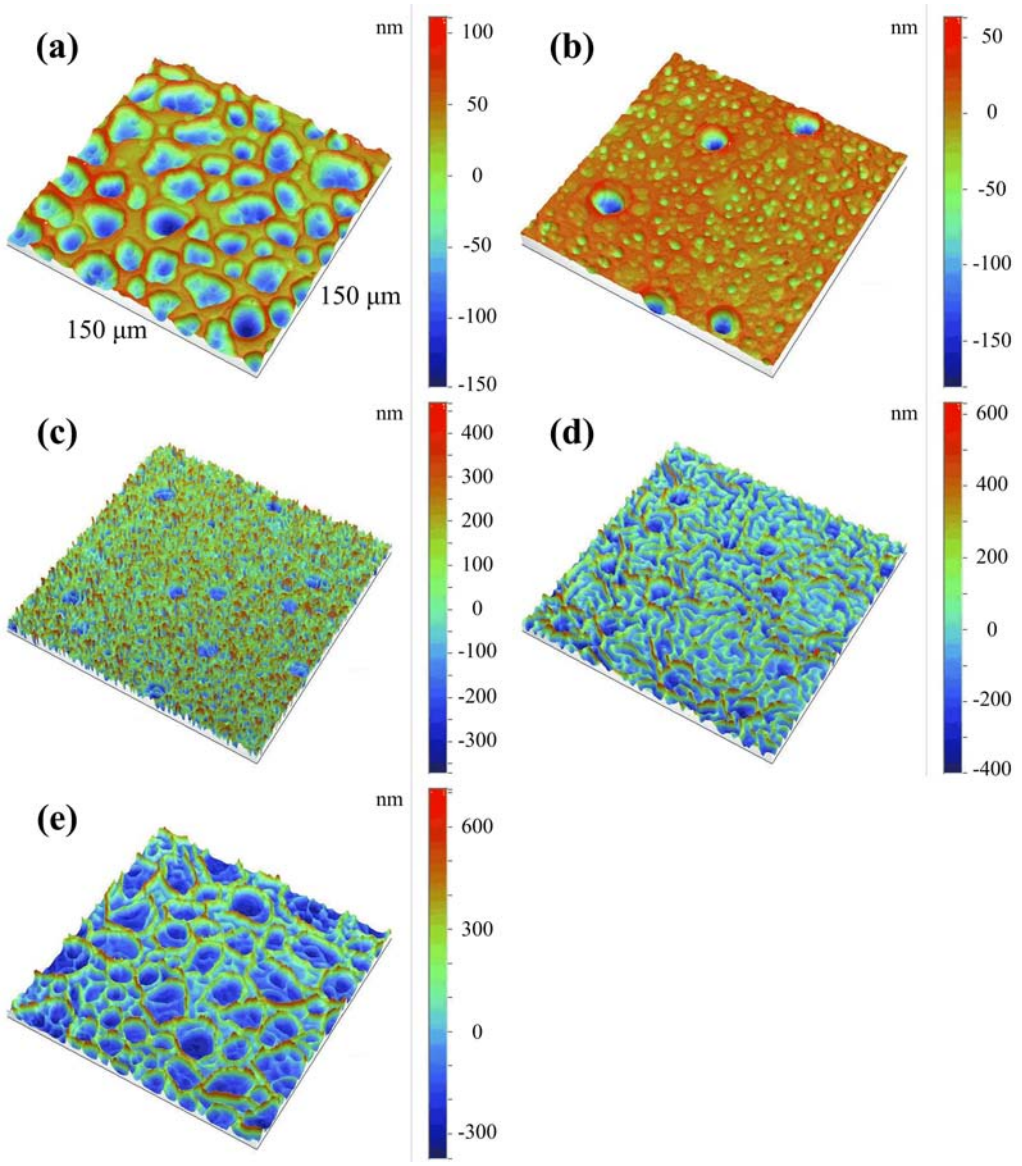

Figure 3.11. Three-dimensional topographic images of ion-implanted C-20 PU films: (a) Pristine, (b) 1×10^{13} ions/cm^2, (c) 1×10^{14} ions/cm^2, (d) 1×10^{15} ions/cm^2 and (e) 1×10^{16} ions/cm^2.

In addition to the surface chemical state of polymers, the surface morphology is also a very important factor when polymer materials are used for biomedical applications. Figures 3.9, 3.10 and 3.11 show the 3-dimensional topographic images of Ar^+-implanted PU films as a function of ion dose (for more information, see Appendix A). In the case of non-treated PU films, although they seemed transparent to the naked eye, there were lots of craters on their surfaces due to the rapid evaporation of THF during the curing process. Wrinkle formation and its pattern were not clearly seen for these samples. However, unlike non-treated samples, C90 and C-20 PU samples had surface wrinkles whose size was dependent on ion dose. The root mean square surface roughness of PU films as a function of ion dose is presented in Table 3.2. In the cases of C90 and C-20 PU films, the surface roughness of these PU films increased with increasing ion dose. However, due to the existence of craters, the surface roughness of non-treated PU films did not show any consistent trend as a function of ion dose.

Table 3.2. Root mean square surface roughness of PU films.

Ion dose	**Surface roughness (nm)**		
(ions/cm^2)	Non-treated	C90	C-20
Pristine	333.89	85.93	51.36
1×10^{13}	637.77	43.07	24.20
1×10^{14}	740.32	143.41	146.07
1×10^{15}	406.00	133.23	157.36
1×10^{16}	253.82	146.78	192.17

3.4. Discussion

Thermal treatment can be used to alter the physical properties of polymer materials. In this study, two different types of PU films were prepared depending on the degree of phase separation and the distribution of hard and soft segments by thermal treatment. During the heating process, the hard and soft segments of PU films are mixed together and become an amorphous state because heating temperature is above the T_m of the hard segment. After heating, subsequent cooling processes will definitely make different characteristics of PU films. At a lower cooling temperature (-20 °C), due to increase in the free energy of mixing of the system, a relatively higher degree of phase separation in PU films will occur. In this case, as indicated in Table 3.1, a lower glass transition temperature and a higher melting temperature were observed. In contrast, at a higher temperature (90 °C), a relatively lower degree of phase separation should take place.

If the degree of phase separation is high enough to develop crystalline form, the size and amount of crystalline structure will be increased. Figure 3.12 shows XRD patterns for C-20 and C90 PU films before ion implantation. Both PU films showed only broad weak patterns around 20° which corresponds to the d-spacing value of 4.4 Å [92]. This implies that both PU films did not have long-range order and therefore they had poorly-developed crystalline structure, which was also confirmed by the disappearance of T_2 after thermal treatment. Furthermore, similar peak intensities of both thermally treated PU films also indicate that they had almost same low crystallinity. Thus, from these results, it is expected that the effect of the crystalline phase of PU films on the changes of surface properties would not be significant.

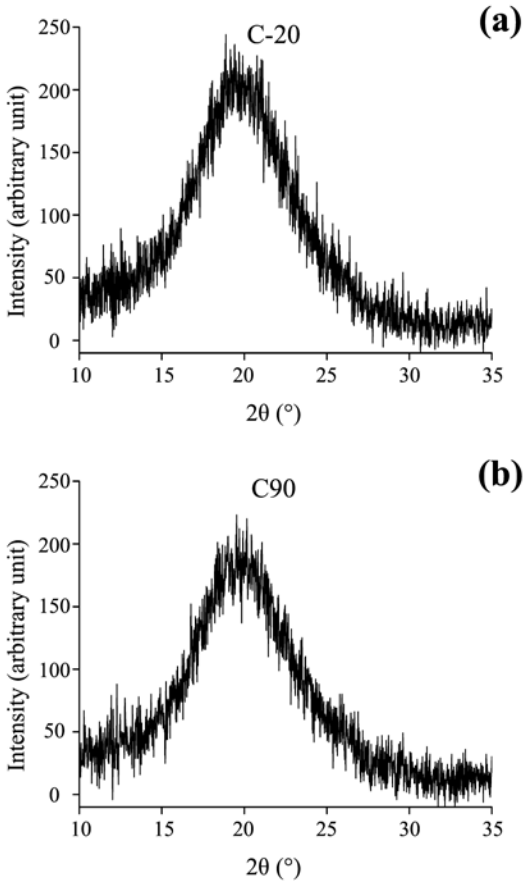

Figure 3.12. HRXRD patterns for PU films before ion implantation: (a) C-20 and (b) C90.

Eventually, the decisive factors for the changes in surface properties are the amount of hard segment domains and the distribution of them on the surfaces of PU films. Since the T_g of soft segments is lower than room temperature, the surface layer of a PU film can be easily reorganized depending on the environmental condition to minimize interfacial free energy. When the PU film faces the air, hydrophobic methylene groups ($-CH_2-$), the main part of the soft segment of PU films, tends to move towards the surface resulting in the enrichment of the soft segment at the surface [93-96]. Therefore,

due to the higher cooling temperature, relatively more carbon-containing functional groups would exist on the surfaces of C90 films compared to C-20 ones before ion implantation. On the other hand, because of the improved phase separation of the C-20 PU films and the blunted molecular mobility of their soft segments, more and larger hard segment domains would be located on the surface. Meanwhile, the molecular reorganization of thermally treated PU films is a temperature-dependent process. Thus, it is reasonable to assume that the surface properties of non-treated and C90 PU films were quite similar to each other because the curing temperature of non-treated samples and the cooling temperature of C90 ones are the same. As shown in Figure 3.8, the results of the surface wettability confirm this assumption.

The ion implantation caused the changes in surface chemical states of PU films. It has been observed that it is difficult to analyze the effect of ion dose on the amount of functional groups. Because radicals produced by collision with Ar^+ ions are very reactive, related chemical reactions are a kind of fast kinetics. Considering chemical bond strength, C-C, C-N, C-O and N-H bonds are susceptible to be broken by collision with Ar^+ ions and they turn into reactive free radicals. And a considerable number of these free radicals reacts with oxygen in the air and produces hydrophilic functional groups. In addition, surface carbonization confirmed by electron spin resonance spectra (see Appendix B) also takes place during ion implantation. As a result, due to the complicated chemical reactions, the amount of each functional group seems to be rather independent of applied ion dose as shown in Figures 3.5, 3.6 and 3.7. If reactive oxygen ions are applied to PU samples instead of non-reactive argon ions, oxygen-containing hydrophilic functional groups such as C=O and COO will be increased until carbonization becomes a dominant process.

The effect of surface chemical state on the surface wettability of a PU film is strongly dependent on the degree of carbonization and the amount of existing

functional groups on the surface of the PU film. The surface roughness of the PU film is also closely related to the surface wettability. Hence, surface wettability is a function of the chemical and morphological changes. In the cases of non-treated and C90 PU films, as shown in Figure 3.8, the water contact angle of them decreased with increasing ion dose up to 1×10^{14} ions/cm^2 in spite of increasing surface roughness. Thus, the formation of hydrophilic functional groups on the surfaces of these PU films is a major determinant of their surface wettability. However, at higher ion doses, the water contact angle slightly increased with increasing ion dose up to 1×10^{16} ions/cm^2. The carbonization of the surface layer and the increased surface roughness causes relatively more hydrophobic surfaces. In the case of C-20 PU films, surface wettability increased as a function of ion dose (up to 1×10^{16} ions/cm^2). Compared with the results of non-treated and C90 PU films, this continuous increase in surface wettability may be attributed to relatively smaller surface roughness and increased oxygen-containing hydrophilic functional groups on the surface even at high ion doses.

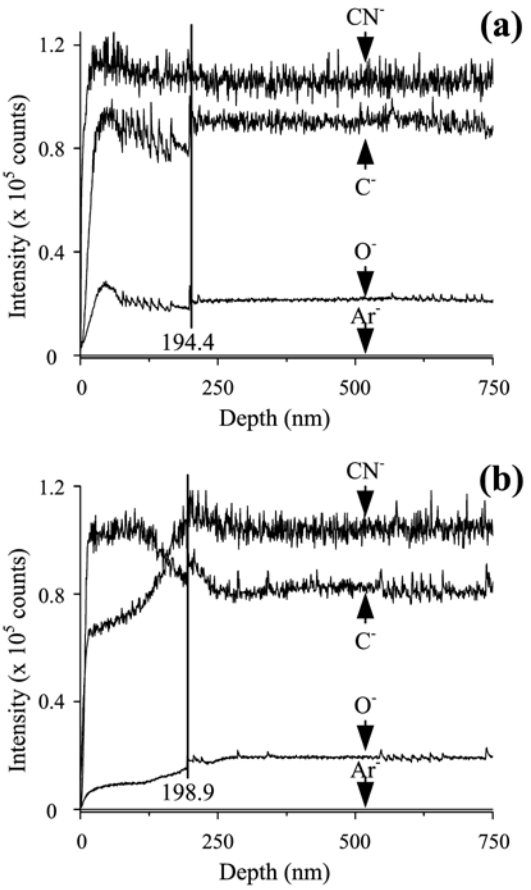

Figure 3.13. TOF-SIMS results of ion-implanted PU films: (a) 1×10^{15} ions/cm^2 and (b) 1×10^{16} ions/cm^2.

During ion implantation, a polyurethane film thermally expands and hard skin is formed on its surface at the same time. In this study, as shown in Figure 3.13, its thickness was approximately 200 nm. After cooling at ambient temperature, the ion-implanted polyurethane film spontaneously contracts and compressed stress arises from this process. As a result, hard skin which is formed on the surface of a PU film can be cracked or wrinkled [1]. As for the non-treated PU samples, polymer chains

would be locally concentrated on the surface of craters due to the fast evaporation of THF resulting in relatively solid surface. Therefore, the formation and propagation of wrinkles are restrained by these hard-skinned craters and no wrinkle patterns are clearly observed. On the other hand, as for the C90 PU samples, because of the mixing and reorganization of polymer chains during thermal treatment, polymer chains were evenly distributed on their surfaces resulting in the disappearance of craters. The ion implantation resulted well-developed wrinkled structures on the surface. It seems that the size of surface wrinkles increases with increasing ion dose. This result may be attributed to the increased thickness and hardness of modified surface layer during ion implantation. In the case of C-20 PU samples, they had relatively small surface roughness compared with the non-treated and C90 PU samples within the ion dose range adopted in this study. Due to the increased hard domains on the surfaces of C-20 samples induced by phase separation, the wrinkle formation and its propagation might be interrupted as shown in Figures 3.11(b), 3.11(c) and 3.11(d).

The ion-implanted samples showed that the wrinkle patterns were independent of applied ion dose. Even though the determinants of the wrinkle patterns are not fully understood, it is speculated that residual stress, which created in pristine PU films during fabrication and sampling processes, would play an important role in determining the wrinkle patterns of ion-implanted PU films. For example, if a PU film has unidirectional residual stress, surface wrinkles will be aligned perpendicular to the direction of the residual stress. On the other hand, if there is no residual stress, irregular patterns will be created on the surface of a PU film. To confirm this, a PU film was prepared by unidirectional stretching combined with thermal treatment. With the help of thermal treatment, the elongated PU film contracted very slowly until it reached a constant length. A SEM and an AFM images of the film are shown in Figure 3.14 and 3.15, respectively. Evidently, the surface wrinkles were aligned in one direction with

similar size.

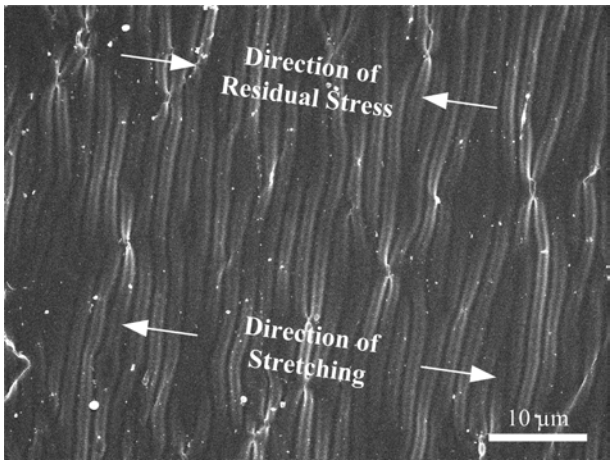

Figure 3.14. A SEM image of a unidirectionally stretched and thermally treated PU film after Ar^+ ion implantation (thermal treatment temperature = 90 °C, thermal treatment time = 25 min, elongation = 100 %, ion dose = 1×10^{14} ions/cm^2).

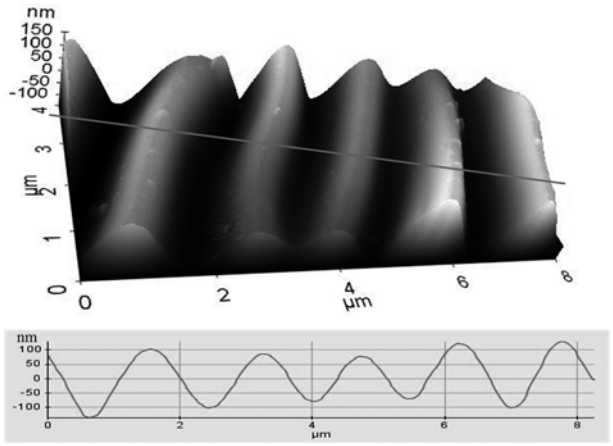

Figure 3.15. An AFM image and an example of line profiles of unidirectionally aligned surface wrinkles on the surface of an ion-implanted PU film (thermal treatment temperature = 90 °C, thermal treatment time = 25 min, elongation = 100 %, ion dose = 1×10^{14} ions/cm^2).

3.5. Conclusions

Two different types of thermal treatment were applied to polyurethane (PU) films fabricated by solvent casting method. After argon ion implantation, the influence of thermal treatment on the surface properties of ion-implanted PU films was examined. From the results, it is evident that the phase separation of polyurethane and the distribution of soft segment matrix and hard segment domains on the surfaces of a PU film, both of which are induced by thermal treatment, can affect its surface morphology as well as surface chemical state during ion implantation. Therefore, if the surface property changes are controlled by simple thermal treatment before ion implantation, the fabrication of wrinkled PU films with good surface wettability can be achieved using ion implantation. These PU films are expected to be used for the growth substrates for cells such as an endothelial cell lining of artificial blood vessels.

IV. Enhanced Biocompatibility of Polyurethane Substrates using Focused Ion Beam Treatment

4.1. Introduction

Polymeric materials as biomaterials should possess a broad range of mechanical strength which covers not only soft tissues such as human blood vessel and skin but also hard tissues such as bone and ligament of human body. Furthermore, they should have good biocompatibility with no toxicity. The mechanical properties of elasticity are also required for polymers which are applicable to the replacements of human soft tissues.

A large number of polymeric materials have been used in biological and medical applications. Above all, polyurethane (PU) and its derivatives which show essential characteristics of biomaterials depending on their composition of soft and hard segments have been well employed in the last few decades. As a result, large quantities of commercially produced PUs have been used for the fabrication of artificial blood vessels, catheters, pacemaker leads and so on [8]. Nevertheless, due to the hydrophobic nature of PUs themselves, side effects including poor adhesion as well as poor proliferation of cells, inflammation and thromboembolism triggered by immune system are still a matter of concern.

To resolve these problems, various methods of surface modification are commonly introduced. The surface modification can improve the biocompatibility of materials without altering their bulk properties. In the case of PU, coating of biocompatible silk fibroin [97-98], chemical or plasma-assisted grafting of bioactive agents such as

prostacyclin, heparin, hexamethylated disiloxane, L-lactide, sulfonated PEO and collagen [28-29, 99-102], plasma treatment for adopting functional groups [91, 103] and ion implantation [9, 12-14, 104-105] have been applied onto the surfaces of PU films or PU foams. Among these methods, ion implantation has attracted great attention from biomaterial researchers over the past two decades. It is well known that ion implantation can change the chemical and physical properties of polymer materials and increase their biocompatibility by implanting ion particles on the polymer surface [106].

Here, focused ion beam (FIB), one of beam-line type ion implantation methods, was utilized to modify the surfaces of PU substrates. In most cases, the contribution of FIB to biomedical area has been limited to the preparation and site-specific analysis of samples which can show cell-substrate interfaces by milling process in combination with scanning electron microscopy (SEM) [15-18]. However, we concentrated our efforts to very interesting feature of FIB treatment – formation of various wrinkle patterns on the surface of polymer – because wrinkles could possibly play an important role in the growth of cells on the surfaces of biomaterial substrates. It has been reported that nanoscale or microscale topography of substrates can affect cell growth behavior such as adhesion, spreading, orientation and proliferation [36, 38, 46, 107-111].

Therefore, both wrinkle formation and chemical changes induced by FIB treatment may synergistically enhance both cell adhesion and cell growth on the surface of the modified polymer substrate. In this study, we applied gallium ion (Ga^+) implantation using FIB onto the surfaces of PU substrates. In order to check out the toxicity of FIB-treated PU substrates, RAW 264.7 monocytes/macrophages were seeded on the modified PU and their morphological changes were observed. Also, the morphology and wrinkle pattern of the FIB-treated PU substrates were observed and their surface chemical state and elemental composition were analyzed. To verify the influence of the

physico-chemically modified PU surface on the adhesion and growth of cells, immunofluorescence staining was conducted. For the quantitative assessment of cell proliferation, NIH3T3 fibroblasts were cultured on the PU substrates for 3 days and the MTT cell proliferation assay was performed. The obtained results from FIB-treated PU substrates were compared with those of non-treated and argon ion (Ar^+) implanted PU samples.

4.2. Experimental

4.2.1. Materials

Pellethane® 2103-80AE (Dow Chemical Co., USA), commercial ether based thermoplastic PU, was obtained and used after thorough washing with distilled water. Dimethylformamide (DMF) and tetrahydrofuran (THF) were purchased from Samchun Chemical Co. Ltd. (Republic of Korea) and used without further purification. Dulbecco's modified Eagle's medium (DMEM) and MTT assay kit were obtained from Sigma-Aldrich Co. (Saint Louis, MO, USA) and fetal bovine serum (FBS) was purchased from GIBCO (Chagrin Falls, OH, USA).

4.2.2. Preparation of PU thin films

An 11 wt% PU solution was prepared by dissolving 9.0 g of Pellethane® 2103-80AE in a mixture of DMF and THF (70:30 w/w) with stirring at room temperature for 6 hours to obtain homogeneous solution. And then, the PU solution was kept in a thermostat oven at 25 °C overnight to be stabilized. With this solution, PU thin films were fabricated by solvent casting method and cured in a vacuum oven at 80 °C for 72

hours to remove residual solvent from the PU films. The thickness of the PU films was about 130 μm. Some part of samples were cut into circular discs having a diameter of 5 mm and washed with distilled water and ethanol.

4.2.3. Ion implantation into PU substrates

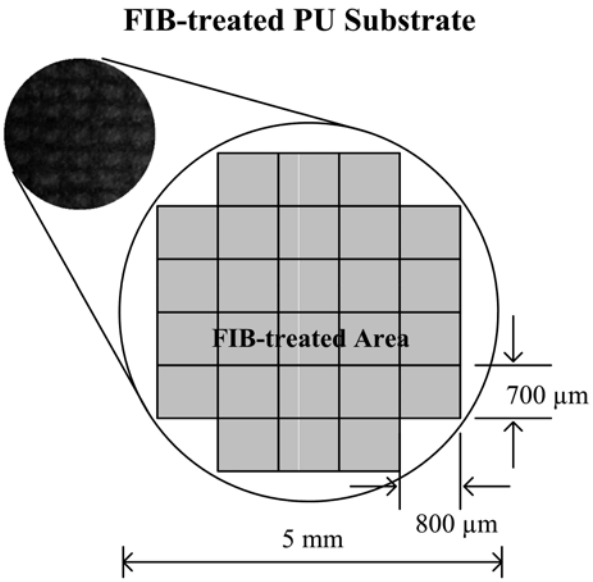

Figure 4.1. A schematic representation of a FIB-treated PU substrate: A photograph of a FIB-treated substrate captured against dark background is located at the top-left corner.

For Ga^+ irradiation on the surfaces of PU substrates, a dual beam system which combined ultrahigh resolution field emission scanning electron microscope (FE-SEM) and accurate focused ion beam (Nova 600 NanoLab; FEI Company, USA) was employed. The specimens were placed in the vacuum chamber under a pressure of 1×10^{-5} Pa during the FIB treatment. The acceleration voltage and ion current were kept at 30 kV and 9.3 nA, respectively. The irradiation angle between the incident beam and

the surface normal was fixed at 0° and the beam dwell time was kept at 10 μs for all samples. In most cases, the applied ion dose was 1×10^{13} ions/cm^2 except in the case of the observation of surface morphology changes; in this case, the applied ion dose ranged from 1×10^{12} to 1×10^{15} ions/cm^2. The FIB-treated area was 800×700 μm^2 for each scan when the dual beam system was operated in digital raster mode. Unfortunately, due to the characteristic of the apparatus, the whole surface area of a specimen could not be Ga^+-irradiated. Instead, as shown in Figure 4.1, 26 scans which covered about 74.2 % of entire surface area were performed on the surfaces of the substrates without overlapping areas.

For the comparative analysis, Ar^+-implanted PU substrates were fabricated using a custom-made ion implanter installed at Korea Atomic Energy Research Institute (KAERI, Republic of Korea). The Ar^+ implantation was performed in the vacuum chamber under a pressure of 1×10^{-5} Pa at room temperature. The ion energy and ion fluence were 30 keV and 1×10^{15} ions/cm^2, respectively. To prevent thermal effect, the beam current was kept constant at 2 μA/cm^2. On the contrary to the FIB-treated sample, the surface area of the Ar^+-implanted one was entirely ion-implanted.

4.2.4. Observation of surface morphologies and wrinkle patterns of PU substrates

Surface morphologies of non-treated and ion-implanted samples were analyzed using FE-SEM (JSM-6700F; JEOL, Japan). In order to obtain more detailed information about the wrinkle patterns of the FIB-treated samples, atomic force microscopy (AFM) (XE-100; Park Systems Corp., Republic of Korea) was also carried out in dynamic non-contact mode with a silicon tip. Square frames having edges of 2 μm with 102 × 102 data points were used to acquire AFM images. The scan rate for

measurements was 1 Hz.

4.2.5. Measurement of implanted Ga^+ content of FIB-treated PU substrates

The amount of implanted Ga^+ was determined by inductively coupled plasma mass spectrometry (ICP-MS) (ELAN 6100; Perkin-Elmer SCIEX, USA). Argon plasma (6000 K) source was used in this experiment. The RF power and the sample injection flow rate were 1100 W and 1.00 ml/min, respectively. FIB-treated samples were analyzed three times and average values were obtained.

4.2.6. Surface chemical analysis of PU substrates

The surface chemical composition of PU samples were confirmed by X-ray photoelectron spectroscopy (XPS) system (AXIS-His; KRATOS, Japan). To minimize the charging effects of the nonconductive PU specimens, neutralizing was carried out. The Mg-Kα (150 W) source was used in the hybrid mode with 90° take-off angles. The survey scan was performed within the binding energy range of 0 - 1000 eV. The pass energy of 160 eV was applied to the samples during the survey scan. In order to obtain the elemental composition of the PU samples, the XPS spectra were employed using an iterative least-squares fitting routine on the basis of Gaussian and Lorentzian functions as well as the Shirley-type background subtraction. The binding energies of all the spectra were referenced to the 285 eV corresponding to the peaks of C-C and/or C-H groups (C1s).

4.2.7. Cell culture and seeding on PU substrates

The NIH3T3 fibroblasts cell line derived from mouse embryo and the RAW 264.7 monocytes; macrophage cell line derived from mouse, which were obtained from the Korean Cell Line Bank (KCLB, Seoul, Republic of Korea), were cultured in DMEM supplemented with 10 % (v/v) FBS and 1 % (v/v) antibiotic/antimycotic solution at 37 °C in a humidified 5 % CO_2 atmosphere. For seeding on PU substrates, the NIH3T3 cells were detached from tissue culture flasks with 0.25 % trypsin/EDTA solution and the RAW 264.7 cells were disconnected by scraping. As a result, a single cell suspension (2×10^3 cells/μl) was prepared for later experiments.

Before cell seeding, PU substrates were sterilized with 70 % (v/v) ethanol and washed three times with 1× phosphate buffer saline (PBS) containing 1 % (v/v) antibiotics. For cellular attachment onto PU substrates, 5 μl of cell stock was seeded directly onto each wetted sample and incubated for 20 minutes in a humidified chamber without culture medium. Then, the cell-seeded substrates were moved into culture medium and cultured for 3 days.

4.2.8. Observation of the morphological changes of monocytes/macrophages on PU substrates

To check out the foreign body reaction to PU substrates, RAW 264.7 cells were seeded on them. One day after cell seeding, the cell-seeded PU substrates were washed twice with PBS, and fixed in 4 % (v/w) glutaraldehyde, postfixed with 1 % (w/v) OsO_4, dehydrated stepwise with increasing concentrations of ethanol and finally dried in a critical point drier. Samples were then coated with gold in a JFC-1100 unit (Jeol Inc., Japan) and observed under SEM (JEM-T300; Jeol Inc., Japan).

4.2.9. Immunofluorescence staining

The NIH3T3-seeded PU substrates at 6 and 24 hours after cell seeding were washed three times with PBS and treated with 3 % (v/v) hydrogen peroxide (H_2O_2) for 20 minutes, and then blocked with 1 % bovine serum albumin (BSA) in PBS for 30 minutes at room temperature. Then, samples were incubated overnight at 4 °C with the following primary antibodies: Alexa 488 conjugated filamentous actin (F-actin) (1:250, A12379, Invitrogen Ins., Grand Island, NY) and mouse monoclonal anti-focal adhesion kinase (FAK) (1:100, BD610087, BD Biosciences Biotech., San Diego, CA). Other samples at 1 and 3 days after seeding were incubated with the following primary antibodies; rabbit polyclonal anti-AKT (1:250, #9272, Cell signaling Ins., Danvers, MA) and goat polyclonal anti-caspase 3 (1:250, SC1225, Santa Cruz Biotech., Santa Cruz, CA) after equal processing with 6 and 24 hours samples. The samples were washed three times with PBS and incubated with appropriate secondary antibodies (goat anti-mouse IgG TRITC, goat anti-rabbit IgG FITC, donkey anti-goat IgG TRITC, 1:500 for double labeling, Santa Cruz Biotech.) for 2 hours at room temperature with gently shaking. All antibodies were diluted in PBS containing 1% BSA. After further washes in PBS, coverslips were mounted using fluoroshield mounting medium with DAPI (ab104139, Abcam, UK), and fluorescence-stained samples were analyzed under confocal microscopy (FV-300, OLYMPUS, Japan).

4.2.10. MTT assay

At 1, 2 and 3 days after cell seeding, the NIH3T3 cell-seeded PU samples (n = 3 per group) for the MTT assay were transferred to 1.5 ml plastic tubes after washing

with PBS, mixed with 1 ml serum-free DMEM supplemented with 0.5 g MTT (3-(4,5-dimethylthiazol-2-yl)-2,5-diphenyltetrazolium bromide), and incubated in the dark at 37 °C and 5 % CO_2 atmosphere for 2 hours. The plastic tubes were centrifuged for 10 min at 2,000 g and the supernatant was aspirated. For solubilization, purple formazan was extracted with 1 ml of 0.04 M HCl in 2-propanol. The absorbance of the extracted solution was measured at 570 nm using an ultraviolet-visible (UV/VIS) spectrophotometer (Biospec, UK). Results were expressed as mean ± standard deviation. Statistical differences in the cell proliferation of different substrates were assessed by one-way analysis of variance. When the *P*-values were less than 0.05, differences were considered statistically significant.

4.3. Results

4.3.1. Surface morphologies and wrinkle patterns of PU substrates

Figure 4.2 shows SEM images of the surfaces of PU substrates. Non-treated PU substrates had smooth surfaces. In contrast, as for Ar^+-implanted PU substrates, it seemed that wrinkles showing irregular pattern were formed on their surface and the wavelength and amplitude of surface wrinkles were in the micron range. However, depending on applied ion doses, FIB-treated samples had different surface morphologies. In the cases of ion doses lower than 1×10^{12} ions/cm^2, surface wrinkles were not formed by FIB treatment. Surface wrinkles that were aligned in one direction were formed at low ion doses in the range of $1 \times 10^{12} - 1 \times 10^{13}$ ions/cm^2 as shown in Figures 4.2(c) and 4.2(d). The wavelength of wrinkles slightly decreased but their amplitude increased with increasing ion influence. Both their wavelength and amplitude were in the submicron range. When the applied ion dose ranged from 1 ×

10^{13} to 1×10^{15} ions/cm^2, herringbone-like wrinkle pattern was observed as shown in Figure 4.2(e). In the cases of ion doses higher than 1×10^{15} ions/cm^2, the greater part of the surface area of PU substrates was melted by generated heat and irregular pattern was created (Figure 4.2(f)) during FIB treatment.

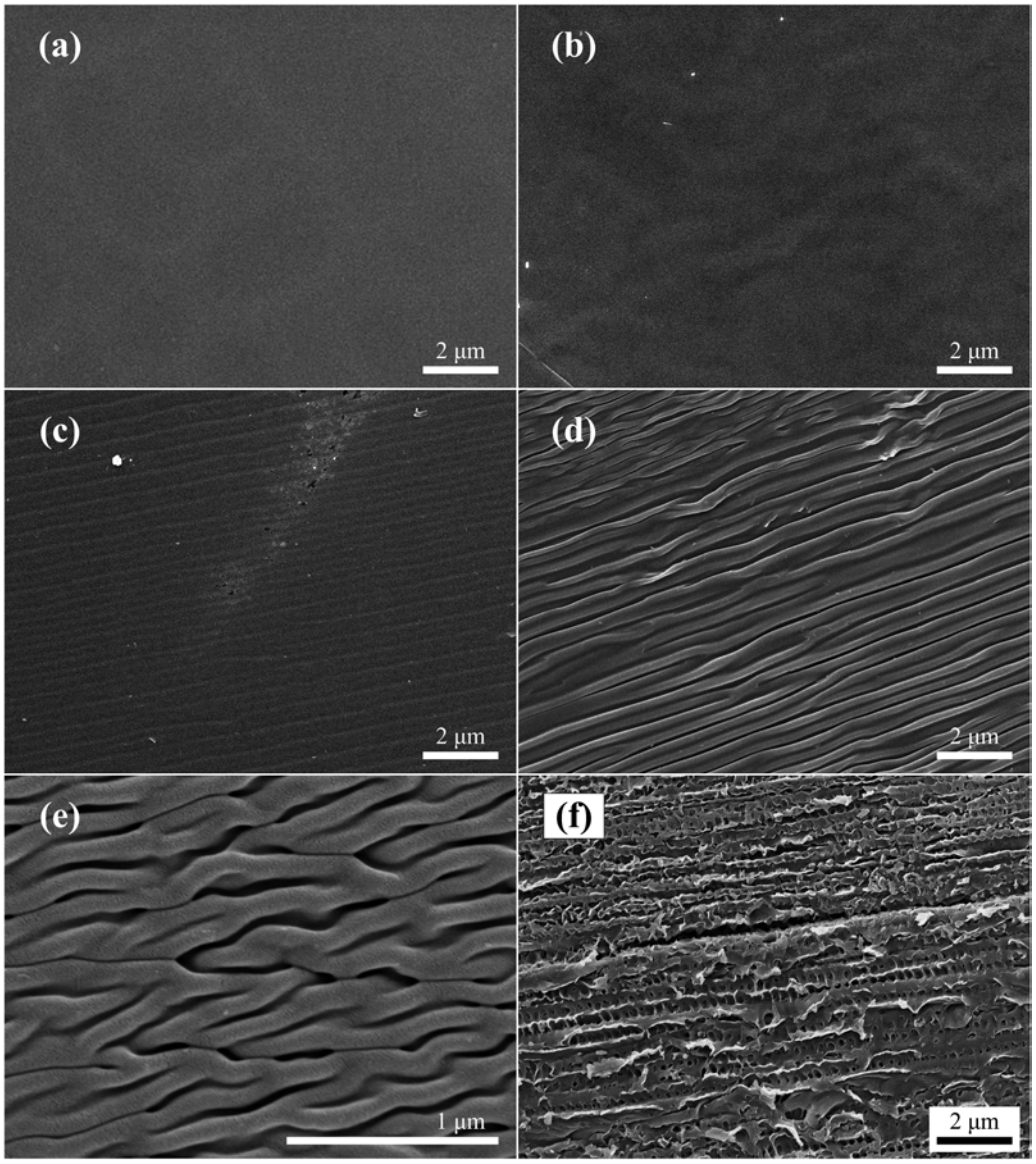

Figure 4.2. SEM images of PU substrates: (a) Non-treated, (b) Ar^{+}-implanted, ion dose = 1×10^{15} ions/cm^2, (c) FIB-treated, ion dose = 1×10^{12} ions/cm^2, (d) FIB-treated, ion dose = 1×10^{13} ions/cm^2, (e) FIB-treated, ion dose = 1×10^{14} ions/cm^2 and (f) FIB-treated, ion dose = 1×10^{15} ions/cm^2.

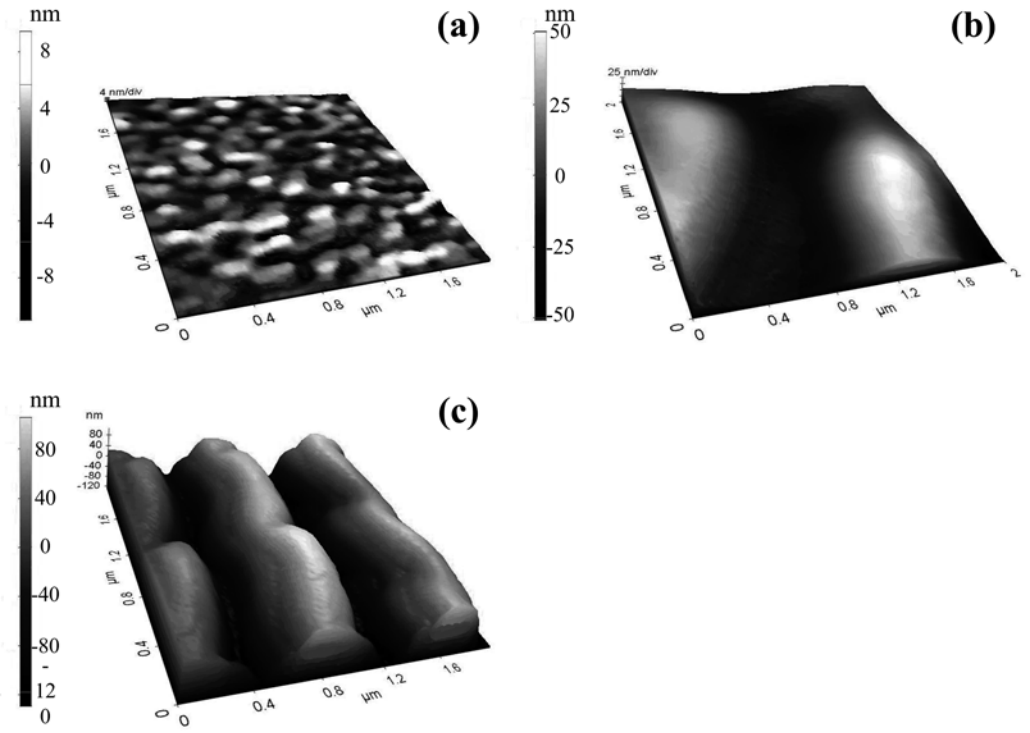

Figure 4.3. AFM images of PU substrates (bar located at the left side of each image = z-axis height): (a) Non-treated, (b) Ar^+-implanted, ion dose = 1×10^{15} ions/cm^2 and (c) FIB-treated, ion dose = 1×10^{13} ions/cm^2.

Figure 4.3 shows AFM images of the surface morphologies of PU substrates. Topological properties are summarized in Table 4.1 and values are expressed as mean ± standard deviation. Compared with the surface roughness of the non-treated PU substrate, those of the Ar^+-implanted and FIB-treated PU substrates increased considerably.

Table 4.1. Surface morphological properties of PU substrates.

Sample	Aligned wrinkle		Root mean square roughness (nm)
	Wavelength (nm)	Amplitude (nm)	
Non-treated PU	-	-	2.9 ± 0.7
Ar^+-implanted PU (1×10^{15} ions/cm^2)	-	-	32.5 ± 6.7
FIB-treated PU (1×10^{13} ions/cm^2)	788.8 ± 29.9	201.9 ± 9.3	58.8 ± 4.7

4.3.2. Implanted Ga^+ content of FIB-treated PU substrates

Table 4.2. ICP-MS results of FIB-treated PU substrates.

Sample status	Amount of the implanted Ga^+ (ppb)
After FIB-treatment	33 ± 12
After washing with distilled water and ethanol	-
After 3 days of cell culture	-
After immersion in PBS for 14 days	-

Up to the present, the influence of Ga^+ on cells and their metabolism is not clearly known. Although Ga^+ and its compounds are not considered to be particularly toxic, they might induce inflammation [112-113]. It is necessary that the amount of implanted Ga^+ in FIB-treated PU substrates should be measured. As shown in Table 4.2, its amount was very infinitesimal after FIB-treatment. Moreover, after washing, gallium ions were not detected by ICP-MS.

4.3.3. Surface chemical analysis of PU substrates

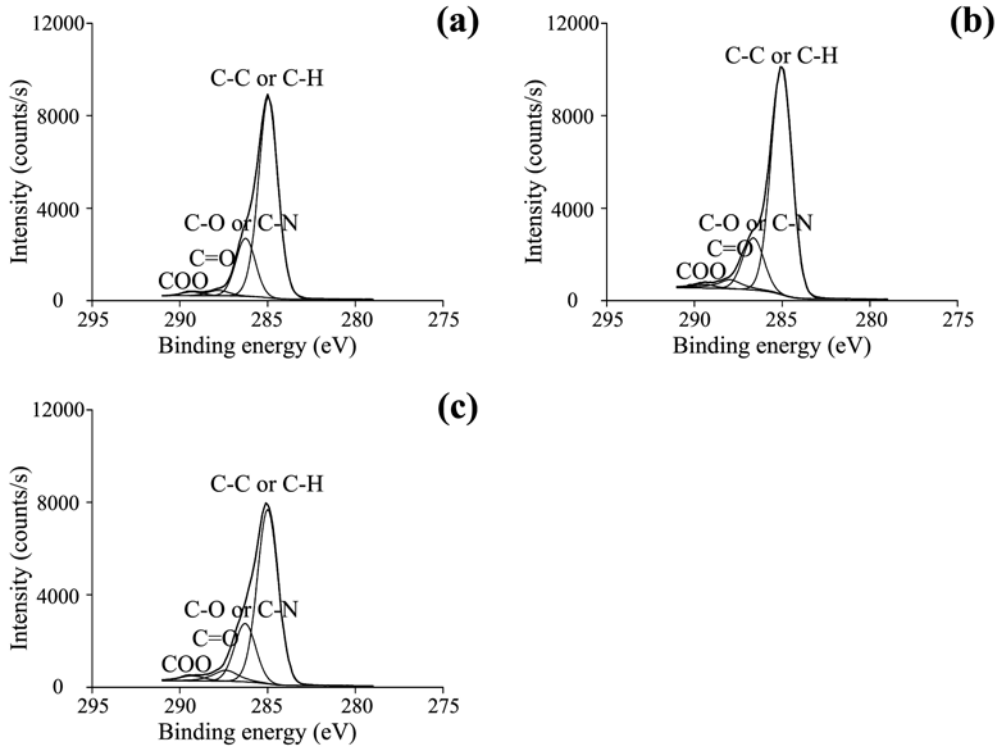

Figure 4.4. Cls XPS spectra of PU substrates: (a) Non-treated, (b) Ar^{+}-implanted, ion dose = 1 × 10^{15} ions/cm^2 and (c) FIB-treated, ion dose = 1 × 10^{13} ions/cm^2.

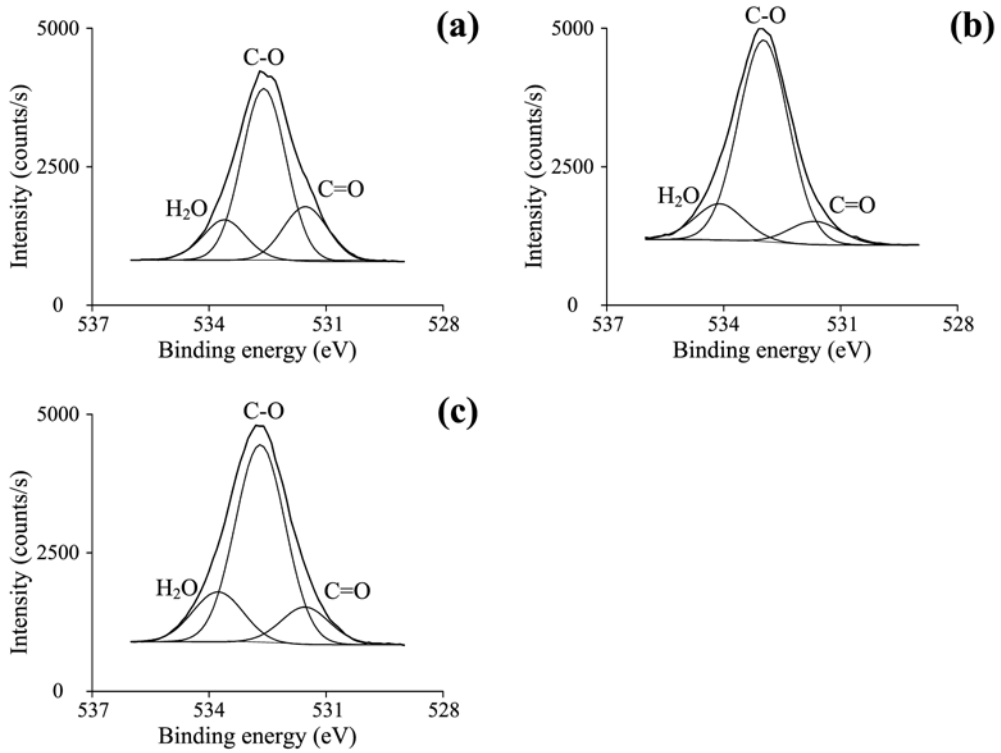

Figure 4.5. Ols XPS spectra of PU substrates: (a) Non-treated, (b) Ar^+-implanted, ion dose = 1 × 10^{15} ions/cm^2 and (c) FIB-treated, ion dose = 1 × 10^{13} ions/cm^2.

Figures 4.4, 4.5 and 4.6 show the C1s, O1s and N1s XPS spectra of PU substrates, respectively. Table 4.3 summarizes the functional groups and surface elemental composition of the PU substrates. Note that analyzed element is expressed as a right-hand superscript * in Table 4.3. Compared with the results of the non-treated and Ar^+-implanted PU substrates, it was revealed that C-O or C-N, C=O and COO functional groups on the surface of the FIB-treated substrate appreciably increased but C-C or C-H functional groups decreased. In addition, the amount of adsorbed H_2O also increased and new C=N functional group was created after FIB treatment in comparison with the

non-treated PU substrate.

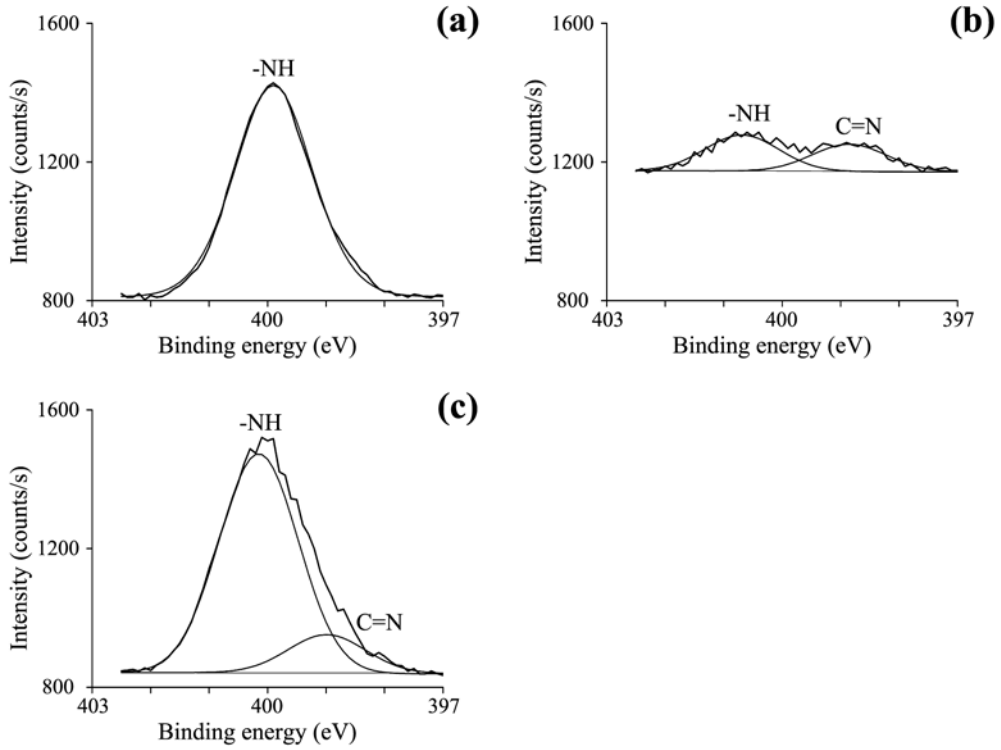

Figure 4.6. Nls XPS spectra of PU substrates: (a) Non-treated, (b) Ar^+-implanted, ion dose = 1 × 10^{15} ions/cm^2 and (c) FIB-treated, ion dose = 1 × 10^{13} ions/cm^2.

Table 4.3. Functional groups and surface elemental composition of PU substrates.

Element	Functional group	Surface elemental composition of PU substrate (%)		
		Non-treated	FIB-treated (1×10^{13} ions/cm^2)	Ar^+-implanted (1×10^{15} ions/cm^2)
C	C*-C or C*-H	63.62	57.2	67.28
	C*-O or C*-N	18.32	19.17	15.42
	C*=O	1.91	4.52	3.88
	C*OO	1.34	1.93	1.11
	Total	**85.19**	**82.82**	**87.69**
N	-N*H	2.95	2.94	0.42
	C=N*	-	0.52	0.32
	Total	**2.95**	**3.46**	**0.74**
O	C-O*	7.64	9.51	8.92
	C=O*	2.44	1.78	1.05
	H_2O*	1.79	2.42	1.61
	Total	**11.87**	**13.71**	**11.58**

4.3.4. Foreign body reaction to PU substrates

When the immune system is activated, it attempts to remove or isolate a foreign body. In this case, macrophage fusion takes place and leads to the formation of multinucleated giant cell. Therefore, by observing the morphological changes of RAW 264.7 cells, the toxicity of PU substrates can be detected. In all cases, as shown in Figure 4.7, any aspects of cell fusion were not observed for 24 hours in this study. In the case of non-treated PU substrates, most of RAW 264.7 cells were round-shaped and their filopodia were not formed within 24 hours after seeding. Furthermore, they did

not adhere well onto the surface of PU samples and agglomerated together to form larger clusters. On the other hand, in the cases of Ar^+-implanted and FIB-treated PU substrates, RAW 264.7 cells adhered well and spread out onto the surface. Also, they had well-developed filopodia compared to those cultured on the non-treated PU substrates.

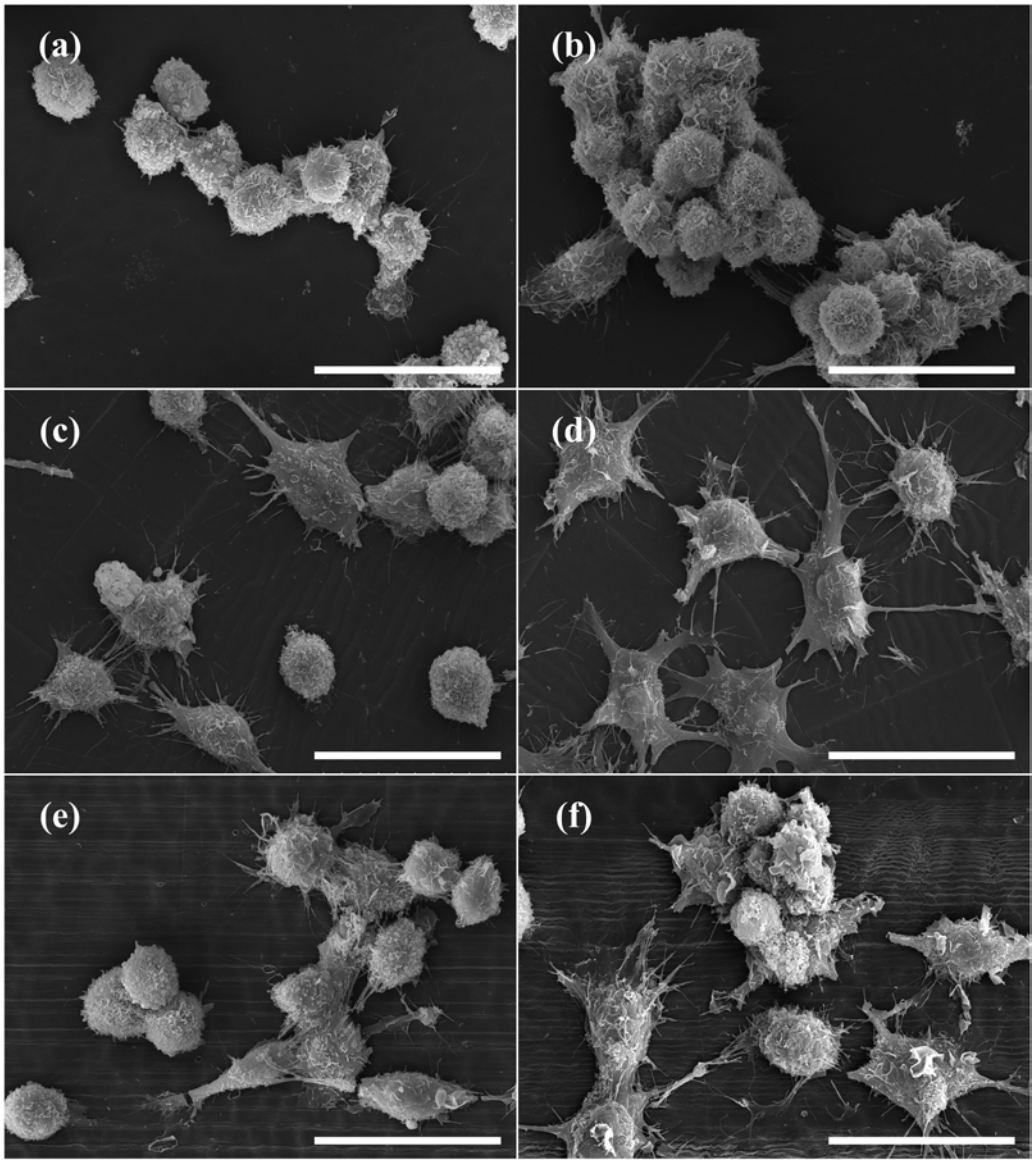

Figure 4.7. SEM images of RAW 264.7 cells on PU substrates 6 hours after seeding (left column) and 24 hours after seeding (right column) (bar size = 30 μm): (a)-(b) Non-treated, (c)-(d) Ar^+-implanted, ion dose = 1×10^{15} ions/cm^2 and (e)-(f) FIB-treated, ion dose = 1×10^{13} ions/cm^2.

4.3.5. Immunofluorescence staining of NIH3T3 fibroblasts

To explore the activation of biological molecules which produce various cellular processes including cell adhesion, cell proliferation and cell apoptosis, immunofluorescence staining was carried out and confocal images of cultured NIH3T3 cells were captured. Here, four kinds of biological molecules were studied; F-actin is a protein molecule involved in cell motility, cell cytokinesis and maintenance of cell shape; FAK is a protein kinase that mainly participates in cell adhesion and cell spreading; AKT is a protein kinase that plays an very important role in cell survival, cell proliferation and cell migration; Caspase 3 is a protease that is closely related to cell apoptosis. Figures 4.8, 4.9, 4.10 and 4.11 show the immunofluorescent images of NIH3T3 fibroblasts cultured on the surfaces of PU substrates. During 1 day of culture, compared with NIH3T3 cells adhered onto Ar^+-implanted and FIB-treated PU substrates, those adhered onto non-treated PU substrates synthesized only a trace amount of F-actin and FAK. Meanwhile, the expression of F-actin and FAK in the cells cultured on the Ar^+-implanted and FIB-treated PU substrates seemed to be on a similar level. Also, no obvious caspase 3 expression was detected for all PU substrates even after 3 days of culture. In contrast, AKT expression was clearly observed in all NIH3T3 fibroblasts cultured on the PU substrates.

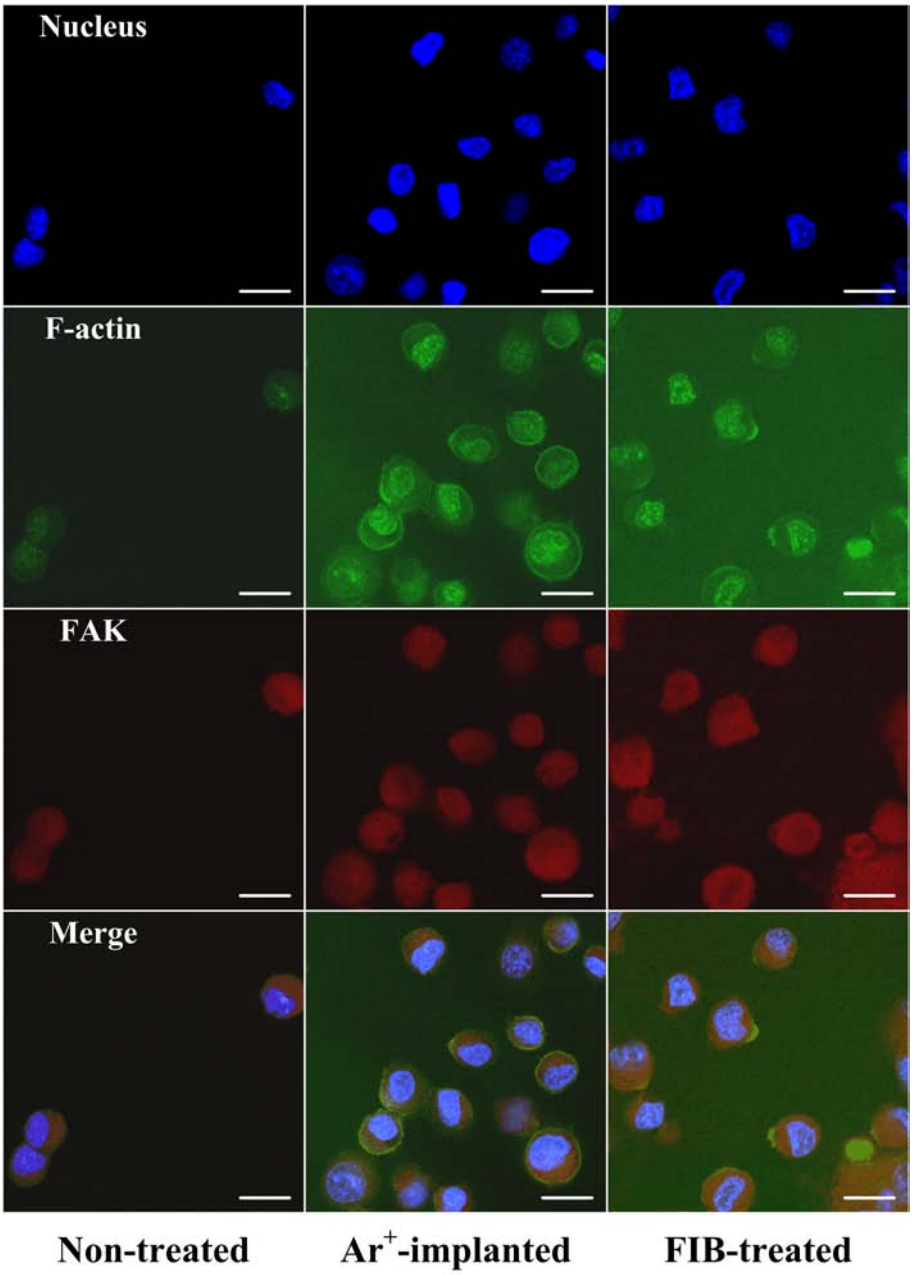

Figure 4.8. Confocal images of NIH3T3 fibroblasts after 6 hours of culture (bar size = 20 μm). F-actin and FAK are stained green and red, respectively.

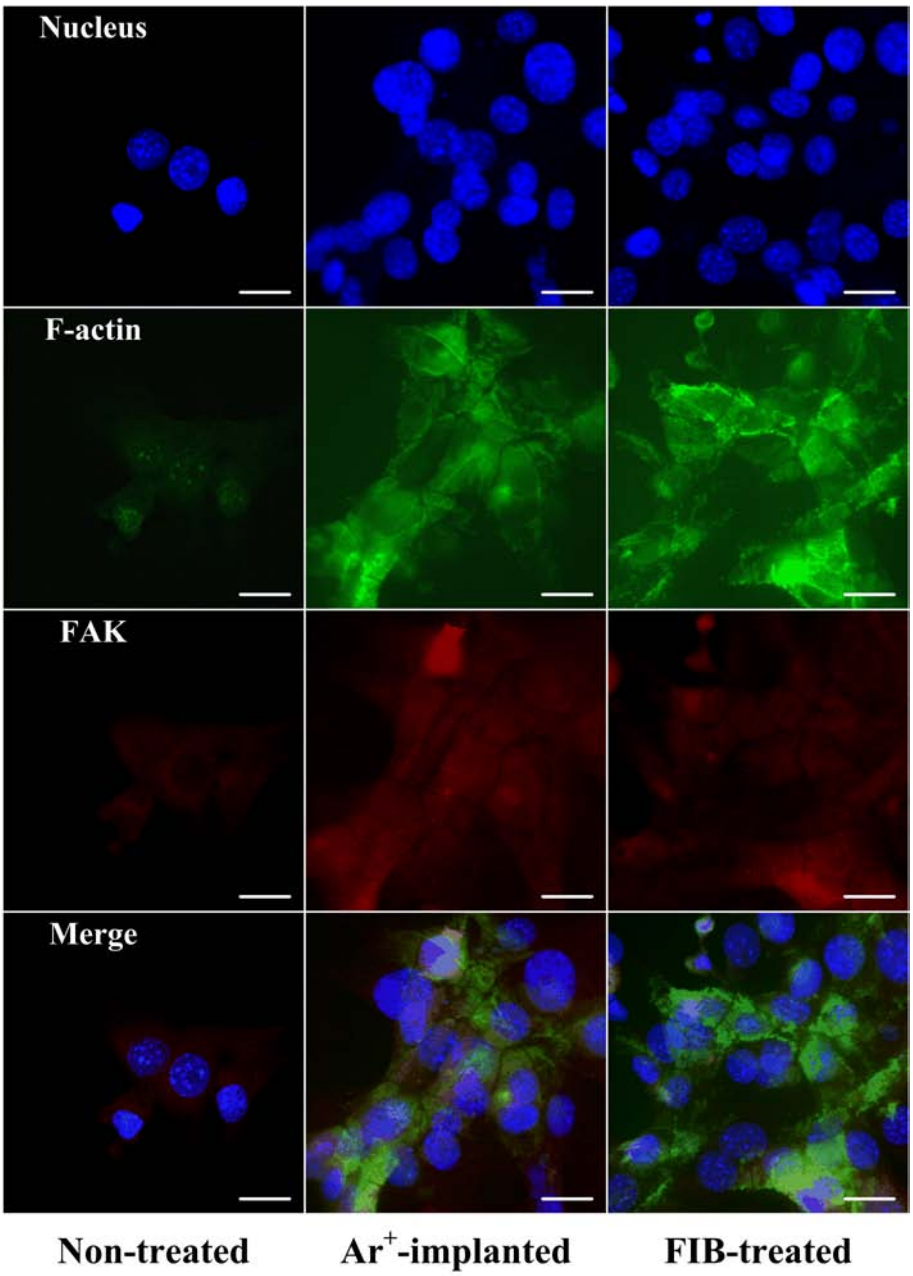

Figure 4.9. Confocal images of NIH3T3 fibroblasts after 1 day of culture (bar size = 20 μm). F-actin and FAK are stained green and red, respectively.

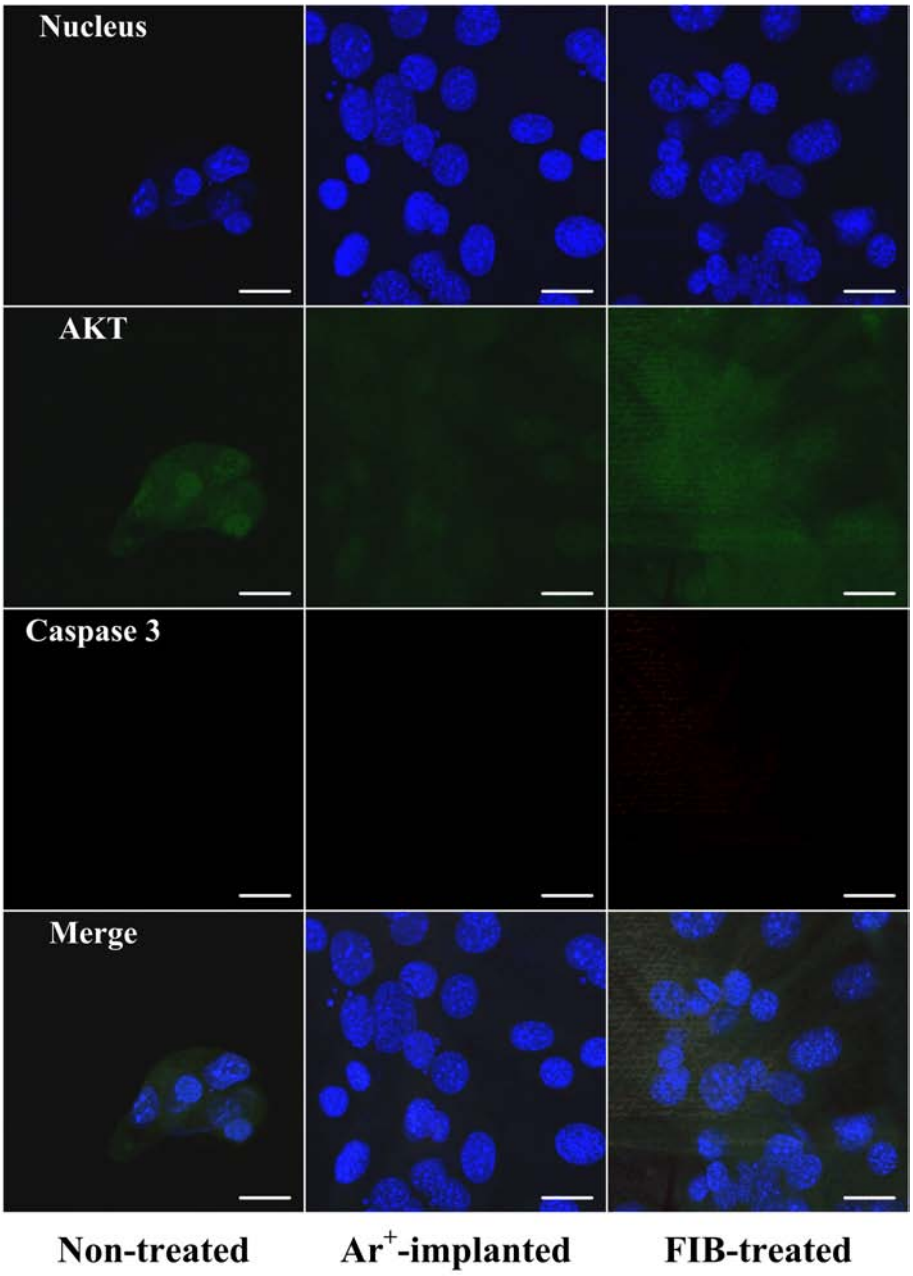

Figure 4.10. Confocal images of NIH3T3 fibroblasts after 1 day of culture (bar size = 20 μm). AKT and caspase 3 are stained green and red, respectively.

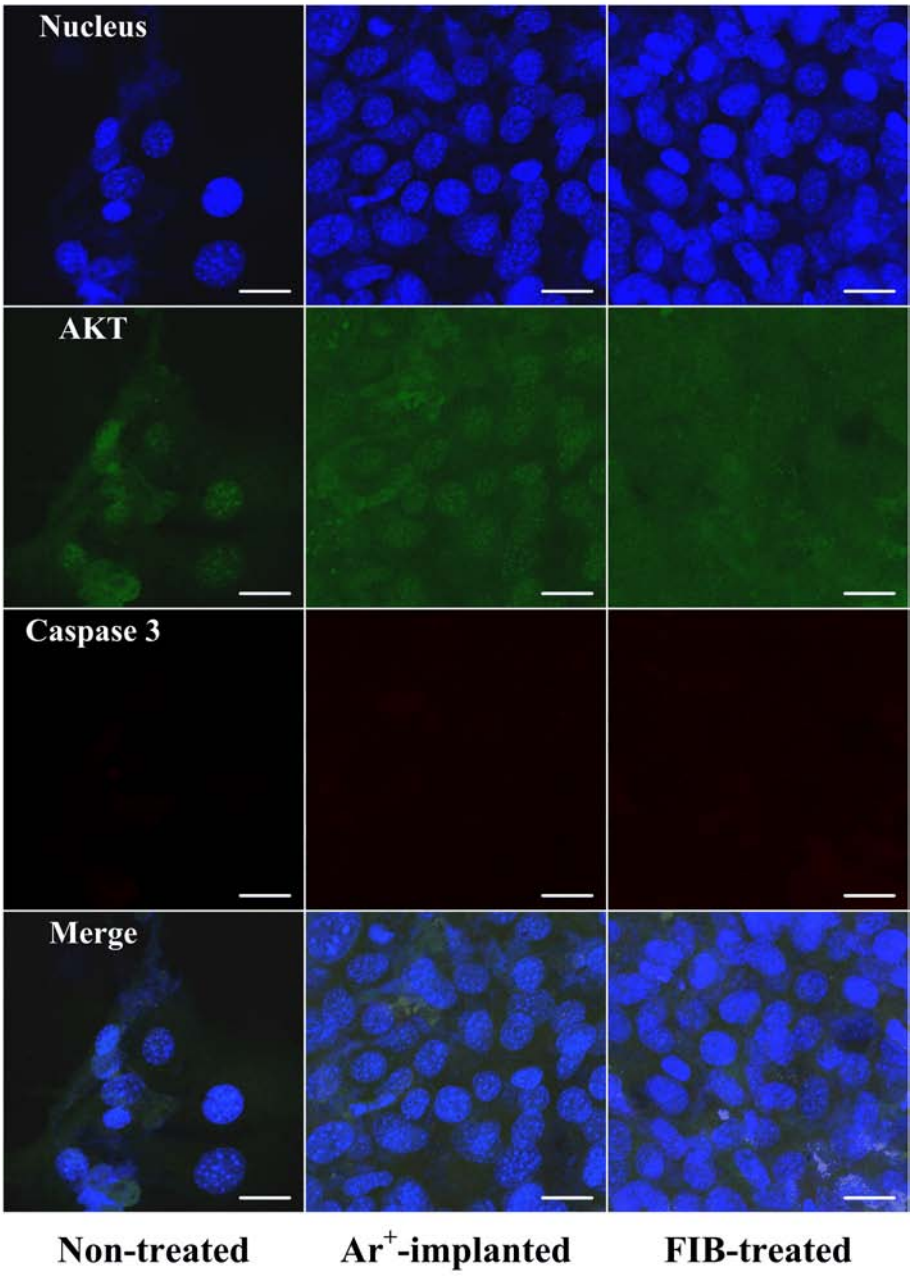

Figure 4.11. Confocal images of NIH3T3 fibroblasts after 3 days of culture (bar size = 20 μm). AKT and caspase 3 are stained green and red, respectively.

4.3.6. Cell proliferation assay

Figure 4.12 shows MTT assay results of NIH3T3 fibroblasts during 3 days of culture. During cell culture, cell proliferation on FIB-treated and Ar^+-implanted PU substrates was significantly increased ($P < 0.05$) compared with non-treated ones. Furthermore, at day 2 and day 3, cell proliferation on the FIB-treated PU substrates was also significantly increased ($P < 0.05$) compared with the Ar^+-implanted ones. The degree of cell proliferation of each group between 1 and 3 days of culture was quite different. The number of NIH3T3 cells cultured on the non-treated, Ar^+-implanted and FIB-treated PU substrates increased by 415, 324 and 386 % during cell culture, respectively.

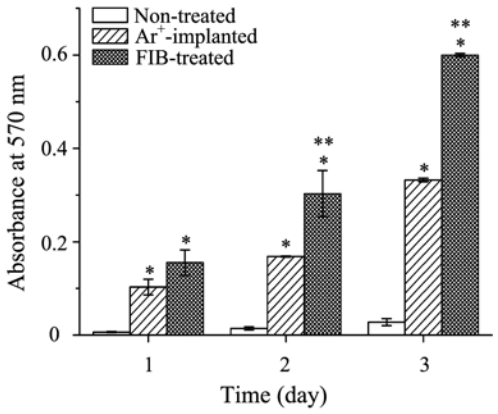

Figure 4.12. Cell proliferation assay results of NIH3T3 fibroblasts cultured on PU substrates (n = 3): Values are expressed as mean ± standard deviation; P^* < 0.05 when compared with non-treated; P^{**} < 0.05 when compared with Ar^+-implanted.

4.4. Discussion

It has been demonstrated that FIB has been used for the preparation of three-dimensional samples showing cell-substrate interfaces by milling process. In this study, however, it is confirmed that FIB can be used for surface modification as a tool for ion implantation like well-established plasma immersion ion implanters and other ion beam implanters. Compared with the existing ion beam implanters, the surface modification of polymeric materials by FIB treatment has many advantages. Firstly, fast physico-chemical modification is possible for small surface areas. It should be noted that only 800 × 700 μm^2 can be modified by each scan even at very low resolution in a very short time. Secondly, wrinkles can be formed even at low ion doses. In this study, aligned wrinkles were formed on the surfaces of FIB-treated PU substrates when ion doses were between 1×10^{12} and 1×10^{13} ions/cm^2. However, in the cases of Ar^+-implanted PU substrates, wrinkles were not formed under the same conditions. Moreover, in the cases of Kr^+-implanted PU substrates (see Appendix C), surface wrinkles whose size were similar to those of the FIB-treated PU substrates were formed when ion doses higher than 1×10^{15} ions/cm^2 were applied. Lastly, because modified area can be controlled by its position and scanning range, simple fabrication of hybrid patterns on polymeric substrates is feasible without mask.

The mechanism of the formation of surface wrinkles on a polymeric substrate using FIB treatment is very similar to that of conventional ion implantation. During FIB treatment, the surface layer of a polymer substrate is thermally expanded. At the same time, the crosslinking and carbonization of polymer chains inside the surface layer occurs to form hard skin on the surface of the polymer substrate. Afterwards, releasing heat from the polymer substrate induces compressed stress and surface deformation. This deformation can play an important role in the creation of various surface wrinkles

with straight, herringbone and hierarchical patterns [82-84]. Furthermore, the formation of surface wrinkles are dependent on polymer substrate used, temperature and parameters of ion irradiation such as ion species, ion energy and ion dose.

Because different ion species are used for surface modification in this study, their effects on the formation of surface wrinkles may not be ignored. In general, heavier ions tend to form thinner hard skin at the same ion energy. Besides, while ion beams irradiated from conventional ion beam sources can modify the entire area of target surface at one time, those irradiated from FIB source can sweep target surface from top left to bottom right (raster scanning). In addition, treatment time is also different between FIB treatment and conventional ion implantation even if same ion dose is applied. Therefore, the diffusion of generated heat and compressed stress of FIB-treated PU samples might be different from that of Ar^+-implanted PU substrates. Hence, as shown in Figures 4.2 and 4.3, submicron surface wrinkles can be formed on PU substrates by FIB treatment even at low ion doses.

As shown in Table 4.3, after FIB treatment, C=O and C-O functional groups on the surfaces of PU substrates increased to an appreciable extent. During the implantation process of ion particles, collision between polymer chains and ion particles takes place in the surface layer of polymer substrates. As a result, some of the polymer chains are broken and radicals are subsequently formed. And these radicals transform into the functional groups such as C-O, C=O and COO through depolymerization, crosslinking and reactions with atmospheric oxygen [114]. The generated functional groups increase the surface energy and wettability of the polymer substrates. It is noteworthy that, compared with conventional Ar^+ implantation (1×10^{15} ions/cm^2), FIB treatment brought about better chemical modification of PU surfaces even at comparatively low ion dose (1×10^{13} ions/cm^2).

Meanwhile, gallium that liquefies above room temperature is typically used for FIB

source. Because gallium ions are not the product of cell metabolism, if they are released from inner surface of a PU substrate to outer environment, they might exert a harmful influence on cellular immune system during cell culture. Therefore, the amount of implanted Ga^+ should be checked out before and after cell culture. From the results of ICP-MS and XPS, it is confirmed that gallium ions were not detected after washing samples with distilled water and ethanol. This also means that the amount of Ga^+ was extremely small, which lay beyond the detection range, or implanted ions were released before cell culture by washing. It is clear that cell growth was not affected by Ga^+ which might exist on the surface or inside of PU substrates. In addition to the measurement of implanted Ga^+ content, foreign body reaction was also tested to confirm that FIB treatment PU substrates do not trigger a response of the immune system. As shown in Figure 4.7, like RAW 264.7 cells cultured on non-treated and Ar^+-implanted PU substrates, those cultured on FIB-treated PU substrates did not transform into multinucleated giant cells. Hence, this result also indicates that FIB treatment did not induce any cellular immune responses in this study.

Because the activation of biological molecules such as protein kinase and protease produces various cellular responses, the identification of these proteins involved in cell adhesion, cell survival and cell apoptosis is very important to understand the influence of FIB treatment. As shown in Figures 4.8 and 4.9, the expression of F-actin and FAK, which are closely related to cell adhesion, was clearly observed in NIH3T3 fibroblasts cultured on FIB-treated PU substrates compared with those on non-treated PU substrates, implying enhanced cell adhesion to the FIB-treated PU substrates. Moreover, considering the expression of AKT and caspase 3, it showed that cells cultured on the FIB-treated PU substrates kept proliferating well without any symptoms associated with cell death within short-term cell culture. Therefore, it is evident that FIB treatment can improve the biocompatibility of PU substrates.

Compared to conventional ion implantation, FIB treatment enables morphological and chemical modification of PU substrates even at low ion doses. Although foreign body reactions to both PU substrates seem to be similar to each other, physico-chemical changes induced by FIB treatment will enhance initial adhesion of NIH fibroblasts. As a result, cell proliferation on FIB-treated PU substrates was significantly increased during cell culture compared to non-treated and Ar^+-implanted ones. Also, this trend may be attributed to increased adsorption of cell adhesion proteins like collagen, fibronectin and laminin onto the FIB-treated PU substrates at the early stage of cell culture.

4.5. Conclusions

The focused ion beam (FIB) has proven to be a useful tool for ion implantation of polyurethane (PU) substrates like other conventional ion implanters. Increased functional groups such as C=O, COO and C-O on the surfaces of FIB-treated PU substrates improved surface wettability. Furthermore, even at low ion doses, FIB treatment created surface wrinkles whose wavelength and amplitude were in the submicron range. These physico-chemical changes led to enhanced biocompatibility of FIB-treated PU substrates so that NIH3T3 fibroblasts exhibited better adhesion and proliferation than non-treated and Ar^+-implanted ones. Therefore, the utilization of FIB-treatment will be applicable to surface modification of polymer-based biomaterials. For example, because various wrinkles can mimic the morphologies of the extracellular matrix of connective tissue in animals or human body, the FIB-treated polymer substrates might be used as templates for in vitro cell studies.

V. Fabrication of Extracellular Matrix-like Scaffolds using Focused Ion Beam and Oxygen Plasma Treatments

5.1. Introduction

Studies of cellular responses to micro- and nano-structured surfaces have had a long history in the field of tissue engineering. One of central issues in current tissue engineering is the physio-chemical mimicry of the extracellular matrix (ECM) of human body which mainly consists of interlocking meshes of fibrous proteins and glycosaminoglycan. The ECM is an intricate structural entity providing structural support and anchorage to human cells, regulating intercellular communication and activating various cellular functions in combination with cellular growth factors. From a morphological point of view, the ECM is composed of wrinkles, pores, fibers and pits with sizes ranging from several tens to hundreds of nanometers [36]. Therefore, the development of ECM-like scaffolds is necessary for understanding and improving the cellular behavior such as adhesion, spreading, migration and proliferation of cells during *in vitro* or *in vivo* studies.

Due to the softness and elasticity of polymers, they have been used to fabricate scaffolds for soft tissues. For structural mimicry of native ECM, various methods such as photolithography [42, 44, 47, 50, 74, 115-117], electrospinning [61, 118-122] and phase separation [123-125] have been applied to polymeric materials. Unfortunately, because these methods are solution-based processes, the removal of residual resist or solvent is naturally needed. Furthermore, in most cases, related wet processes are not eco-friendly. Therefore, environment-friendly dry processes for the fabrication of

ECM-like scaffolds are more common practice.

The surface modification using focused ion beam (FIB) emerges as one of the leading candidates because it is a completely dry process. In addition, like other ion implantation, FIB treatment can induce the physico-chemical changes of polymeric surfaces. During FIB treatment, depending on ion energy, ion dose and polymer substrate used, surfaces with various wrinkle types such as unidirectional alignment, herringbone pattern and hierarchical structure can be formed on a polymeric substrate in just one step process [82-83]. Also, due to the radicals created by collision between gallium ions (Ga^+) and polymer molecules, a considerable number of hydrophilic functional groups, resulting from reactions with oxygen in the air, are produced on the surface of the polymer substrate. With these morphological and chemical modifications, FIB treatment can be adopted to mimic the complex structures of ECM. However, in spite of the increased hydrophilic functional groups, the surface wettability of a FIB-treated substrate is not improved as well as can be expected due to the existence of surface wrinkles whose size ranges from several tens to hundreds of nanometers.

In this study, to develop ECM-like scaffolds, oxygen (O_2) plasma treatment was applied to the FIB-treated polyurethane (PU) substrates. Plasma treatment is well-known and effective method for the enhanced surface wettability of polymers [102, 126-128]. With O_2 plasma treatment, the surface morphologies of FIB-treated PU substrates were observed and the topological properties of them were analyzed. In order to examine the improved surface wettability of FIB-treated PU substrates after O_2 plasma treatment, water contact angles were measured and the surface chemical composition also analyzed. To verify the influence of O_2 plasma treatment on the adhesion and proliferation of cells, human skin fibroblasts were cultured on the PU scaffolds for 5 days and cell proliferation assay was conducted for quantitative assessment using cell counting kit-8 (CCK-8). The morphologies of cultured

fibroblasts were also observed. The obtained results from PU scaffolds fabricated by FIB and O_2 plasma treatments were compared with those of non-treated and FIB-treated PU substrates.

5.2. Experimental

5.2.1. Materials

Pellethane® 2103-80AE (Dow Chemical Co., USA), commercial ether based thermoplastic PU, was obtained and used after thorough washing with distilled water. Dulbecco's modified Eagle's medium (DMEM) was obtained from Sigma-Aldrich Co. (Saint Louis, MO, USA) and fetal bovine serum (FBS) was purchased from GIBCO (Chagrin Falls, OH, USA). A CCK-8 was obtained from Dojindo Laboratories (Kumamoto, Japan).

5.2.2. Preparation of PU films

An 11 wt% PU solution was prepared by dissolving 5.0 g of Pellethane® 2103-80AE in THF with stirring at room temperature for 6 hours to obtain homogeneous solution. And then, the PU solution was kept in a thermostat oven at 25 ℃ overnight to be stabilized. With this solution, PU thin films were fabricated by solvent casting method and cured in a vacuum oven at 50 ℃ for 72 hours to remove residual solvent in the PU films. The thickness of the produced PU films was about 120 μm. For later experiments, they were cut into circular discs having a diameter of 13 mm and washed with distilled water and ethanol.

5.2.3. FIB and O_2 plasma treatments of PU substrates

For Ga^+ irradiation on the surfaces of PU substrates, a dual beam system (NOVA 200; FEI Company, Hillsboro, OR, USA) which combined field emission scanning electron microscope (FE-SEM) and focused ion beam was utilized. The PU substrates were placed in the vacuum chamber under a pressure of 5×10^{-5} Pa during FIB treatment. The acceleration voltage and ion current were kept at 30 kV and 5 nA, respectively. The irradiation angle between the incident beam and the surface normal was fixed at 0° and the beam dwell time was kept at 30 μs for all samples. The applied ion dose was 4.3×10^{12} ions/cm^2 and the FIB-treated area was 930 × 780 μm^2 for each scan when the dual beam system was operated in digital raster mode. As shown in Figure 5.1(a), 72 scans which covered about 39.3 % of entire surface area of the PU substrate were performed without overlapping areas (Figure 5.1(b)).

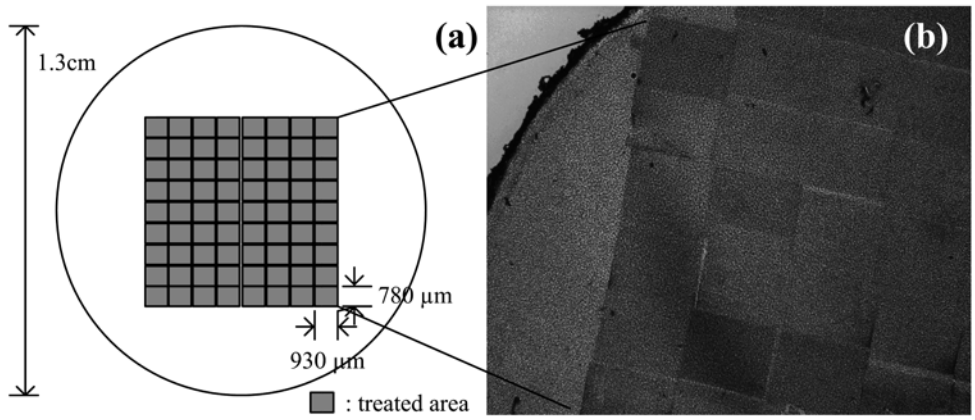

Figure 5.1. FIB treatment of a PU substrate: (a) A schematic drawing of a FIB-treated PU sample and (b) An image of a FIB-treated PU substrate magnified to 13 times its actual size.

O_2 plasma treatment of FIB-treated PU substrates was performed using a lab-scale low temperature and pressure plasma treatment device (Europlasma, Belgium). As a power source, a 300 W RF generator was used. The gas flow rate and treatment time were 100 sccm and 10 minutes, respectively. The plasma treatment was conducted on the FIB-treated area with the help of PU masks. Hereafter, PU substrates fabricated by FIB and O_2 plasma treatments are referred to as FIB/PL-treated PU scaffolds.

5.2.4. Observation of surface morphologies of PU substrates

The surface morphologies of PU samples were analyzed using FE-SEM (JSM-6700F; JEOL, Japan). Because PU films are highly nonconductive, a layer of gold (4 nm thickness) was coated onto their surface by a sputter coater to avoid surface charging. The beam voltage of 5 kV was used in this study.

To analyze the topological properties of the surface wrinkles of FIB-treated substrates, atomic force microscopy (AFM) (XE-100; Park Systems Corp., Republic of Korea) was carried out in dynamic non-contact mode with a silicon tip. Square frames having edges of 3 μm with 153 × 153 data points were used to acquire AFM images. The scan rate for measurements was 1 Hz.

5.2.5. Measurement of implanted Ga^+ content in FIB-treated PU substrates

The amount of implanted Ga^+ ions was determined by inductively coupled plasma mass spectrometry (ICP-MS) (ELAN 6100; Perkin-Elmer SCIEX, USA). Argon plasma (6000 K) source was used in this experiment. The RF power and the sample injection flow rate were 1100 W and 1.00 ml/min, respectively. FIB-treated samples were analyzed three times and average values were obtained.

5.2.6. Surface chemical analysis of PU substrates

The surface chemical composition of PU samples were confirmed by X-ray photoelectron spectroscopy (XPS) system (AXIS-His; KRATOS, Japan). To minimize the charging effects of the nonconductive PU specimens, neutralizing was carried out. The Mg-Kα (150 W) source was used in the hybrid mode with 90° take-off angles. The survey scan was performed within the binding energy range of 0 - 1000 eV. The pass energy of 160 eV was applied to the samples during the survey scan. To calculate the elemental composition of the PU samples, the XPS spectra were processed using an iterative least-squares fitting routine on the basis of Gaussian and Lorentzian functions as well as the Shirley-type background subtraction. The binding energies of all the spectra were referenced to the 285 eV corresponding to the peaks of C-C and/or C-H groups (C1s).

To get more information about the chemical bonds and molecular structural change of PU substrates, attenuated total reflectance Fourier transform infrared spectroscopy (ATR FT-IR) was also carried out (Nicolet 6700 FT-IR spectrometer; Thermo Scientific, USA). The absorbance spectra of PU substrates in the range of 4000 - 600 cm^{-1} were measured with 32 scans per sample at a spectral resolution of 4 cm^{-1}.

5.2.7. Surface wettability measurement of PU substrates

To check out the surface wettability of PU substrates, water contact angles were measured using a contact angle measuring instrument (DSA 100; KRŰSS, Germany). The static sessile drop method was applied. A drop of distilled water with a volume of about 5 µl was used for each measurement.

5.2.8. Cell culture and seeding on PU substrates

Under informed consent, human dermal fibroblasts were extracted from the forehead skin tissue of a male patient undergoing plastic surgery. These cells were cultured in a culture flask containing DMEM supplemented with 10 % FBS and 1 % antibiotics at 37 ℃ and 5 % CO_2. They were serially passaged at every 80 % confluence level. During passaging, the growth media was removed and the cells were washed with phosphate buffered saline (PBS). And then, trypsinization was done at 37 ℃ for 5 minutes to detach the cells from the bottom of the culture flask. After the addition of PBS and growth media, the detached cells and the culturing media were mixed and transferred to new plates for the next passage.

Before cell seeding, the FIB-treated and FIB/PL-treated PU substrates were washed with warm distilled water (40 ℃) to remove implanted Ga^+. Prepared PU substrates sterilized by ethylene oxide gas were put onto 24-well plates. A suspension containing 1×10^4 fibroblasts of their second passage was carefully transferred to each well. The cells were cultured for 1, 3 and 5 days at 37 ℃ and 5 % CO_2. The basal growth media was DMEM containing 10 % FBS and fresh culturing media was replenished every two days. For comparative study, cell culture on tissue culture polystyrene (TCPS) dishes was also carried out and non-treated PU substrates were used as controls.

5.2.9. Observation of cell morphologies

After 1 day and 5 days of culture, morphological observation of fibroblasts cultured on PU substrates was performed using fluorescence microscopy (Croscope Inverte; Olympus, Japan) equipped with a digital camera. The cell-seeded PU substrates were

washed two times with PBS and then stained with PBS solution containing 0.1 % crystal violet and 50 % methanol for 5 minutes. After the dye solution was aspirated, the cell-seeded PU substrates were rinsed with PBS twice. Images of the cell-seeded PU samples were captured at a magnification of 100×.

FE-SEM (JSM-6700F; JEOL, Japan) was also used to characterize the cell morphology on the PU samples. Primary fixation of the fibroblasts was carried out with modified Karnovsky's fixative containing 2 % paraformaldehyde and 2 % glutaraldehyde in 0.05 M sodium cacodylate buffer (pH 7.2) at 4 °C for 2 hours. After washing with 0.05 M sodium cacodylate buffer (pH 7.2) at 4 °C for 10 minutes, post-fixation was done with 1 % osmium tetroxide in 0.05 M sodium cacodylate buffer (pH 7.2) at 4 °C for 2 hours. And then, the cell/substrate complexes were washed twice with distilled water at room temperature. After dehydration with a series of graded ethanols of 30, 50, 70, 80, 90 and 100 %, the dried samples were sputter-coated with gold and SEM images were obtained.

5.2.10. CCK-8 assay

For quantitative analysis of cell proliferation, CCK-8 assay was conducted according to manufacturer's technical manual [129] with some modifications for a 24-well plate version. After measuring the absorbance at 450 nm with an ultraviolet-visible (UV/VIS) spectrophotometer (Biospec, UK), the absorbance value was converted into the number of cells per well on the basis of standard curve. In particular, to investigate the effects of FIB and O_2 plasma treatments separately, fibroblasts cultured on plasma-treated PU substrates were also assayed. For this assay, all experiments were carried out in triplicate. Results were expressed as mean ± standard deviation. Statistical differences in the cell proliferation of different substrates were

analyzed by one-way analysis of variance (ANOVA). When the *P*-values were less than 0.05, differences were considered statistically significant.

5.3. Results

5.3.1. Surface morphologies of a FIB/PL-treated PU scaffold

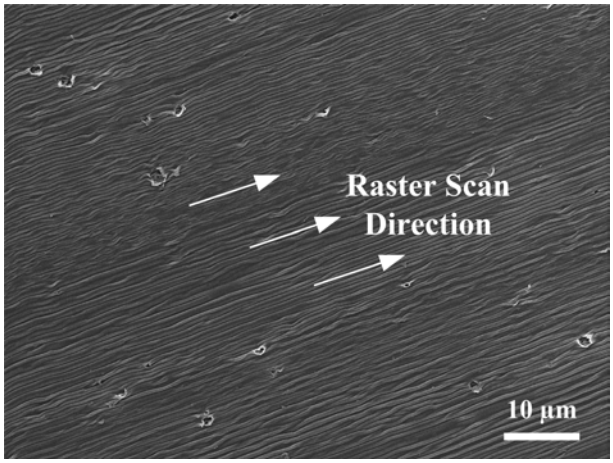

Figure 5.2. A SEM image of a FIB/PL-treated PU scaffold.

Figure 5.2 shows a SEM image of a FIB/PL-treated PU scaffold. There were no significant morphological differences between before and after O_2 plasma treatment of FIB-treated PU substrates. Figure 5.3 shows various types of surface wrinkles of FIB/PL-treated PU scaffolds. In this study, it appeared that, in most parts of FIB-treated area, surface wrinkles with various wavelengths and amplitudes were aligned parallel to the direction of raster scan. However, herringbone-like surface wrinkles (Type D) were also created during FIB treatment. In the case of unidirectional aligned wrinkles, small-sized (Type A), medium-sized (Type B) and large-sized (Type C)

surface wrinkles whose wavelength and amplitude were in the submicron range were observed. Their wavelength and amplitude are summarized in Table 5.1. Figure 5.4 shows the root-mean square surface roughness of FIB/PL-treated PU scaffolds. Because surface roughness depends on the amplitude of surface wrinkles, Type B had the largest value of surface roughness compared to that of non-treated PU substrates.

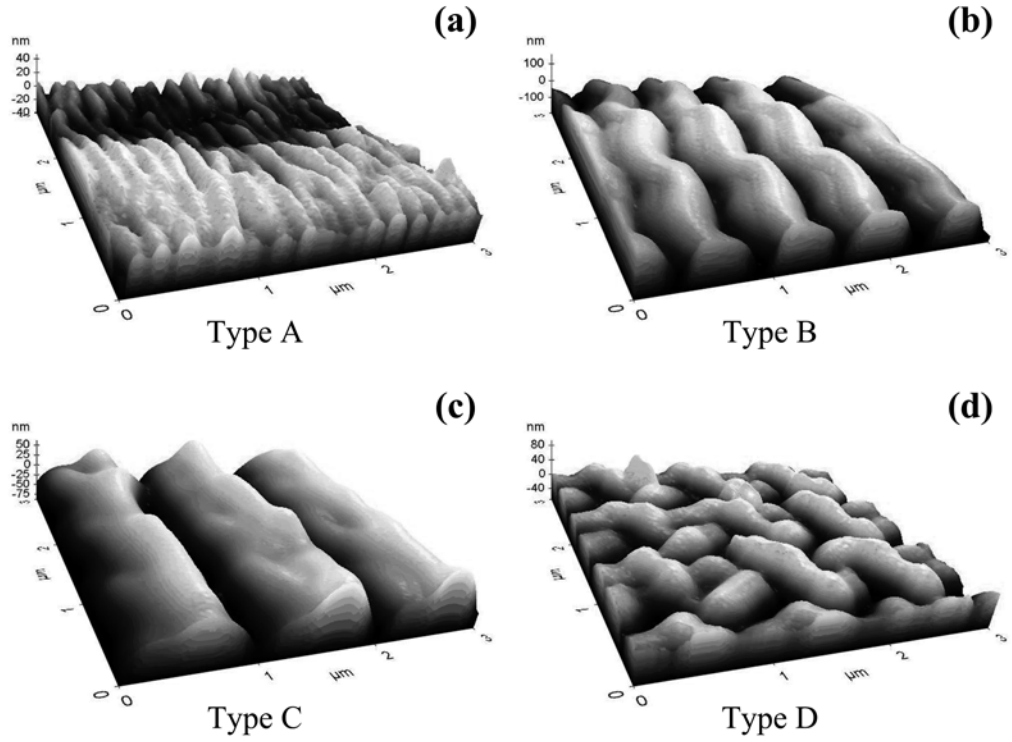

Figure 5.3. AFM images of the surface wrinkles of FIB/PL-treated PU scaffolds: (a) Unidirectional, small-sized, (b) Unidirectional, medium-sized, (c) Unidirectional, large-sized and (d) Herringbone-like.

Table 5.1. Aligned surface wrinkles of FIB/PL-treated PU scaffolds.

Sample	Aligned wrinkle	
	Wavelength (nm)	Amplitude (nm)
FIB/PL-treated (Type A)	180.39 ± 13.41	38.81 ± 4.16
FIB/PL-treated (Type B)	682.41 ± 10.99	220.26 ± 18.99
FIB/PL-treated (Type C)	1041.02 ± 58.83	129.20 ± 12.86

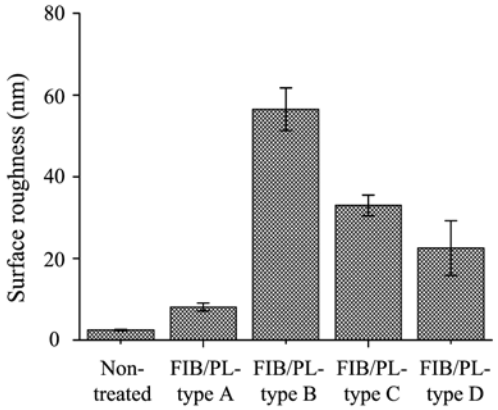

Figure 5.4. Root-mean square surface roughness of FIB/PL-treated scaffolds.

5.3.2. Implanted Ga^+ content of FIB/PL-treated PU scaffolds

Table 5.2. Ga^+ content of FIB/PL-treated PU samples.

Sample status	Amount of implanted Ga^+ (ppb)
After FIB-treatment	358 ± 67
After washing with distilled water (20 °C)	33 ± 16
After washing with distilled water (40 °C)	-

Although gallium ions and gallium compounds are not considered to be particularly toxic to the human body in low doses, they might induce inflammation [112-113]. Therefore, the Ga^+ amount of FIB/PL-treated PU scaffolds should be measured. As shown in Table 5.2, the amount of implanted Ga^+ after washing with cold distilled water decreased by 90.8 % compared to the amount measured after FIB-treatment. After washing with warm distilled water, the implanted gallium ions were not detected. In this study, to avoid the side effects of Ga^+ on cell growth, FIB-treated PU substrates for cell culture were washed with 40 °C distilled water before cell seeding.

5.3.3. Surface chemical analysis of PU substrates

Figures 5.5, 5.6 and 5.7 show the C1s, O1s and N1s XPS spectra of PU substrates, respectively. Also, Table 5.3 shows the quantitative summary of the functional groups and surface elemental composition of PU substrates. Analyzed element is expressed as a right-hand superscript *. Considering the C1s and O1s spectra of a non-treated PU substrate, its surface were enriched with the -C-C- and C-O-C functional groups of the soft segments of PU to minimize interfacial free energy. After FIB-treatment, new functional groups such as -C=NH and $-CNH_2$ were created on the surfaces of PU substrates. In addition, after O_2 plasma treatment, $(C=O)NH_2$ functional group was also created.

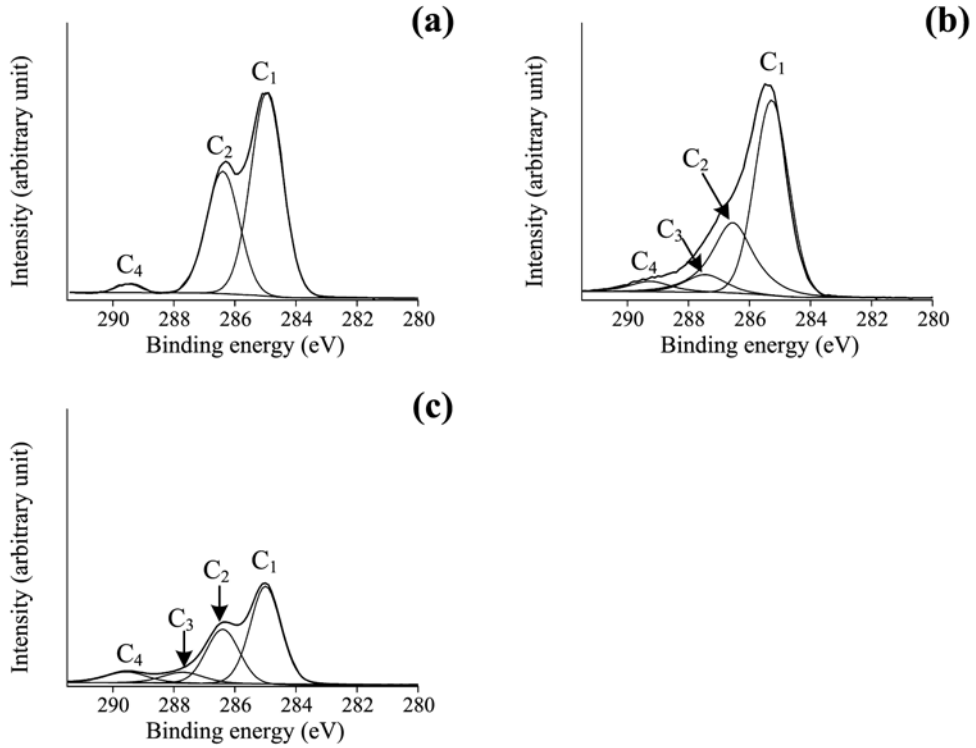

Figure 5.5. C1s XPS spectra of PU substrates: (a) Non-treated, (b) FIB-treated and (c) FIB/PL-treated.

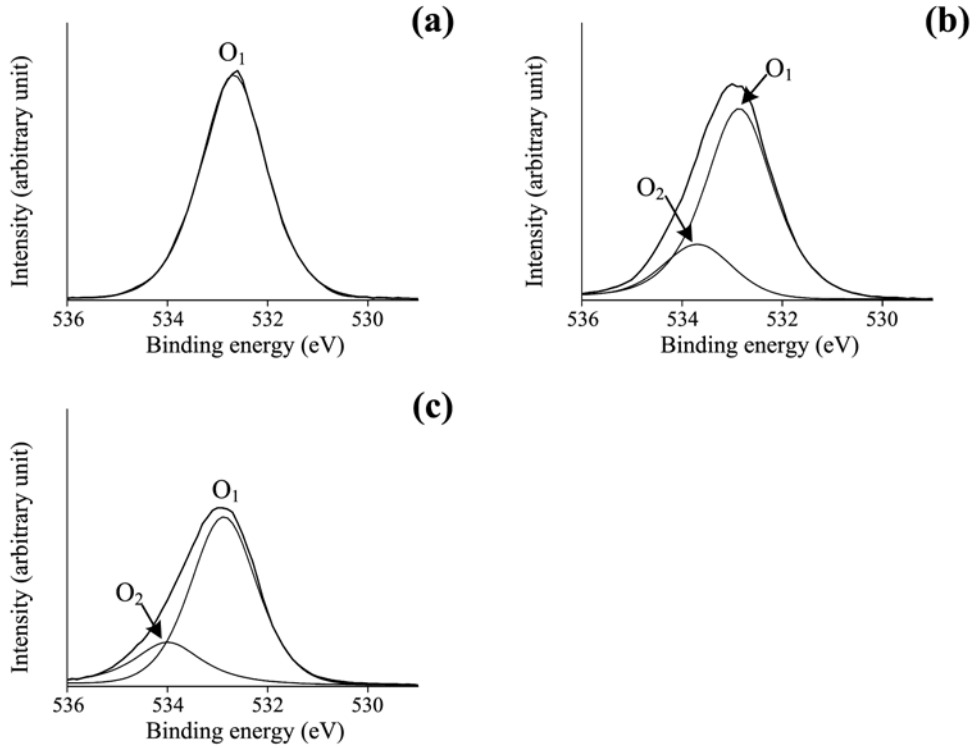

Figure 5.6. O1s XPS spectra of PU substrates: (a) Non-treated, (b) FIB-treated and (c) FIB/PL-treated.

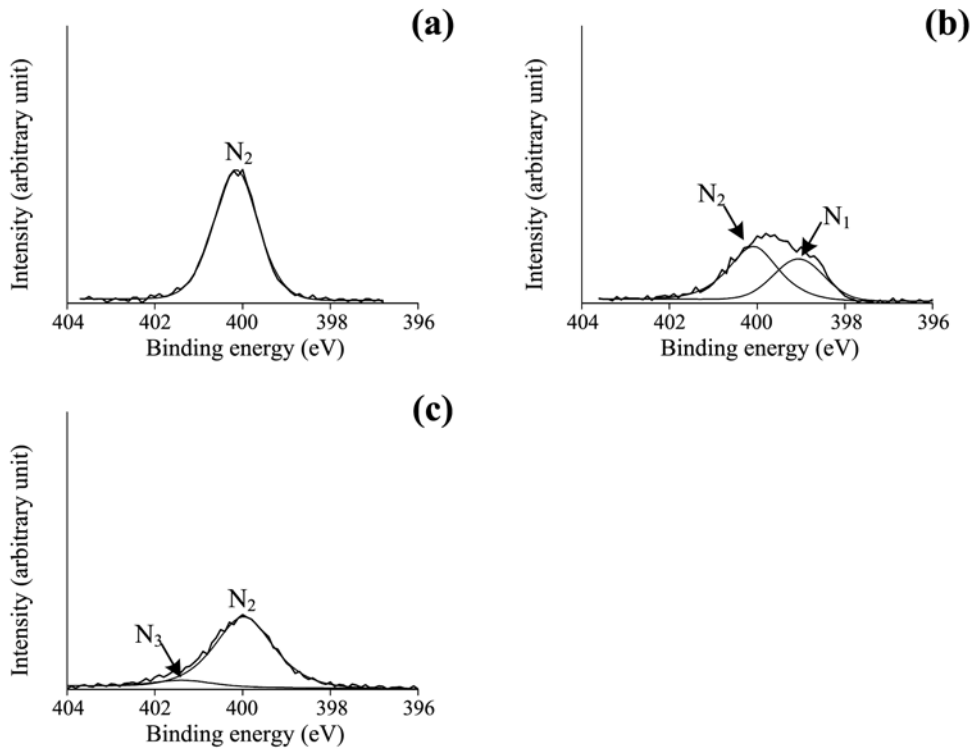

Figure 5.7. N1s XPS spectra of PU substrates: (a) Non-treated, (b) FIB-treated and (c) FIB/PL-treated.

Because the peaks of C-O-C and C-OH functional groups overlapped each other at a binding energy of around 286.6 eV, their identification was not easy from the XPS spectra of PU substrates. In addition, the peaks of -(C=O)O- or -(C=O)OH also overlapped each other at a binding energy of around 289.5 eV. However, as shown in Figure 5.8, the ATR FT-IR spectra clearly demonstrated the increase of C-OH and -(C=O)OH functional groups of FIB/PL-treated PU substrates. After FIB treatment, the intensity of the characteristic peaks of PU, which are located at 1597 and 1416 cm^{-1} from benzene rings, at 1527 cm^{-1} from N-H bending and C-N stretching mode of the

urethane group and at 3325 cm^{-1} from the stretching band of hydrogen bonded N-H [8, 130-131], were decreased. Furthermore, the peaks at 1728 cm^{-1} from the ester stretching band of C=O and 1076 cm^{-1} from the stretching band of C-O-C [8] were also decreased implying that the molecular chains of PU were broken by implanted gallium ions during FIB treatment. However, after O_2 plasma treatment, the increase of absorbance in the range of 3300 - 3500 cm^{-1} which is characteristics of hydroxyl group (-OH) vibration [86] was observed indicating that a substantial portion of the ether and urethane functional groups of PU was transformed into C-OH and -(C=O)OH ones. In addition, Because C-H is most abundant and easy to be broken, its related peaks should be observed to examine the crosslinking process and the formation of radicals or new functional groups. The peaks at 1477 cm-1 from the bending band of C-H, 1365 cm-1 from the wagging band of C-H, 2329 cm-1 from the symmetric stretching band of C-H, and 2858 cm-1 and 2796 cm-1 from the symmetric stretching band of C-H were also slightly decreased.

As a result, it was confirmed that hydrophilic functional groups such as C-OH and -(C=O)OH on the surface of the FIB/PL-treated substrate appreciably increased in comparison with those of the non-treated and FIB-treated ones. On the other hand, the relatively hydrophobic -C-C- and C-O-C functional groups on the surface of the FIB/PL-treated substrate considerably decreased. Overall, oxygen-containing hydrophilic functional groups were increased or created by FIB and O_2 plasma treatments. As shown in Table 5.4, the O/C ratio of the FIB/PL-treated PU scaffolds was increased by 59.5 % compared to that of the non-treated PU substrates.

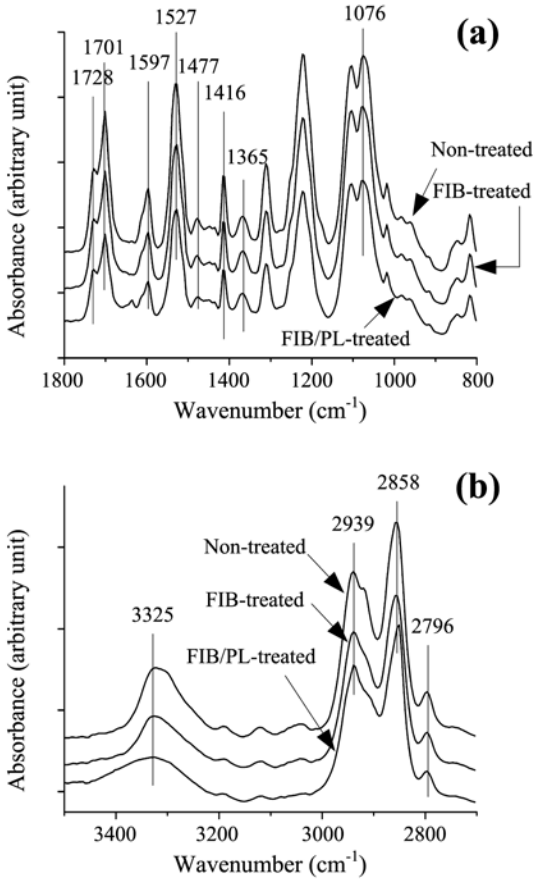

Figure 5.8. ATR FT-IR spectra of PU substrates in the wavenumber range of: (a) 1800 - 800 cm^{-1} and (b) 3500 - 2700 cm^{-1}.

Table 5.3. Functional groups and surface elemental composition of PU substrates.

Element		Functional group	Binding energy (eV)	Surface elemental composition of PU substrate (%)		
				Non-treated	FIB-treated	FIB/PL-treated
C	C_1:	-C*-C- or -C*-H	285.1	48.95	47.65	34.28
	C_2:	C*-O-C or C*-OH	286.6	29.78	23.37	27.30
	C_3:	-(C*=O)N-	287.6	-	5.19	5.24
	C_4:	-(C*=O)O- or -(C*=O)OH	289.5	1.50	3.23	5.31
N	N_1:	-C=N*H or -CN*H_2	339.4	-	0.84	-
	N_2:	-N*H(C=O)	400.1	2.49	1.15	2.85
	N_3:	-(C=O)N*H_2	401.4	-	-	0.25
O	O_1:	C-O*-C or C-O*H	532.9	17.27	14.73	19.41
	O_2:	-(C=O)O*- or -(C=O)O*H	534.0	-	3.83	5.36

Table 5.4. Total surface elemental composition and O/C ratio of PU substrates.

Sample	Element (%)			O/C ratio
	C	O	N	
Non-treated	80.23	17.27	2.49	0.215
FIB-treated	79.44	18.56	1.99	0.234
FIB/PL-treated	72.13	24.77	3.10	0.343

5.3.4. Surface wettability of PU substrates

Although the surfaces of PU substrates can be chemically modified by FIB treatment resulting in enhanced surface wettability, morphological changes such as wrinkles on the PU substrates during FIB treatment may reduce their surface

wettability. As shown in Figure 5.9, the FIB-treated and non-treated PU substrates did not show any significant differences in contact angle. However, soon after O_2 plasma treatment, the contact angle of the FIB-treated PU substrates considerably decreased from 81.4° to 15.4° due to the formation of hydrophilic function groups on the surfaces of them. Furthermore, it seemed that the effects of O_2 plasma treatment on the surface wettability of the non-treated and FIB-treated PU substrates were very similar to each other (Figure 5.9(b)).

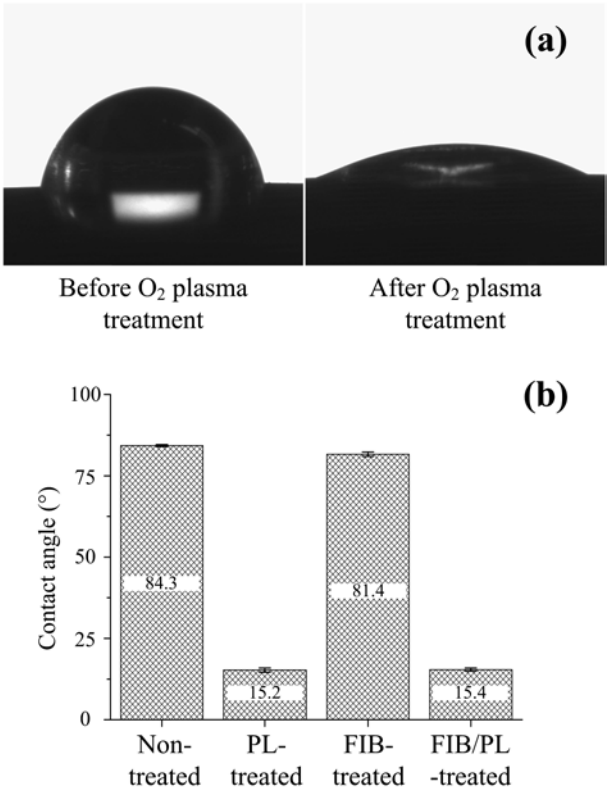

Figure 5.9. Water contact angles of PU substrates: (a) Photographs of water drops on FIB-treated PU substrates before and after O_2 plasma treatment and (b) Results of contact angle measurement.

5.3.5. Fibroblasts cultured on PU substrates

Figures 5.10 and 5.11 show fluorescent images of human dermal fibroblasts cultured on PU substrates and TCPS. Overall, fibroblasts cultured on different substrates were similar in size and shape. However, the number of adhered cells and the patterns of cell distribution were dependent on the substrates. After 1 day of culture, most of fibroblasts seeded on the non-treated PU substrates did not adhere to the surfaces of the non-treated PU substrates. Fibroblasts adhered to the non-treated PU substrates migrated and gathered together forming areas of locally dense population (Figure 5.10(a)). On the other hand, separated cells did not spread out and maintained their circular shape. In the case of fibroblasts cultured on FIB-treated PU substrates, it seemed that they also formed areas of locally dense population especially on the wrinkled surfaces of the FIB-treated PU substrates as shown in Figure 5.10(c). Even with FIB treatment, fibroblasts did not adhere to relatively smooth surfaces and they moved to the wrinkled surfaces. However, with the help of O_2 plasma treatment, fibroblasts were evenly distributed on the entire surface area of FIB/PL-treated scaffolds as shown in Figure 5.10(d). Even distribution of fibroblasts was also observed on the surfaces of TCPS (Figure 5.10(e)). After 5 days of culture, fibroblasts cultured on the non-treated PU substrates were evenly distributed (Figure 5.11(a)) but they did not cover the whole surface area of PU substrates. On the other hand, fibroblasts cultured on the FIB-treated and FIB/PL-treated PU substrates formed cell layers (Figures 5.11(c) and 5.11(d)). In some cases of cell culture on the FIB-treated PU substrates, fibroblasts still formed cell clusters showing highly dense population on the wrinkled surfaces.

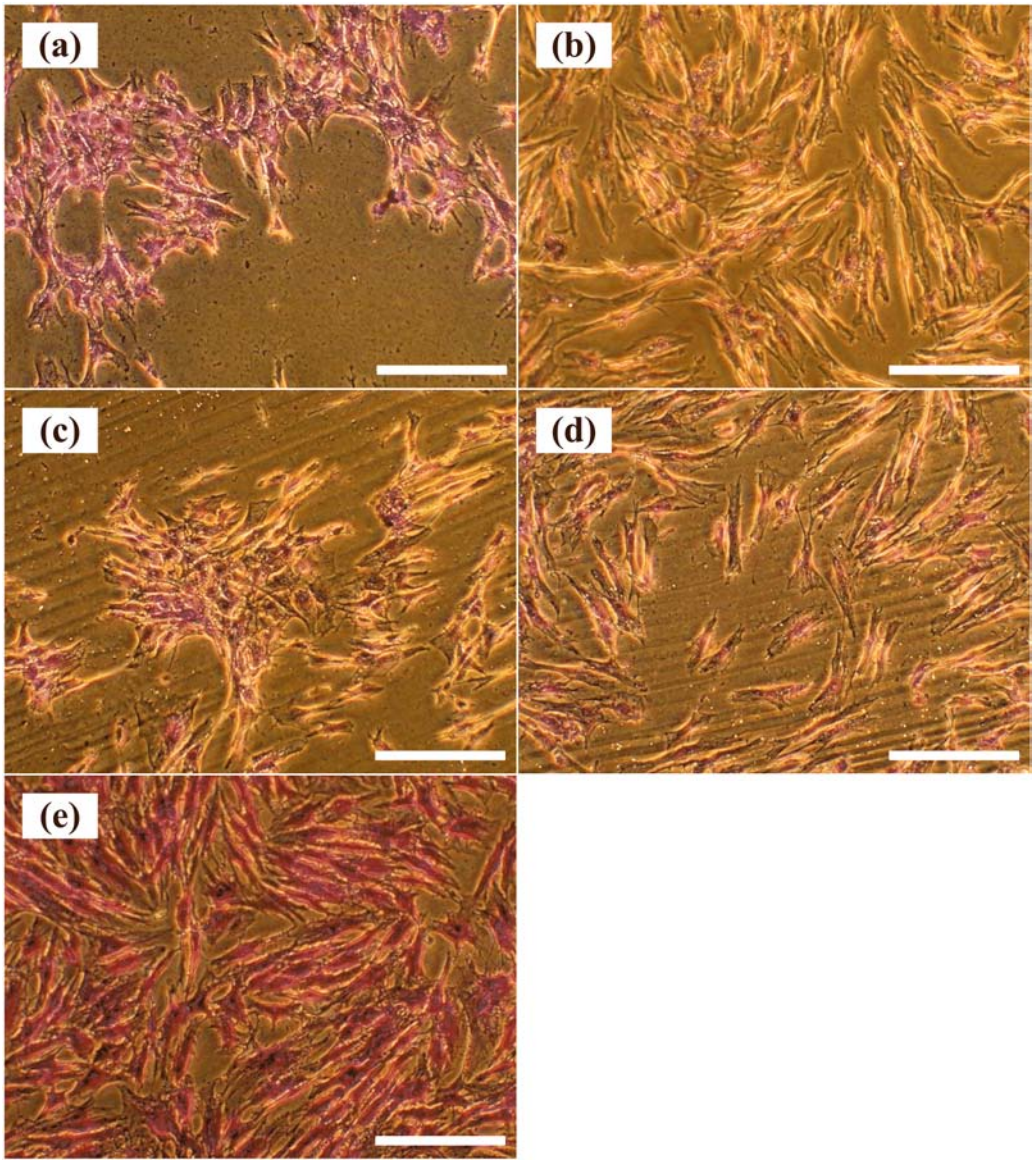

Figure 5.10. Fluorescent images of human dermal fibroblasts on PU substrates and TCPS after 1 day of culture (bar size = 25 μm): (a) Non-treated, (b) PL-treated, (c) FIB-treated, (d) FIB/PL-treated and (e) TCPS.

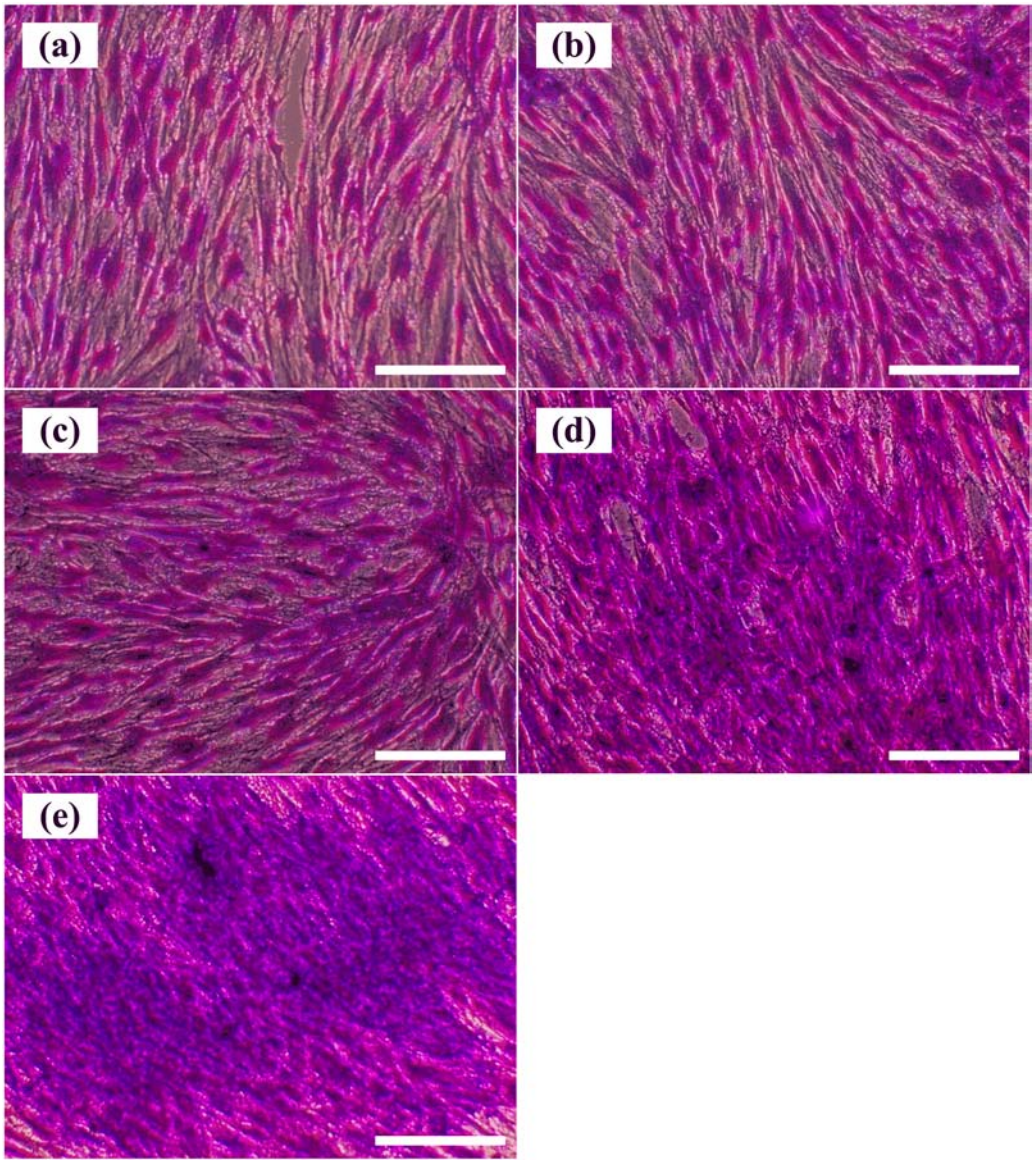

Figure 5.11. Fluorescent images of human dermal fibroblasts on PU substrates and TCPS after 5 days of culture (bar size = 25 μm): (a) Non-treated, (b) PL-treated, (c) FIB-treated, (d) FIB/PL-treated and (e) TCPS.

To ascertain how the surface morphologies of the FIB/PL-treated substrates can affect cell growth, SEM images were obtained. Figure 5.12 shows SEM images of human dermal fibroblasts on non-treated and FIB/PL-treated PU substrates after 3 days of culture. Compared with a fibroblast cultured on a non-treated substrate (Figure 5.12(a)), more filopodia protruded from the cell body of a fibroblast which adhered to a FIB/PL-treated wrinkled surface (Figure 5.12(b)). Furthermore, the inset of Figure 5.12(b) clearly shows filopodia protrusion guided by the surface wrinkles on the FIB/PL-treated PU substrates.

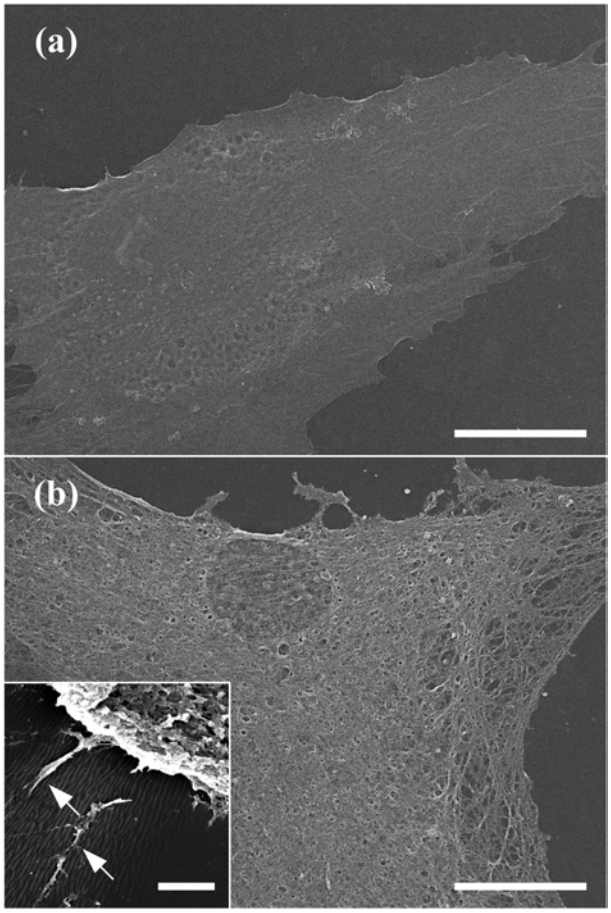

Figure 5.12. SEM images of human dermal fibroblasts on PU substrates after 3 days of culture (bar size = 10 μm): (a) Non-treated and (b) FIB/PL-treated.

5.3.6. Cell proliferation assay

Figure 5.13 shows CCK-8 assay results of human dermal fibroblasts cultured on PU substrates and TCPS. Compared to the number of fibroblasts cultured on non-treated PU substrates, those on PL-treated and FIB/PL-treated substrates were significantly increased ($P < 0.05$) throughout the culture period. Considering four

different types of PU substrates, the average cell density of FIB/PL-treated PU substrates was the highest during cell culture. In addition, the cell density of the FIB/PL-treated PU substrates was 5.50, 2.24 and 2.55 times greater than that of the non-treated PU substrates after 1, 3 and 5 days of culture, respectively. Figure 5.14 shows the cell proliferation efficiency of the PU substrates in comparison with TCPS. The FIB/PL-treated PU substrates definitely showed excellent efficiency compared with three other types of PU substrates. Their efficiency reached about 60 % during the culture period.

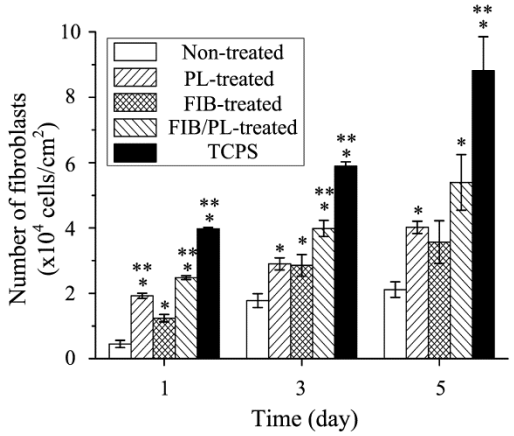

Figure 5.13. Cell Proliferation assay results of human dermal fibroblasts cultured on various substrates (n = 3): Results are expressed as mean ± standard deviation; $P^{*} < 0.05$ when compared with non-treated; $P^{**} < 0.05$ when compared with FIB-treated.

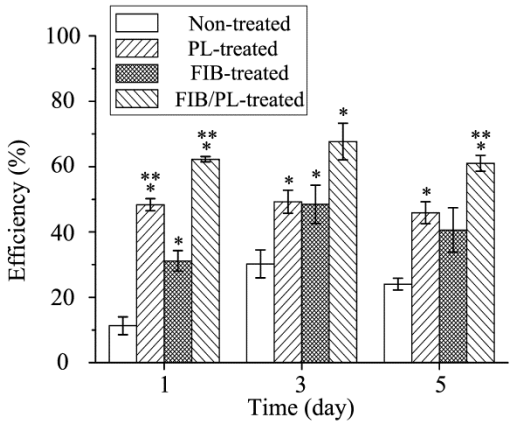

Figure 5.14. Cell proliferation efficiency of PU substrates during cell culture (n = 3): Results are expressed as mean ± standard deviation; $P^{*} < 0.05$ when compared with non-treated; $P^{**} < 0.05$ when compared with FIB-treated.

5.4. Discussion

Considering implanted gallium ions, they may exist in the form of stable elemental gallium or gallium oxide. Because higher temperatures than the T_m of PU, which ranges between 182 - 210 °C [132], are required for the formation of gallium oxide [133], it is believed that most gallium ions were reduced to elemental gallium in this study. As shown in Table 5.2, after washing with distilled water whose temperature is above the melting point of gallium (29.76 °C), implanted gallium was not detected. Therefore, the effect of implanted gallium ions on cell growth can be considered negligible. A plausible explanation for the disappearance of gallium is that elemental gallium changed from solid state to liquid one and it was released from FIB-treated PU substrates during washing. In addition, no conspicuous immune responses during cell culture also indicate the dissipation of implanted gallium ions.

FIB treatment of materials can produce various structures whose size is in the nano- or micro-scale range on the surfaces of them. For hard materials such as metals, these structures can be created by milling process at high ion doses. On the other hand, for soft materials such as polymeric materials, they can also be created in the form of wrinkles by gallium ion implantation even at low ion doses. In the latter case, due to the formation of hard skin on the surfaces of Ga^+-implanted polymer substrates, the ion-implanted substrates consists of two layers, namely a thin hard surface layer and a untreated inner layer. It is well known that the formation of wrinkles on the surfaces of ion-implanted polymer substrates are caused by thermally and mechanically compressive stresses [41, 134-136]. Furthermore, the morphological changes of polymeric surfaces induced by FIB treatment are mainly affected by the parameters of FIB treatment including scan mode, beam size, dwell time and overlap [76, 137-138] as well as the thermal and structural properties of polymer used. Therefore, numerous patterns of surface wrinkles can be formed by controlling these variables.

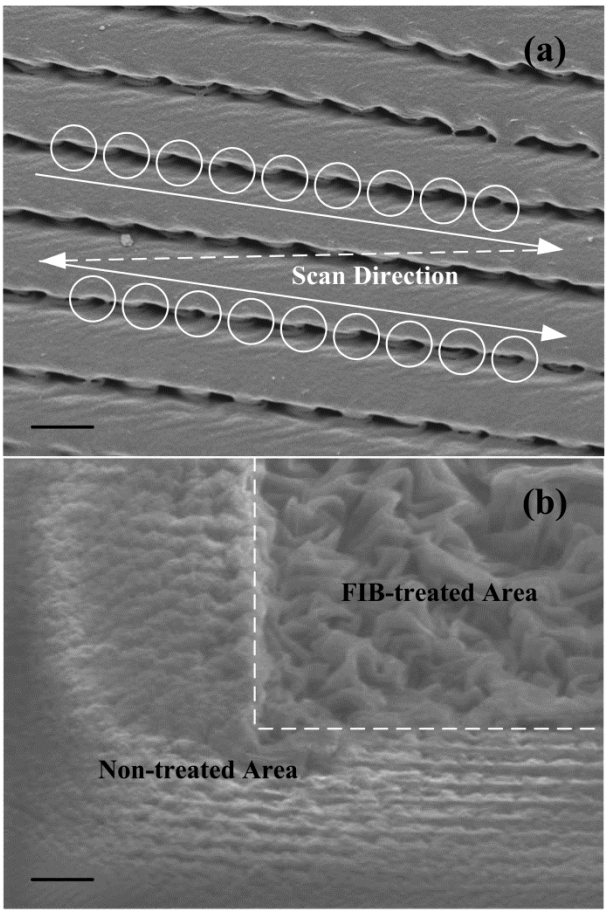

Figure 5.15. SEM images of FIB-treated PU substrates (bar size = 1 μm): (a) Raster scan of FIB over a PU substrate (circle = FIB-treated region, dwell time = 150 μs) and (b) FIB-treated and non-treated areas (dotted line = borderline, applied ion dose = 5×10^{13} ions/cm^2).

Figure 5.15(a) shows a SEM image of a FIB-treated PU substrate fabricated by milling process under raster scan without beam overlap. Arrows indicate the direction of raster scan and a dotted line indicates beam movement without irradiation. To identify FIB-irradiated points, FIB treatment was performed under the same conditions stated above in experimental part except the dwell time. It clearly shows FIB-treated

regions and surface ripples around them. These surface ripples were also observed around the borderline between FIB-treated and non-treated areas as shown in Figure 5.15(b). The FIB-treated area is clearly seen in the top right-hand corner of the image. As a result, in the case of small-sized wrinkles as shown in Figure 5.3(a), they could be formed around FIB-treated area because milling process did not take place under the conditions of low ion dose and dwell time in this study. On the other hand, one-directional (Figures 5.3(b) and 5.3(c)) and herringbone-like (Figure 5.3(d)) surface wrinkles would be created within the FIB-treated area.

Because the ion distribution of a FIB generally follows a Gaussian distribution [76, 138-139], more dramatic effect of a FIB on the morphological change of PU substrates will take place at sites closer to the center of a beam. Due to the ion distribution of a FIB, a wide range of the elasticity of FIB-treated PU substrates will be expected. Applying the theory of the buckling of elastic thin layers on a substrate, the wavelength of surface wrinkles (λ) can be calculated as [41, 82-83, 135, 140]:

$$\lambda = 2\pi h[(1-\nu_b^2)E_s / 3(1-\nu_s^2)E_b]^{1/3} \quad (1)$$

where h is the thickness of ion-implanted hard skin. E and ν are the Young's modulus and Poisson's ratio of ion-implanted surface layer (s) and bulk layer (b). Because applied ion energy was fixed at 30 kV in this study, h would be constant for all samples. Therefore, if $(1-\nu_b^2)/(1-\nu_s^2)$ is assumed to vary within a narrow range before and after FIB treatment, λ can be simplified to $K(E_s/E_b)^{1/3}$ where K is constant (see Appendix D). In this case, the estimated Young's modulus of Type B and Type C (Figure 5.3(b) and 5.3(c)) is 54.14 and 192.19 times greater than that of Type A (Figure 5.3(a)), respectively. Thus, various surface wrinkles can be formed by this unevenness of the Young's modulus of FIB-treated PU substrates.

The chemical change of a FIB-treated region is also affected by the ion distribution leading to the unevenness of surface wettability of FIB-treated PU substrates. However, compared to O_2 plasma treatment, it seems that the effect of gallium ion implantation on the chemical surface modification of PU substrates may be not so crucial because oxygen ions are more reactive species than gallium ions. Furthermore, as shown in Table 5.4, the O/C ratio of the FIB-treated PU scaffolds was increased by only 8.8 % compared to that of the non-treated PU substrates. In addition to this, due to the existence of submicron scale surface wrinkles, surface hydrophobicity will be increased after FIB treatment. As a result, as shown in Figure 5.9, the contact angles of PU substrates before and after FIB treatment did not show any significant differences in this study. In this case, even though surface wrinkles will be helpful to cell adhesion and proliferation, initial adsorption of cell adhesion-related proteins in culture media may be reduced.

To resolve this problem, O_2 plasma treatment was applied. Unlike FIB-treatment, plasma treatment can be evenly applied to the entire surface of a PU substrate. Due to reactive oxygen ions in plasma, O_2 plasma treatment will complement the unevenness of the surface wettability of FIB-treated PU substrates. From the results of XPS and ATR FT-IR, it was confirmed that oxygen-containing hydrophilic functional groups such as -OH and -(C=O)OH were considerably increased after O_2 plasma treatment. These functional groups can facilitate the adsorption of protein molecules which play an important role in cell adhesion onto biomaterials. As a result, as shown in Figure 5.10(d), even distribution of fibroblasts on the surfaces of FIB/PL-treated PU substrates was observed. Thus, it is noted that the FIB/PL-treated PU substrates showed enhanced surface wettability compared to the FIB-treated ones in spite of surface wrinkles.

It is well known that, at the early stages of cell culture, the number of cells which

adhere to the surface of a substrate is dependent on the amount and distribution of adsorbed cell adhesion-related proteins such as fibronectin and vitronectin in culture media onto the surface of the substrate [141-145]. Furthermore, the adsorption amount of these proteins increases with increasing surface wettability of the substrate [146-51]. As mentioned above, due to the unevenness of surface wettability, fibroblasts cultured on the surfaces of FIB-treated PU substrates shows a migration propensity to more hydrophilic wrinkled surface area. In some cases, this migration of fibroblasts may form cell clusters showing highly dense population and induce contact inhibition leading to deterioration in supplies of oxygen and nutrients. However, in the case of FIB/PL-treated PU substrates, the enhancement of surface wettability results in better cell adhesion than non-treated and FIB-treated ones.

After 1 day of culture, although the surfaces of PL-treated PU substrates were smooth, more fibroblasts were cultured compared to FIB-treated ones due to the even distribution of hydrophilic functional groups on the surfaces of them. However, after 3 and 5 days of culture, the numbers of cells cultured on both PU substrates did not show statistically significant differences as shown in Figure 5.13. Even though initial adhesion of fibroblasts is dependent on the amount of hydrophilic functional groups on the surface of PU substrates, this result implies that cell proliferation would be affected by not only hydrophilic functional group formation but also surface wrinkle formation. Therefore, afore-mentioned physico-chemical modifications of FIB/PL-treated PU substrates can improve cell adhesion and proliferation. By controlling parameters of FIB and O_2 plasma treatments, numerous ECM-like scaffolds can be made. Also, if related problems such as the time-dependence on the performance of O_2 plasma treatment and the small area processing of FIB treatment are overcome, the ECM-like scaffolds fabricated by both treatments will be good candidates for various bio-medical applications such as artificial blood vessel and artificial cornea.

5.4. Conclusions

To mimic the morphologies of the extracellular matrix, FIB treatment was applied to PU substrates. Due to the characteristics of a FIB, various types of wrinkles whose wavelength and amplitude were in the submicron range were formed on the surfaces of PU substrates. However, in spite of slight increase in hydrophilic functional groups, the surface wettability of the FIB-treated PU substrates did not show a big increment because of surface wrinkles. To solve this problem, O_2 plasma treatment was also carried out on the FIB-treated PU substrates. As a result, the amount of hydrophilic functional groups such as -OH and -(C=O)OH were considerably increased and evenly distributed on the entire surface area of the FIB-treated PU substrates. With the help of these physico-chemical surface modifications, the initial adsorption of cell adhesion-related proteins and the adhesion and proliferation of human dermal fibroblasts were enhanced. Thus, ECM-like PU scaffolds fabricated by FIB and O_2 plasma treatments showed better biocompatibility compared to non-treated, O_2 plasma-treated and FIB-treated PU substrates. Because ECM-like scaffolds with various surface wrinkles can be made, a wide range of bio-medical uses of them will be expected.

VI. Concluding Remarks

The present study attempted the morphological mimicking of extracellular matrix (ECM) using ion implantation to form wrinkles on the surface of a highly flexible and blood-compatible polyurethane (PU) substrate compared to other polymeric materials. Further, the study explored the opportunities to enhance the biocompatibility of the PU substrate by introducing hydrophilic functional groups onto the surface via oxygen plasma treatment. Fibroblasts were cultured on the ion-implanted and plasma-treated PU substrate in order to examine the influence of physico-chemical surface modification on cell adhesion and growth. From the results, it was found that the more surface wrinkles and hydrophilic functional groups were created on the surface of the polyurethane substrate, the better cell adhesion and growth were improved. The surface modification of PU substrates by ion implantation is favorable for large-area treatment but it can be only possible to form a single pattern of wrinkles with wavelengths of hundreds of nanometers, whereas the surface modification by focused ion beam (FIB) treatment can promptly form a variety of different wrinkle patterns with wavelengths of tens to hundreds of nanometers but is only useful for small-area treatment. It was also found that, for wrinkles formed on the surface of the PU substrate, it was possible to control their sizes and patterns via heat treatment and elongation to induce residual stress. Therefore, the ECM-like PU scaffolds fabricated by ion implantation and oxygen plasma treatment will be applied to artificial organs such as blood vessels. Unfortunately, since this study provides the results obtained from short-term cell cultures, long-term cell cultures are still needed for better understanding of cell behavior on the ECM-like PU scaffolds. However, it will become feasible to fabricate

cell-compatible scaffolds customized for specific cells, through steady long-term *in vitro* and *in vivo* experiments and further studies of *in vivo* biodegradation of polyurethane.

With the increased average life expectancy of human beings, there are an increasing number of people with organs damaged due to accidents or degenerated due to aging and the demand for treatment is also increasing. There should be sufficient supply to meet the increasing demand, but in fact the donation of vital organs is far from enough. In this reality, tissue engineering must be the only way to meet the demand. Although many studies have been attempted with focus on the development of more biocompatible and regenerative artificial organs, we still have a long way to go. As a result of decades-long studies, a number of biomedical products made from biodegradable polymeric materials have appeared on the market, most of them are polyester polymers such as poly(lactic acid) (PLA), poly(glycolic acid) (PGA), poly(ε-caprolactone) (PCL) and their copolymers. Although they have the greatest advantage of being biodegradable, they are considered inappropriate for the replacement of soft tissues because they are hard and inflexible. Therefore, there are many ongoing studies of polymeric materials that can compensate such problems, and more recently with the synthesis of biodegradable polyurethanes by the copolymerization of those polyester-based polymers and highly elastic polyurethanes, their applications to tissue engineering are being studied. If the physico-chemical surface modification by ion implantation and plasma treatment used in this study is performed on the scaffolds fabricated with biodegradable polyurethanes, the scaffolds will exhibit excellent biocompatibility. In addition to this, their combination with peptide-based polymers is expected to pave the way to developing optimal biocompatible polymers.

REFERENCES

[1] Langer R, Vacanti JP. Tissue Engineering. Science 1993;260:920-6.

[2] MacArthur BD, Oreffo ROC. Bridging the gap. Nature 2005;433:19.

[3] Courtney JM, Lamba NMK, Gaylor JDS, Ryan CJ, Lowe GDO. Blood-Contacting Biomaterials: Bioengineering Viewpoints. Artif Organs 1995;19:852-6.

[4] Williams DF. The Williams Dictionary of Biomaterials. Liverpool University Press; 1999.

[5] Williams DF. On the mechanisms of biocompatibility. Biomaterials 2008;29:2941-53.

[6] Ratner BD. The blood compatibility catastrophe. J Biomed Mater Res 1993;27:283-7.

[7] Alberts B, Johnson A, Lewis J, Raff M, Roberts K, Walter P. MOLECULAR BIOLOGY OF THE CELL. 4th ed. New York: Garland Science; 2002.

[8] Lamba NMK, Woodhouse KA, Cooper SL. POLYURETHANES in Biomedical Applications. Boca Raton: CRC Press; 1998.

[9] Pignataro B, Conte E, Scandurra A, Marletta G. Improved cell adhesion to ion beam-irradiated polymer surfaces, Biomaterials 1997;18:1461-70.

[10] Bambauer R, Mestres P, Schiel R, Klinkmann J, Sioshansi P. Surface-Treated Catheters with Ion Beam-Based Process Evaluation in Rats. Artif Organs 1997;21:1039-41.

[11] Kondyurin AV, Maitz MF, Romanova VA, Begishev VP, Kondyurina IV, Guenzel R. Drug release from polyurethane coating modified by plasma immersion ion

implantation. J Biomat Sci-Polym E 2004;15:145-59.

[12] Huang N, Yang P, Leng YX, Wang J, Sun H, Chen JY, Wan GJ. Surface modification of biomaterials by plasma immersion ion implantation. Surf Coat Tech 2004;186:218-26.

[13] Wong KH, Zinke-Allmang M, Wan WK, Zhang JZ, Hu P. Low energy oxygen ion beam modification of the surface morphology and chemical structure of polyurethane fibers. Nucl Instrum Meth B 2006;243:63-74.

[14] Özkucur N, Richter E, Wetzel C, Funk RHW, Monsees TK. Biological relevance of ion energy in performance of human endothelial cells on ion-implanted flexible polyurethane surfaces. J Biomed Mater Res A 2010;93A:258-68.

[15] Stokes DJ, Morrissey F, Lich BH. A New Approach to Studying Biological and Soft Materials Using Focused Ion Beam Scanning Electron Microscopy (FIB SEM). Journal of Physics: Conference Series 2006;26:50-53.

[16] Bittermann AG, Burkhardt C, Lühmann T, Hall H. FIB milling of critical point-dried neurons for characterization of cell-substrate interfaces. Microsc Microanal 2007;13(Suppl 3):208-9.

[17] Edwards HK, Coe SC, Fay MW, Scotchford CA, Grant DM, Brown PD. Site-specific, cross-sectional imaging of biomaterials and the cell/biomaterial interface using focused ion beam/scanning electron microscopy. Journal of Physics: Conference Series 2008;126:012097.

[18] Martínez E, Engel E, López-Iglesias C, Mills CA, Planell JA, Samitier J. Focused ion beam/scanning electron microscopy characterization of cell behavior on polymer micro-/nanopatterned substrates: A study of cell-substrate interactions. Micron 2008;39:111-6.

[19] Pal S, Weiss H, Keller H, Müller-Plathe F. Effect of Nanostructure on the Properties of Water at the Water-Hydrophobic Interface: A Molecular Dynamics

Simulation. Langmuir 2005;21:3699-709.

[20] Kim P, Kim DH, Choi SK, Lee SH, Khademhosseini A, Langer R, Suh KY. Fabrication of nanostructures of polyethylene glycol for applications to protein adsorption and cell adhesion. Nanotechnology 2005;16:1-7.

[21] Rios PF, Dodiuk H, Kenig S, McCarthy S, Dotan A. The effects of nanostructure and composition on the hydrophobic properties of solid surfaces. J Adhes Sci Technol 2006;20:563-87.

[22] Boduroglu S, Cetinkaya M, Dressick WJ, Singh A, Demirel MC. Controlling the Wettability and Adhesion of Nanostructured Poly-(*p*-xylylene) Films. Langmuir 2007;23:11391-5.

[23] Dumitriu S. POLYMERIC BIOMATERIALS. New York: Marcel Dekker; 2002.

[24] Lelah MD, Cooper SL. POLYURETHANES in MEDICINE. Boca Raton: CRC Press; 1986.

[25] Engbers GHM, Dost L, Hennink WE, Aarts PAMM, Sixma JJ, Feijen J. An *in vitro* study of the adhesion of blood platelets onto vascular catheters. Part I. J Biomed Mater Res 1987;21:613-27.

[26] Takahara A, Tashita J, Kajiyama T, Takayanagi M, MacKnight WJ. Microphase separated structure, surface composition and blood compatibility of segmented poly(urethaneureas) with various soft segment components. Polymer 1985;26:987-96.

[27] Park KD, Kim YS, Han DK, Kim YH, Bae EH, Suh H, Choi KS. Bacterial adhesion on PEG modified polyurethane surfaces. Biomaterials 1998;19:851-9.

[28] Park KD, Kim WG, Jacobs H, Okano T, Kim SW. Blood compatibility of SPUU-PEO-Heparin graft copolymers. J Biomed Mater Res 1992;26:739-56.

[29] Kim YH, Han DK, Park KD, Kim SH. Enhanced blood compatibility of polymers grafted by sulfonated PEO via a negative cilia concept. Biomaterials

2003;24:2213-23.

[30] Morimoto N, Watanabe A, Iwasaki Y, Akiyoshi K, Ishihara K. Nano-scale Surface modification of a segmented polyurethane with a phospholipid polymer. Biomaterials 2004;25:5353-61.

[31] Clark P, Connolly P, Curtis ASG, Dow JAT, Wilkinson CDW. Cell guidance by ultrafine topography *in vitro*. J Cell Sci 1991;99:73-7.

[32] Webb A, Clark P, Skepper J, Compston A, Wood A. Guidance of oligodendrocytes and their progenitors by substratum topography. J Cell Sci 1995;108:2747-60.

[33] Rajnicek AM, McCaig CD. Guidance of CNS growth cones by substratum grooves and ridges: effects of inhibitors of the cytoskeleton, calcium channels and signal transduction pathways. J Cell Sci 1997;110:2915-24.

[34] Rajnicek AM, Britland S, McCaig CD. Contact guidance of CNS neurites on grooves quartz: influence of groove dimensions, neural age and cell type. J Cell Sci 1997:110:2905-13.

[35] Könönen M, Hormia M, Kivilahti J, Hautaniemi J, Thesleff I. Effect of surface processing on the attachment, orientation, and proliferation of human gingival fibroblasts on titanium. J Biomed Mater Res 1992;26:1325-41.

[36] Flemming RG, Murphy CJ, Abrams GA, Goodman SL, Nealey PF. Effects of synthetic micro- and nano-structured surfaces on cell behavior. Biomaterials 1999;20:573-88.

[37] Curtis A, Wilkinson C. Nanotechniques and approaches in biotechnology. Trends Biotechnol 2001;19:97-101.

[38] Park GE, Webster TJ. A Review of Nanotechnology for the Development of Better Orthopedic Implants. J Biomed Nanotech 2005;1:18-29.

[39] Mendonça G, Mendonça DBS, Aragão FJL, Cooper LF. Advancing dental

implant surface technology -From micron- to nanotopography. Biomaterials 2008;29:3822-35.

[40] Tay CY, Irvine SA, Boey FYC, Tan LP, Venkatraman S. Micro-/Nano-engineered Cellular Responses for Soft Tissue Engineering and Biomedical Applications. Small 2011;7:1361-78.

[41] Schweikart A, Fery A. Controlled wrinkling as a novel method for the fabrication of patterned surfaces. Microchim Acta 2009;165:249-63.

[42] den Braber ET, de Ruijter JE, Smits HTJ, Ginsel LA, von Recum AF, Jansen JA. Effect of parallel surface microgrooves and surface energy on cell growth. J Biomed Mater Res 1995;29:511-8.

[43] Meyle J, Gültig K, Wolburg H, von Recum AF. Fibroblast anchorage to microtextured surfaces. J Biomed Mater Res 1993;27:1553-7.

[44] Chesmel KD, Black J. Cellular responses to chemical and morphologic aspects of biomaterial surfaces. I. A novel *in vitro* model system. J Biomed Mater Res 1995;29:1089-99.

[45] Meyle J, Gültig K, Nisch W. Variation in contact guidance by human cells on a microstructured surface. J Biomed Mater Res 1995;29:81-8.

[46] den Braber ET, de Ruijter JE, Smits HTJ, Ginsel LA, von Recum AF, Jansen JA. Quantitative analysis of fibroblast morphology on microgrooved surfaces with various groove and ridge dimensions. Biomaterials 1996;17:2037-44.

[47] Chehroudi B, Gould TR, Brunette DM. Effects of a grooved epoxy substratum on epithelial cell behavior *in vitro* and *in vivo*. J Biomed Mater Res 1988;22:459-73.

[48] van Kooten TG, Whitesides JF, von Recum AF. Influence of Silicone (PDMS) Surface Texture on Human Skin Fibroblast Proliferation as Determined by Cell Cycle Analysis. J Biomed Mater Res (Appl Biomater) 1998;43:1-14.

[49] Clark P, Connolly P, Curtis ASG, Dow JAT, Wilkinson CDW. Topographical control of cell behavior: II. multiple grooved substrata. Development 1990;108:635-44.

[50] Hoch HC, Staples RC, Whitehead B, Comeau J, Wolf ED. Signaling for Growth Orientation and Cell Differentiation by Surface Topography in *Uromyces*. Science 1987;235:1659-62.

[51] Green AM, Jansen JA, van der Waerden JPCM, von Recum AF. Fibroblast response to microtextured silicone surfaces: Texture orientation into or out of the surface. J Biomed Mater Res 1994;28:647-53.

[52] Schmidt JA, von Recum AF. Macrophage response to microtextured silicone. Biomaterials 1992;13:1059-69.

[53] Schmidt JA, von Recum AF. Texturing of polymer surfaces at the cellular level. Biomaterials 1991;12:385-9.

[54] Teo WE, Ramakrishna S. A review on electrospinning design and nanofibre assemblies. Nanotechnology 2006;17:R89-106.

[55] Mo XM, Xu CY, Kotaki M, Ramakrishna S. Electrospun P(LLA-CL) nanofiber: a biomimetic extracellular matrix for smooth muscle cell and endothelial cell proliferation. Biomaterials 2004;25:1883-90.

[56] Lee CH, Shin HJ, Cho IH, Kang YM, Kim IA, Park KD, Shin JW. Nanofiber alignment and direction of mechanical strain affect the ECM production of human ACL fibroblast. Biomaterials 2005;26:1261-70.

[57] Han D, Gouma PI. Electrospun bioscaffolds that mimic the topology of extracellular matrix. Nanomed-Nanotechnol 2006;2:37-41.

[58] Teo WE, He W, Ramakrishna S. Electrospun scaffold tailored for tissue-specific extracellular matrix. Biotechnol J 2006;1:918-29.

[59] Sell S, Barnes C, Smith M, McClure M, Madurantakam P, Grant J, McManus M,

Bowlin G. Extracellular matrix regenerated: tissue engineering via electrospun biomimetic nanofibers. Polym Int 2007;56:1349-60.

[60] Chen F, Li X, Mo X, He C, Wang H, Ikada Y. Electrospun chitosan-P(LLA-CL) nanofibers for biomimetic extracellular matrix. J Biomat Sci-Polym E 2008;19:677-91.

[61] Heydarkhan-Hagvall S, Schenke-Layland K, Dhanasopon AP, Rofail F, Smith H, Wu BM, Shemin R, Beygui RE, MacLellan WR. Three-dimensional electrospun ECM-based hybrid scaffolds for cardiovascular tissue engineering. Biomaterials 2008;29:2907-14.

[62] Schiffman JD, Schauer CL. A Review: Electrospinning of Biopolymer Nanofibers and their Applications. Polym Rev 2008;48:317-52.

[63] Anders A, editor. Handbook of Plasma Immersion Ion Implantation and Deposition. New York: Wiley; 2000.

[64] Conrad JR, Radtke JL, Dodd RA, Worzala FJ, Tran NC. Plasma source ion implantation technique for surface modification of materials. J Appl Phys 1987;62:4591-6.

[65] Mändl S, Rauschenbach B. Improving the biocompatibility of medical implants with plasma immersion ion implantation. Surf Coat Tech 2002;156:276-83.

[66] Suzuki Y. Ion beam modification of polymers for the application of medical devices. Nucl Instrum Meth B 2003;206:501-6.

[67] Nakao A, Kaibara M, Iwaki M, Suzuki Y, Kusakabe M. XPS and SERS studies of Cell Adhesion-controlled Polymer Modified by Ion Implantation. Surf Interface Anal 1996;24:252-6.

[68] Satriano C, Marletta G, Conte E. Cell adhesion on low-energy ion beam-irradiated polysiloxane surfaces. Nucl Instrum Meth B 1999;148:1079-84.

[69] Choi SC, Choi WK, Jung HJ, Park JG, Chung BC, Yoo YS, Koh SK. Relation

Between Hydrophilicity and Cell Culturing on Polystyrene Petri Dish Modified by Ion-Assisted Reaction. J Appl Polym Sci 1999;73:41-6.

[70] Satriano C, Carnazza S, Licciardello A, Guglielmino S, Marletta G. Cell adhesion and spreading on polymer surfaces micropatterned by ion beams. J Vac Sci Technol A 2003;21:1145-51.

[71] Dunn GA, Heath JP. A NEW HYPOTHESIS OF CONTACT GUIDANCE IN TISSUE CELLS. Exp Cell Res 1976;101:1-14.

[72] Ohara PT, Buck RC. CONTACT GUIDANCE IN VITRO: A Light, Transmission, and Scanning Electron Microscopic Study. Exp Cell Res 1979;121:235-49.

[73] Teixeira AI, Abrams GA, Bertics PJ, Murphy CJ, Nealey PF. Epithelial contact guidance on well-defined micro- and nanostructured substrates J Cell Sci 2003;116:1881-92.

[74] Meyle J, Gültig K, Brich M, Hämmerle H, Nisch W. Contact guidance of fibroblasts on biomaterial surfaces. J Mater Sci-Mater M 1994;5:463-6.

[75] Dalby MJ, Hart A, Yarwood SJ. The effect of the RACK1 signalling protein on the regulation of cell adhesion and cell contact guidance on nanometric grooves. Biomaterials 2008;29:282-9.

[76] Tseng AA. Recent developments in micromilling using focused ion beam technology. J Micromech Microeng 2004;14:R15-34.

[77] Sugiyama M, Sigesato G. A review of focused ion beam technology and its applications in transmission electron microscopy. J Electron Microsc 2004;53:527-36.

[78] Raffa V, Pensabene V, Menciassi A, Dario P. Design criteria of neuron/electrode interface. The focused ion beam technology as an analytical method to investigate the effect of electrode surface morphology on neurocompatibility.

Biomed Microdevices 2007;9:371-83.

[79] Niihara K, Kaneko T, Suzuki T, Sato Y, Nishioka H, Nishikawa Y, Nishi T, Jinnai H. Nanoprocessing and Nanofabrication of a Structured Polymer Film by the Focused-Ion-Beam Technique. Macromolecules 2005;38:3048-50.

[80] Kochumalayil JJ, Meiser A, Soldera F, Possart W. Focused ion beam irradiation: morphological and chemical evolution in epoxy polymers. Surf Interface Anal 2009;41:931-40.

[81] Kochumalayil JJ, Meiser A, Soldera F, Possart W. Focused ion beam irradiation - morphological and chemical evolution in PMMA. Surf Interface Anal 2009;41:412-20.

[82] Moon MW, Lee SH, Sun JY, Oh KH, Vaziri A, Hutchinson JW. Controlled formation of nanoscale wrinkling patterns on polymers using focused ion beam. Scripta Mater 2007;57:747-50.

[83] Moon MW, Lee SH, Sun JY, Oh KH, Vaziri A, Hutchinson JW. Wrinkled hard skins on polymers created by focused ion beam. P Natl Acad Sci USA 2007;104:1130-3.

[84] Moon MW, Her EK, Oh KH, Lee KR, Vaziri A. Sculpting on polymers using focused ion beam. Surf Coat Tech 2008;202:5319-24.

[85] Moon MW, Han JH, Vaziri A, Her EK, Oh KH, Lee KR, Hutchinson JW. Nanoscale ripples on polymers created by a focused ion beam. Nanotechnology 2009;20:115301 (7pp).

[86] Kondyurin A, Bilek M. Ion Beam Treatment of Polymers: Application Aspects from Medicine to Space. Amsterdam: Elsevier; 2008.

[87] Zdrahala RJ, Zdrahala IJ. Biomedical Applications of Polyurethanes: A Review of Past Promises, Present Realities, and a Vibrant Future, J Biomater Appl 1999;14:67-90.

[88] Ogawa R, Iwasaki Y, Ishihara K. Thermal property and processability of elastomeric polymer alloy composed of segmented polyurethane and phospholipid polymer. J Biomed Mater Res 2002;62:214-21.

[89] Takahashi A, Kita R, Kaibara M. Effects of thermal annealing of segmented-polyurethane on surface properties, structure and antithrombogenicity. J Mater Sci-Mater M 2002;13:259-64.

[90] Lee HS, Hsu SL. An Analysis of Phase Separation Kinetics of Model Polyurethanes. Macromolecules 1989;22:1100-5.

[91] De S, Sharma R, Trigwell S, Laska B, Ali N, Mazumder MK, Mehta JL. Plasma treatment of polyurethane coating for improving endothelial cell growth and adhesion. J Biomat Sci-Polym E 2005;16:973-89.

[92] Martin DJ, Meijs GF, Gunatillake PA, Yozghatlian SP, Renwick GM. The Influence of Composition Ratio on the Morphology of Biomedical Polyurethanes. J Appl Polym Sci 1999;71:937-52.

[93] Takahara A, Jo NJ, Kajiyama T. Surface molecular mobility and platelet reactivity of segmented poly(etherurethaneureas) with hydrophilic and hydrophobic soft segment components. J Biomat Sci-Polym E 1989;1:17-29.

[94] Takahara A, Takahashi K, Kajiyama T. Effect of polyurethane surface chemistry on its lipid sorption behavior. J Biomat Sci-Polym E 1993;5:183-96.

[95] Santerre JP, Woodhouse K, Laroche G, Labow RS. Understanding the biodegradation of polyurethanes: From classical implants to tissue engineering materials. Biomaterials 2005;26:7457-70.

[96] Nakamae K, Nishino T, Asaoka S, Sudaryanto. Microphase separation and surface properties of segmented polyurethane - Effect of hard segment content. Int J Adhes Adhes1996;16:233-9.

[97] Petrini P, Parolari C, Tanzi MC. Silk fibroin-polyurethane scaffolds for tissue

engineering. J Mater Sci-Mater M 2001;12:849-53.

[98] Chiarini A, Petrini P, Bozzini S, Dal Pra I, Armato U. Silk fibroin/poly(carbonate) - urethane as a substrate for cell growth: in vitro interactions with human cells. Biomaterials 2003;24:789-99.

[99] Joseph G, Sharma CP. Prostacyclin immobilized albuminated surfaces. J Biomed Mater Res 1987;21:937-45.

[100] Dejun L, Jie Z. The structure and biomedical behavior of ion bombarded and plasma polymerized segmented polyurethane. Appl Surf Sci 1994;78:195-201.

[101] Hsu S, Chen W. Improved cell adhesion by plasma-induced grafting of L-lactide onto polyurethane surface. Biomaterials 2000;21:359-67.

[102] Li Y, Huang Y. The study of collagen immobilization on polyurethane by oxygen plasma treatment to enhance cell adhesion and growth. Surf Coat Tech 2007;201:5124-7.

[103] Dejun L, Jie Z, Hanqing G, Mozhu L, Fuqing D, Jianfang H. Surface Modification of Medical Polyurethane by Plasma Treatment. Chinese Phys Lett 1992;9:79-82.

[104] Suzuki Y, Kusakabe M. Endothelial cell adhesion to ion implanted polymers. Nucl Instrum Meth B 1992;65:142-7.

[105] Kurotobi K, Kaibara M, Suzuki Y, Iwaki M, Nakajima H, Kaneko S. Ion implantation into collagen-coated surfaces for the development of small diameter artificial grafts. Colloid Surface B 2000;19:227-35.

[106] Kondyurin A, Bilek M. Ion Beam Treatment of Polymers: Application Aspects from Medicine to Space. Amsterdam: Elsevier; 2008. Chapter 9, Biological and medical applications; p.205-41.

[107] Jiang X, Takayama S, Qian X, Ostuni E, Wu H, Bowden N, LeDuc P, Ingber DE, Whitesides GM. Controlling Mammalian Cell Spreading and Cytoskeletal

Arrangement with Conveniently Fabricated Continuous Wavy Features on Poly(dimethylsiloxane). Langmuir 2002;18:3273-80.

[108] Wilkinson CDW, Riehle M, Wood M, Gallagher J, Curtis ASG. The use of materials patterned on a nano- and micro-metric scale in cellular engineering. Mater Sci Eng C 2002;19:263-9.

[109] Palin E, Liu H, Webster TJ. Mimicking the nanofeatures of bone increases bone-forming cell adhesion and proliferation. Nanotechnology 2005;16:1828-35.

[110] Dalby MJ, McCloy D, Robertson M, Wilkinson CDW, Oreffo ROC. Osteoprogenitor response to defined topographies with nanoscale depths. Biomaterials 2006;27:1306-15.

[111] Teixeira AI, McKie GA, Foley JD, Bertics PJ, Nealey PF, Murphy CJ. The effect of environmental factors on the response of human corneal epithelial cells to nanoscale substrate topography. Biomaterials 2006;27:3945-54.

[112] Biological information on the web site of Webelements.com [internet]. [cited 2012 May 1]. Available from: http://www.webelements.com/gallium/biology.html

[113] Material Safety Data Sheets for elements available at ACI Alloys, Inc. [internet]. [cited 2012 May 1]. Available from: http://www.acialloys.com/msds/msds.html

[114] Kondyurin A, Bilek M. Ion Beam Treatment of Polymers: Application aspects from medicine to space. Amsterdam: Elsevier; 2008. Chapter 4, Structure of polymers after ion beam treatment; p.75-145.

[115] Brunette DM. Spreading and Orientation of Epithelial Cells on Grooved Substrata. Exp Cell Res 1986;167:203-17.

[116] den Braber ET, de Ruijter JE, Ginsel LA, von Recum AF, Jansen JA. Orientation of ECM protein deposition, fibroblast cytoskeleton, and attachment complex components on silicone microgrooved surfaces. J Biomed Mater Res

1998;40:291-300.

[117] Meyle J, Wolburg H, von Recum AF. Surface Micromorphology and Cellular Interactions. J Biomater Appl 1993;7:362-74.

[118] Mattews JA, Wnek GE, Simpson DG, Bowlin GL. Electrospinning of Collagen Nanofibers. Biomacromolecules 2002;3:232-8.

[119] Li WJ, Laurencin CT, Caterson EJ, Tuan RS, Ko FK. Electrospun nanofibrous structure: A novel scaffold for tissue engineering. J Biomed Mater Res 2002;60:613-21.

[120] Min BM, Lee G, Kim SH, Nam YS, Lee TS, Park WH. Electrospinning of silk fibroin nanofibers and its effect on the adhesion and spreading of normal human keratinocytes and fibroblasts in vitro. Biomaterials 2004;25:1289-97.

[121] Li WJ, Tuli R, Okafor C, Derfoul A, Danielson KG, Hall DJ, Tuan RS. A three-dimensional nanofibrous scaffold for cartilage tissue engineering using human mesenchymal stem cells. Biomaterials 2005;26:599-609.

[122] Chew SY, Mi R, Hoke A, Leong KW. Aligned Protein-Polymer Composite Fibers Enhance Nerve Regeneration: A Potential Tissue-Engineering Platform. Adv Funct Mater 2007;17:1288-96.

[123] Ma PX, Zhang R. Synthetic nano-scale fibrous extracellular matrix. J Biomed Mater Res 1999;46:60-72.

[124] Hua FJ, Kim GE, Lee JD, Son YK, Lee DS. Macroporous Poly(L-lactide) Scaffold 1. Preparation of a Macroporous Scaffold by Liquid-Liquid Phase Separation of a PLLA-Dioxane-Water System. J Biomed Mater Res 2002;63:161-7.

[125] Zhang R, Ma PX. Synthetic nano-fibrillar extracellular matrices with predesigned macroporous architecture. J Biomed Mater Res 2000;52:430-8.

[126] Chen M, Zamora P, Som P, Peña LA, Osaki S. Cell attachment and

biocompatibility of polytetrafluoroethylene (PTFE) treated with glow-discharge plasma of mixed ammonia and oxygen. J Biomed Sci-Polym E 2003;14:917-35.

[127] van Kooten TG, Spijker HT, Busscher HJ. Plasma-treated polystyrene surfaces: model surfaces for studying cell-biomaterial interactions. Biomaterials 2004;25:1735-47.

[128] Kawamoto Y, Nakao A, Ito Y, Wada N, Kaibara M. Endothelial cells on plasma-treated segmented-polyurethane: Adhesion strength, antithrombogenicity and cultivation in tubes. J Mater Sci-Mater M 1997;8:551-7.

[129] Cell Counting Kit-8 Technical Manual [internet]. [cited 2012 May 1]. Available from: http://www.dojindo.com/store/p/456-Cell-Counting-Kit-8.aspx

[130] Martins MCL, Wang D, Ji J, Feng L, Barbosa MA. Albumin and fibrinogen adsorption on PU-PHEMA surfaces. Biomaterials 2003;24:2067-76.

[131] Bandekar J, Sawyer A. FT-IR spectroscopic studies of polyurethanes: IV. Studies of the effect of the presence of processing aids on the hemocompatibility of polyurethanes. J Biomed Sci-Polym E 1995;7:485-501.

[132] Pellethane® Technical Data Sheets on the web site of Matweb.com [internet]. [cited 2012 June 5]. Available from: http://www. matweb.com/index.aspx

[133] Downs AJ, editor. Chemistry of Aluminium, Gallium, Indium and Thallium. Glasgow: Blackie Academic & Professional; 1993.

[134] Yoo PJ, Lee HH. Evolution of a Stress-Driven Pattern in Thin Bilayer Films: Spinodal Wrinkling. Phys Rev Lett 2003;91:154502. DOI:10.1103/PhysRevLett91.154502.

[135] Zhao Y, Huang WM, Fu YQ. Formation of micro/nano-scale wrinkling patterns atop shape memory polymers. J Micromech Microeng 2011;21:067007 (8pp).

[136] Chan EP, Smith EJ, Hayward RC, Crosby AJ. Surface Wrinkles for Smart Adhesion. Adv Mater 2008;20:711-6.

[137] Hopman WCL, Ay F, Hu W, Gadgil VJ, Kuipers L, Pollnau M, de Ridder RM. Focused ion beam scan routine, dwell time and dose optimizations for submicrometre period planar photonic crystal components and stamps in silicon. Nanotechnology 2007;18:195305 (11pp).

[138] Han J, Lee H, Min BK, Lee SJ. Prediction of nanopattern topography using two-dimensional focused ion beam milling with beam irradiation intervals. Microelectron Eng 2010;87:1-9.

[139] Edinger K, Kraus T. Modeling of focused ion beam induced surface chemistry. J Vac Sci Technol B 2000;18:3190-3.

[140] Harrison C, Stafford CM, Zhang W, Karim A. Sinusoidal phase grafting created by a tunably buckled surface. Appl Phys Lett 2004;85:4016-8.

[141] Webb K, Hlady V, Tresco PA. Relative importance of surface wettability and charged functional groups on NIH 3T3 fibroblast attachment, spreading, and cytoskeletal organization. J Biomed Mater Res 1998;41:422-30.

[142] Arima Y, Iwata H. Effect of wettability and surface functional groups on protein adsorption and cell adhesion using well-defined mixed self-assembled monolayers. Biomaterials 2007;28:3074-82.

[143] Dekker A, Beugeling T, Wind H, Poot A, Bantjes A, Feijen J, van Aken WG. Deposition of cellular fibronectin and desorption of human serum albumin during adhesion and spreading of human endothelial cells on polymers. J Mater Sci-Mater M 1991;2;227-33.

[144] Gan BK, Kondyurin A, Bilek MMM. Comparison of Protein Surface Attachment on Untreated and Plasma Immersion Ion Implantation Treated Polystyrene: Protein Islands and Carpet. Langmuir 2007;23:2741-6.

[145] Nosworthy NJ, Ho JPY, Kondyurin A, McKenzie DR, Bilek MMM. The attachment of catalase and poly-L-lysine to plasma immersion ion implantation-

treated polyethylene. Acta Biomater 2007;3:695-704.

[146] van Kooten TG, Schakenraad JM, van der Mei HC, Busscher HJ. Influence of substratum wettability on the strength of adhesion of human fibroblasts. Biomaterials 1992;13:897-904.

[147] Altankov G, Groth TH. Reorganization of substratum-bound fibronectin on hydrophilic and hydrophobic materials is related to biocompatibility. J Mater Sci-Mater M 1994;5:732-7.

[148] Wei J, Yoshinari M, Takemoto S, Hattori M, Kawada E, Liu B, Oda Y. Adhesion of mouse fibroblasts on hexamethyldisiloxane surfaces with wide range of wettability. J Biomed Mater Res-A 2007;81:66-75.

[149] Campillo-Fernandez AJ, Unger RE, Peters K, Halstenberg S, Santos M, Sánchez MS, Dueñas JMM, Pradas MM, Ribelles JLG, Kirkpatrick CJ. Analysis of the Biological Response of Endothelial and Fibroblast Cells Cultured on Synthetic Scaffolds with Various Hydrophilic/Hydrophobic Ratios: Influence of Fibronectin Adsorption and Conformation. Tissue Eng 2009;15:1331-41.

APPENDIX

Appendix A. SEM images of thermally treated PU films after Ar^+ implantation (bar size = 100 μm).

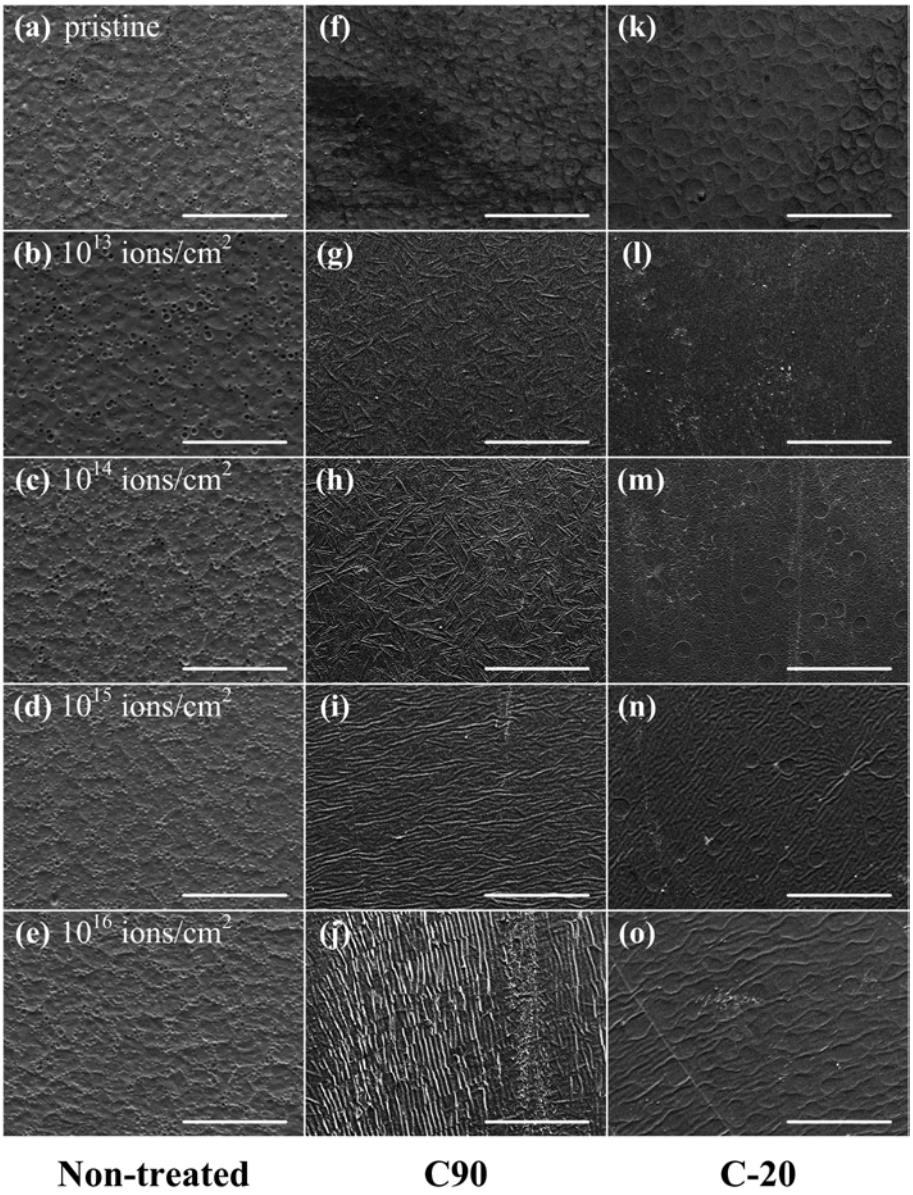

Appendix B. ESR results of Ar^{+}-implanted C90 PU films (g-factor = 2.003).

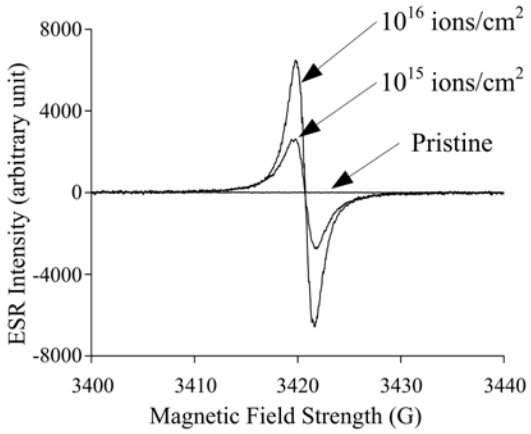

- For amorphous carbon structures, the value of g-factor is 2.0027.
- Free electrons in graphite-like structures were detected at ion doses higher than 1×10^{15} ions/cm^2.

Appendix C. Three-dimensional topographic images of Kr^{+}-implanted PU substrates (at a magnification of 29×): (a) Pristine, (b) 1×10^{13} ions/cm^2, (c) 1×10^{14} ions/cm^2, (d) 1×10^{15} ions/cm^2 and (e) 1×10^{16} ions/cm^2.

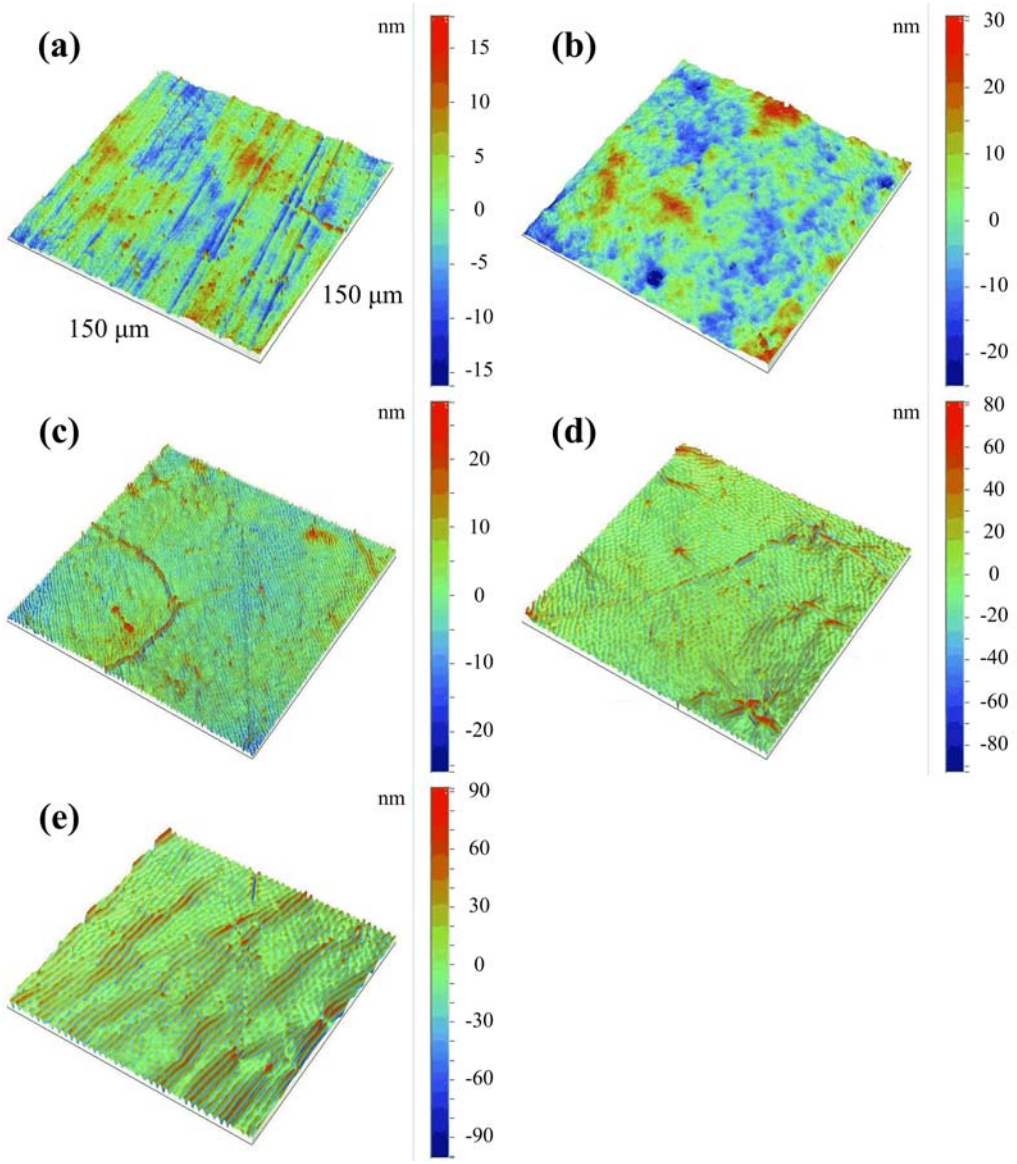

Appendix D. Calculation of K of equation (1).

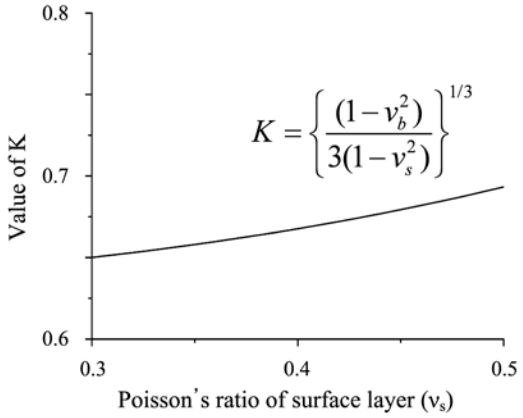

- For elastic polymers, the Poisson's ratio of bulk layer (ν_b) is 0.5.
- For plastic polymers, the Poisson's ratio of bulk layer (ν_b) is 0.3.

Values of K

ν_s	K	ν_s	K	ν_s	K
0.30	0.650079	0.37	0.661647	0.44	0.676804
0.31	0.651538	0.38	0.663575	0.45	0.679313
0.32	0.653059	0.39	0.665577	0.46	0.681916
0.33	0.654643	0.40	0.667657	0.47	0.684619
0.34	0.656292	0.41	0.669817	0.48	0.687424
0.35	0.658008	0.42	0.672060	0.49	0.690337
0.36	0.659792	0.43	0.674388	0.50	0.693361

Appendix E. SEM images of FIB-treated PU films (ion dose = 2.2×10^{13} ions/cm^2).

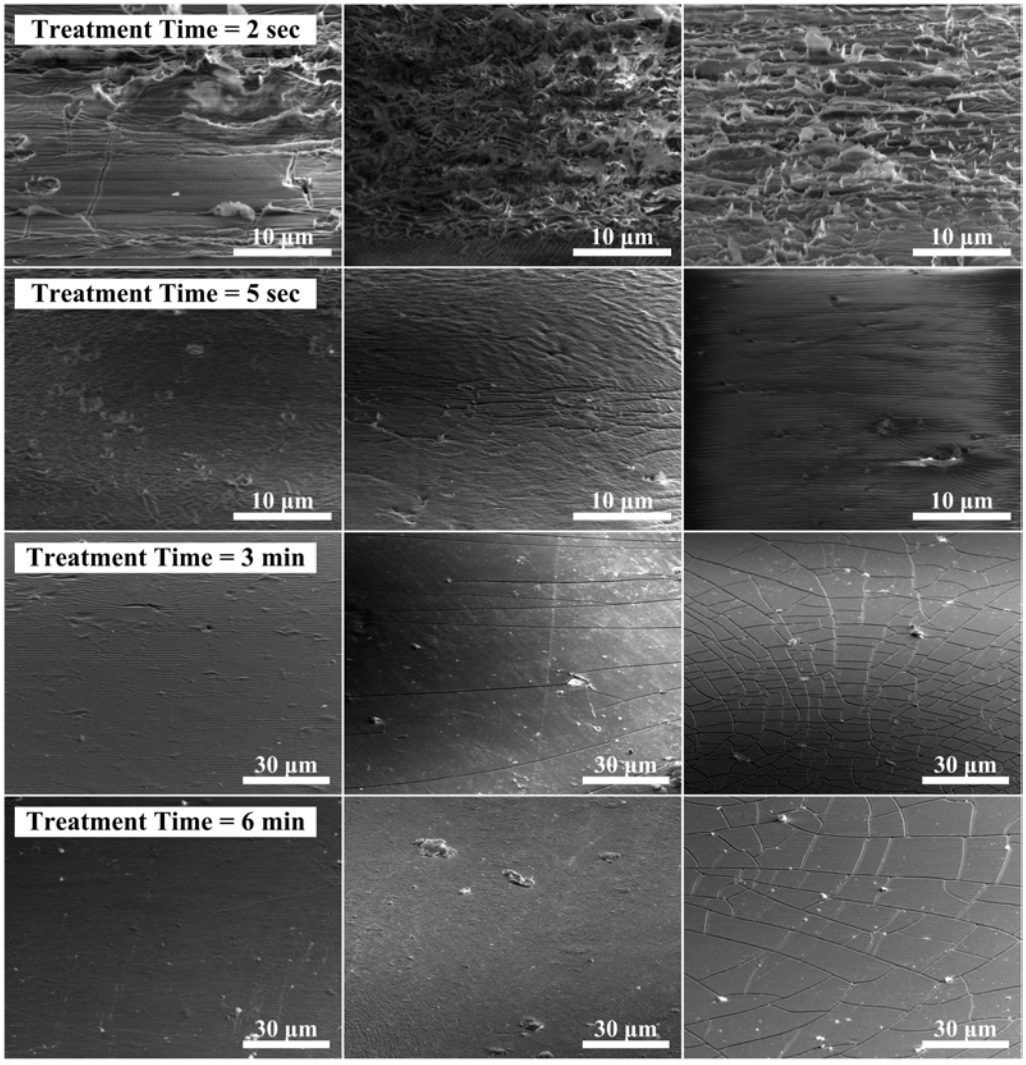

KOREAN ABSTRACT

생체재료(Biomaterials)는 의약품을 제외한 인공, 천연 또는 그들의 복합재료로서 인체 내에서 단기 또는 장기간 동안 인체의 조직이나 기관의 기능을 치료, 보강, 대치 또는 회복시키는데 사용되는 모든 재료를 일컫는다. 생체재료로 사용되는 물질은 생체조직과 유사한 기계적 강도와 기능적 특징 및 생화학적 적합성의 필수적인 특성들을 갖추어야 한다. 1900년대 초반부터 생체재료의 연구는 시작됐지만, 최근 30년간 세계적으로 생체재료 또는 이에 관련된 시장이 급속히 증가하고 있다. 이런 급속한 성장의 주된 이유는 전쟁과 사고로 인한 재활환자의 증가, 수명 연장과 자연 사망률의 감소로 인한 노령인구의 증가, 인간의 높은 삶의 질 추구 등을 들 수 있다. 따라서, 조직공학(Tissue engineering) 분야에서는 성능이 우수한 생체재료의 개발이 시급히 필요한 실정이다.

폴리우레탄(Polyurethane)은 폴리올(Polyol)로 구성된 연질부와 우레탄기(Urethane group)로 구성된 경질부로 이루어진 전형적인 블록 공중합체(Block copolymer)이다. 폴리우레탄의 우수한 기계적 특성과 뛰어난 생체적합성(Biocompatibility) 때문에, 혈액과 접촉하는 의료용품이나 인공장기용 재료에 많이 사용되고 있다. 특히, 생의학 분야에서는 폴리우레탄에 대한 많은 연구 결과로부터, 다른 고분자들에 비해 더 좋은 혈액적합성(Blood compatibility)을 보이는 것으로 알려져 있다. 그러나, 이러한 장점에도 불구하고, 아직까지는 그 자체가 혈액 적합성이 충분하지 못하고 생체 외부 및 생체 내부 실험에서 생분해(Biodegradation)나 칼슘 침착에 의한 칼슘화 현상 및 박테리아 감염이 일어나기 때문에 의료용 재료로 광범위하게 응용되지 못하고 있는 실정이다. 그러므로, 장기간 이식

가능한 의료용 재료로 사용되기 위해서는 폴리우레탄의 혈액적합성뿐만 아니라 생체 내 안정성, 항칼슘화 및 감염 억제 특성이 요구된다. 따라서, 폴리우레탄의 생체적합성을 향상시키기 위해서는 재료 표면의 개질(Surface modification)이 필요하다.

본 논문에서는, 현재 고분자 재료의 생체적합성을 간단하고 효과적으로 향상시키는 방법인 이온 주입법(Ion implantation)을 사용하여 폴리우레탄 표면을 개질하였다. 이온 주입법에 의한 열처리된 폴리우레탄 필름의 표면 개질에 대한 연구를 위해, 기존의 이온 주입 장비를 이용하여 아르곤 이온(Ar^+) 주입하였다. 상분리(Phase separation)와 같은 폴리우레탄 고유 특성을 변화시키기 위해, 아르곤 이온을 주입하기 전 solvent casting 방법으로 만들어진 폴리우레탄 필름에 서로 다른 두 가지 열처리를 적용하였다. 그 결과, 열처리에 의해 폴리우레탄 필름 표면의 상분리 정도 및 연질 매트릭스(Matrix)와 경질 도메인(Domain)의 분포 변화가 발생하는 것을 확인하였다. 이온 주입 전 높은 온도에서 열처리한 폴리우레탄 필름의 경우, 계면 자유 에너지(Interfacial free energy)를 최소화하기 위해 필름 표면은 소수성(hydrophobic)의 연질부가 풍부해졌다. 반면, 낮은 온도에서 열처리한 폴리우레탄 필름의 경우, 상분리 정도의 증가와 연질부의 분자 운동성 감소에 의해 필름 표면은 폴리우레탄 경질부가 증가하였다. 이온 주입 후 고온에서 열처리한 폴리우레탄 필름의 경우, 적은 이온 주입량(1×10^{14} ions/cm^2 이하)에도 표면 젖음성(Surface wettability)이 향상되는 이유는 이온 주입된 폴리우레탄 필름의 표면에 소수성 연질부의 고분자쇄가 끊어지면서 친수성 관능기가 형성되었기 때문이었다. 그러나, 1×10^{14} ions/cm^2보다 많은 이온 주입량에 의한 표면 거칠기(Surface roughness)의 증가와 필름 표면층의 탄화(Carbonization)는 표면 젖음성을 감소시키는 것을 확인하였다. 저온에서 열처리한 폴리우레탄 필름의 경우, 1×10^{13} ions/cm^2에서 1×10^{16} ions/cm^2의 이온 주입량 범위에서 표면

젖음성이 향상되었는데, 이는 친수성 관능기의 향상과 많은 이온 주입량에도 불구하고 고온에서 처리했을 때보다 상대적으로 작게 증가한 표면 거칠기에 기인하였다. 이온 주입에 의한 표면 주름(Surface wrinkles)의 크기는 이온 주입량에 따라 증가하는 경향을 보였다. 하지만, 저온에서 열처리한 폴리우레탄 필름의 경우, 필름 표면의 경질부 도메인에 의해 필름 표면의 주름 형성이 지연됨을 확인하였다.

빔(Beam) 타입의 갈륨 이온(Ga^+) 주입 방법인 집속 이온빔(Focused ion beam, FIB) 또한 폴리우레탄 기질의 표면 개질을 위해 사용되었다. 집속 이온빔으로 처리된 폴리우레탄 기질의 세포 부착 및 성장에 관한 영향을 살펴보기 위해, 쥐 배아(mouse embryo)에서 유래된 NIH3T3 섬유아세포(Fibroblast)를 배양해보았다. 집속 이온빔 처리 후 세척한 폴리우레탄 기질은 주입된 갈륨 이온이 검출되지 않았는데, 이는 갈륨 이온의 세포 성장에 미치는 영향이 거의 무시할 수준임을 의미하였다. 게다가, FIB처리 한 폴리우레탄 기질 표면은 쥐에서 유래된 RAW 264.7 단핵백혈구/대식세포(Monocyte/macrophage)의 다핵거대세포(Multinucleated giant cell)로의 변형을 유발하지 않았기 때문에 세포에 대한 독성이 없음을 보여주었다. 면역형광 염색법의 결과로부터, 3일 동안의 NIH3T3 세포 배양 기간 동안 세포소멸에 관련된 caspase 3의 합성은 미미한 수준임을 알 수 있었고, 이로부터 세포가 건강하게 성장하는 것을 입증하였다. 기존의 아르곤 이온 주입법과 비교했을 때, FIB처리는 carbonyl 그리고 carboxyl과 같은 친수성 관능기를 폴리우레탄 기질 표면에 더 많이 형성하여 표면 젖음성을 향상시켰다. 그리고 상대적으로 적은 이온 주입량에서도 수십에서 수백 나노미터 크기의 표면 주름을 형성하였다. 이 물리화학적 표면 개질에 의해, 집속 이온빔 처리된 폴리우레탄 기질은 향상된 생체적합성을 보였고, 아무 처리도 하지 않은 폴리우레탄 기질 및 아르곤 이온이 주입된 폴리우레탄 기질과 비교했을 때 훨씬 우수한 세포 증식을 보여주었다.

집속 이온빔과 산소 플라즈마 처리 방법은 친환경적인 건식 공정으로 고분자 재료 표면의 물리화학적 개질에 사용될 수 있다. 우리 몸의 세포외기질(Extracellular matrix)의 형태학 및 화학적 모사를 위해, 이 두 가지 방법을 폴리우레탄 기질에 적용해보았다. 그리고 두 가지 표면 개질 방법이 적용된 폴리우레탄 기질이 사람의 피부 섬유아세포의 부착 및 증식에 미치는 영향에 대하여 연구하였다. 그 결과, 이 두 가지 방법을 이용하여 만든 세포외기질과 유사한 폴리우레탄 기지체(Scaffold)의 표면에서는, 섬유아세포의 몸체에서 더 많은 사상위족(Filopodia)이 뻗어 나오는 것을 확인하였다. 수십에서 수백 나노미터 크기의 다양한 표면 주름과 증가된 표면 젖음성으로 인해 세포외기질을 모사한 폴리우레탄 기지체는 세포 배양 기간 동안 향상된 생체적합성과 세포 증식을 보여주었다. 따라서, 세포외기질과 유사한 폴리우레탄 기지체는 인공 혈관 등의 인공 장기 및 세포의 성장 거동을 연구하는 플랫폼(Platform)으로의 사용이 기대된다.

주요어: 폴리우레탄, 이온 주입, 집속 이온빔, 표면 개질, 표면 주름, 표면 젖음성, 생체적합성, 생체재료, 조직 공학

학번: 2001-30386

감사의 글

남들보다 두 배 더 많은 시간을 들여 연구를 했는데도 불구하고, 아직도 아쉬움이 남는 까닭은 부족함이 채워지지 않아서 그런가 봅니다. 조직 공학이라는 매우 흥미로운 분야에 빠져서 즐겁게 연구하였고, 아직 많이 부족한 내용이겠지만, 제 연구 결과가 이 분야에 조그마한 보탬이 되었으면 하는 바램을 가져봅니다. 저 혼자서는 할 수 없었던 큰 그림을 그리는데 도움을 주신 많은 분들께 감사 드립니다.

지금은 곁에 계시지 않지만 항상 묵묵히 믿고 지켜봐 주시던 그리운 아빠, 이제는 아들의 아들까지 돌봐주시느라 고생이신 엄마, 내 인생 최고의 선택이라 자부하는 우리 여보 현아, 그리고 경기도 광명 얼짱 아들 지훈이와 항상 분에 넘치는 사랑을 베푸시는 장모님, 장인어른께 부끄럽지 않은 아들이자, 남편, 아빠, 사위로서 열심히 살겠습니다.

세포 실험에 도움을 주셨던 서울대학교 의과대학 성형외과 장학 교수님, 박영인 연구원님, 이륜숙 연구원님과 서울대학교 치의과대학 김현정 교수님, 박숙영 연구원님, 그리고, 이온빔에 관한 해박한 지식으로 저를 도와주신 한국 원자력 연구원 이재상 박사님, FIB 샘플을 만들어 주시느라 고생하셨던 서울대학교 재료공학부 허은규 박사님께 진심으로 감사 드립니다.

마지막으로 저 때문에 근심이 많으셨던 강태진 지도교수님과, 함께 실험실 생활을 했던 종렬이형, 재홍, 문희, 세영, 덕준, 성환, 희석, 원석, 희윤, 민경, 다영, 선아에게 이제 실험실을 벗어나 좀 더 넓은 세상에서 멋지게 활약하는 제자이자 선후배, 친구가 되기를 다짐해보며 마무리합니다. 감사합니다.